THE UNIVERSITY OF MICHIGAN

7300-1-F

RADANT ANALYSIS STUDIES

Final Report, First Phase
30 April 1965 through 28 February 1966

C. T. Tai, E. S. Andrade and M. A. Plonus

June 1966

Prepared for

THE UNIVERSITY OF MICHIGAN

FOREWORD

This report was prepared by C. T. Tai, E. S. Andrade and M. A. Plonus of the Radiation Laboratory, Department of Electrical Engineering, University of Michigan under Contract AF 33(615)-2811. The primary objective of this effort was to investigate analytically and experimentally the Radant-a unique electromagnetic wave transmission structure developed by AVWE-3 as part of the in-house research effort.

This work was sponsored by the Air Force Avionics Laboratory with Stanley B. Pitts acting as Project Engineer. This report covers the work conducted during the period of 30 April 1965 to 28 February 1966.

This report was submitted by the authors in April 1966.

This technical report has been reviewed and is approved.

JOSEPH A. DOMBROWSKI
Lt Colonel, USAF
Chief, Electronic Warfare Division

THE UNIVERSITY OF MICHIGAN

7300-1-F

ABSTRACT

This is the final report on the first phase of an investigation of radant structures. A theoretical and experimental investigation has been made of a specialized radant structure consisting of an array of loops supported by two dielectric panels. Impedance and pattern performance of the radant structure was examined over a wide frequency range. The radant structure was fed by a ferrite loaded slot, by a ridged horn and by a half wave dipole. The diffracted field due to a finite dielectric panel was analyzed using the Huygens-Kirchhoff principle. The results are evaluated and it is concluded that the performance of the specialized structure was not sufficiently unusual or promising to warrant further study. Recommendations are made for a more general approach in a study of selected radant structures or elements that appear to hold promise.

THE UNIVERSITY OF MICHIGAN

7300-1-F

TABLE OF CONTENTS

I
INTRODUCTION

This is the final report on the first phase of an investigation of a specialized radant structure. The investigation was initiated at The University of Michigan at the request of the Avionics Laboratory following preliminary investigation by personnel of that laboratory. A radant is a structure made up of a radome and an antenna so integrated that they function as a single device. It is hope that such a device will possess advantages in size and weight and that it might be more free from bore site error and also have advantageous polarization characteristics.

The objective of the contract was to analyze, experimentally and theoretically a radant structure consisting of two dielectric sheets supporting a matrix of antenna elements consisting of dipoles and/or loops which were connected by transmission lines. The investigation was to be centered on a radant device similar to a specific structure (described later) fabricated and tested in the Avonics Laboratory. In the course of the investigation, attention was to be given to the effects on performance of various parameters of the radant device as a function of frequency. To be considered were the effect of spacing between input and output matrices, the effect of spacing between the antenna elements and the feasibility of converting from linear polarization to an orthogonal linear or to circular polarization. The impedance characteristics and the propagation constant of the radant structure was to be studied and the optimum method for feeding the structure was to be determined.

In tests made by the Air Force their radant structure had been fed by a narrow band ferrite loaded cavity slot antenna. This antenna developed by Adams et al (1964) had a resonant frequency of 350 MHz and a radiating aperture of 2 inches by 5 inches. The preliminary test results obtained by the Air Force using the ferrite loaded slot to feed the radant structure appeared to indicate the possibility of super-directivity. The University of Michigan was therefore asked to give particular attention to a similar radant and feed arrangement and to account

for any unusual performance characterisitcs.

Although a description of the radant structure was given by Tai and Andrade (1965) it is repeated here for convenience. It consists of an array of conducting loops held in place by two 18" by 18" printed circuit fiber board panels. The exterior parts of the loops are flat strips attached to the fiber board panels. These strips, 3/32 inch wide by 1 5/8 inches long, form parallel rows spaced 1 inch apart with an end to end spacing between elements of 1/2 inch. The loops are not aligned in the lateral direction but are desplaced as shown in Fig. 1. The exterior flat strips of the loops are connected to their counter part on the other panel by a pair of brass machine screws, 0-80 by 1 inch. The threaded screw arrangement permits some adjustment in the thickness of the radant panel. Unless otherwise stated the E vector of the exciting antenna was parallel to the plane of the loops for all pattern and impedance data reported.

In the first Interim Report (Tai et al (1965)) the radant structure was treated analytically as an array of conducting discs. The transmission characteristics of the anisotropic medium thus formed was calculated and numerous curves were presented for the incident plane wave case. Results were given for the E-field both parallel and perpendicular to the plane of the incidence and for anisotropic panels of thickness $\lambda/16$, $\lambda/8$, $\lambda/4$ and $\lambda/2$ and for several values of permittivity and permeability. The purpose of that study was to build a reasonable theoretical model in order to help interpret the electrical characteristic of the loop radome structure.

Also in the first Interim Report the transmission patterns of an anisotropic panel excited by a spherical source was examined. The objective was to simulate illumination by a small electromagnetic horn or dipole placed in the near or far field of the anisotropic panel. The formulations were completed and some preliminary calculations were made. As far as the beamwidth of the resultant field is concerned the result based upon the approximate theory compares favorably
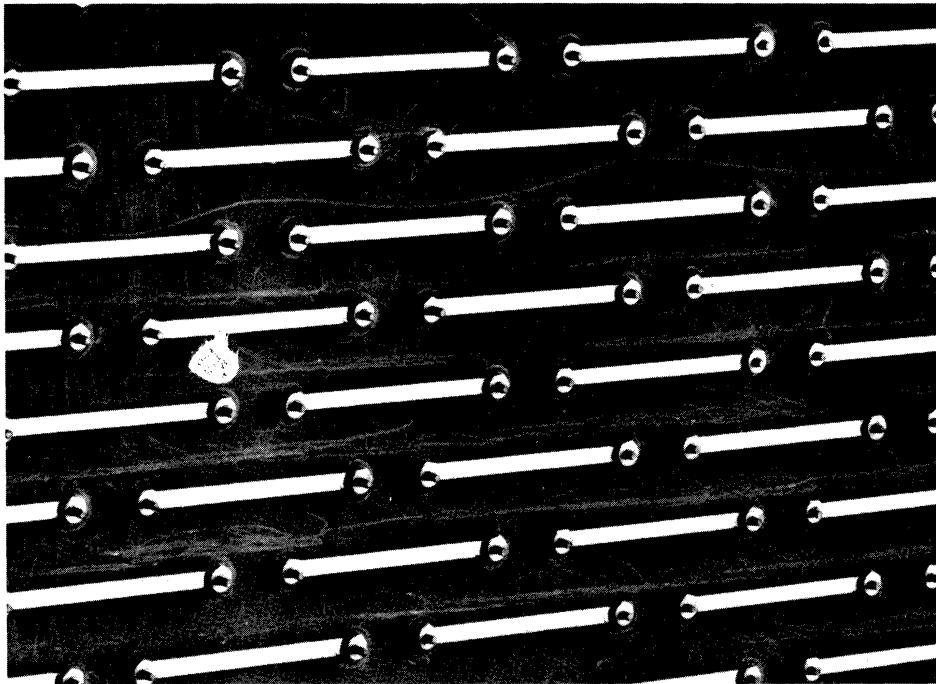
FIG. 1a: PHOTOGRAPH OF SECTION OF RADANT STRUCTURE
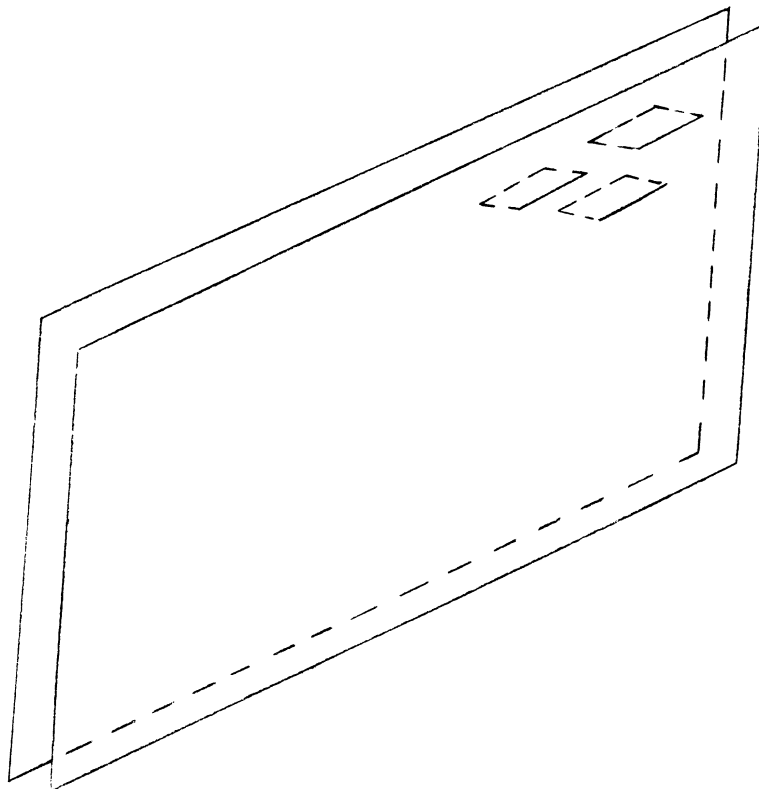

FIG. 1b: RADANT STRUCTURE

with the experimental result.

An extensive experimental program was initiated during the first interim period. The radant panel described above was fabricated, and with the ferrite slot antenna as a feed, pattern and impedance data was obtained for several spot frequencies below 1000 MHz.

The continuation of the experimental study was reported in the second Interim Report(Tai and Andrade, 1965). Further pattern and impedance data was obtained for the radant structure using the ferrite slot feed. Information was obtained on effect of spacing between feed and panel and the effect of a large versus small ground plane was found. It was found that the directivity increased with frequency (350-600 MHz) essentially as was predicted. The maximum change in directivity due to placing the radant structure in front of the ferrite slot antenna was about 8 db; this occurred at 550 MHz. Even with this increased directivity, the absolute gain of the combination was low (-6 to -8 db with respect to a half wave dipole) due/to the poor efficiency of the slot feed at this frequency.

To obtain information on the performance of the radant structure at frequencies not covered by the ferrite slot feed, use was made of other feeds,-e.g. a simple dipole and a broadband ridge waveguide horn. Preliminary results with these feeds are also given in the second Interim Report. With the ridges horn as a feed, VSWR as a function of spacing was measured at several frequencies and resonant spacing effects were noted. With the spacing fixed, VSWR as function of frequency was measured; in general the radant structure caused a much higher VSWR.

Preliminary pattern data obtained at x band with the ridged horn feeding the radant structure showed that for some spacings, the beamwidth was slightly more narrow; in general, the introduction of the radant caused some break-up in the patterns accompanied by an increase in side lobes level.

Work on a theoretical investigation of the scattering characteristics of a pair of dipoles linked by a transmission line was also reported in the second Interim

Report. This work was initiated as a possible model for a future investigation of a radant panel made of dipoles connected by a transmission line.

During the present report period, the experimental investigation of the radant structure described above has been concluded. Using the ridged horn as a primary feed, patterns were taken at 1.0, 1.5, 3.0 and 8.5 GHz. Pattern data was also taken at 0.36, 0.75, 1.5 and 3.0 GHz using half wave dipoles as feeds. Some pattern data was obtained for the radant structure at 2.5 GHz when one of its center loops was excited directly.

Additional experimental work was performed on the transmission and pattern characteristics of a dielectric panel illuminated by a half wave dipole. These results were of interest for comparison with results from a theoretical study described in the first Interim Report (and in Section V of the present report.)

In regard to the theoretical work based upon the Huygen-Kirckhoff's principle, the approximate theory discussed in the first Interim Report was modified with the hope of providing a better analysis of the diffracted field due to a finite dielectric panel. The entire work is now included in Section V of this report. From the analytical point of view, the modification [Eq. (6) of Section V], is a more logical approach to the problem. Unfortunately, as far as the numerical results are concerned, the refined theory yields certain data which can not be easily interpreted. If we refer to Figs. 49-52, it is seen that the resultant field, in many cases, exhibits a split lobe in the forward direction. Such a spliting does not exist according to the approximate theory discussed in Interim Report No. 1. It is very possible that the use of the geometrical optics approximation for the primary field is the main cause of this unexpected result. Since the entire analysis is of some theoretical interest, the work is reported here so we may, perhaps, stimulate some further investigations on this problem.

II
RADANT STRUCTURE WITH RIDGED HORN AS PRIMARY FEED

Initial experimental data using the ridged horn as a primary feed for the aniso-tropic radant panel has been presented (Tai and Andrade, 1965) in the second Interim Report. Data presented were the VSWR, impedance and radiation pattern charac-teristics obtained for 1.0 and 8.5 GHz. To complete the study of the transmission characterisitcs of the radant structure additional patterns have been obtained at 1.5 and 3.0 GHz. The half power beamwidth and side lobe level as a function of ground plane size and spacing is given in Tables I for 3 GHz and in Table II, beam-widths as a function of frequency is given. E-plane patterns were measured in accordance with the coordinate system of Fig. 2. The spacing between the radant structure and the ridged horn was varied in one-half inch increments from 0 to 2 inches. Radiation patterns were measured for two ridged horn configurations which were: 1) the ridged horn flush mounted in an 18 inch square ground plane and 2) ridged horn with no ground plane. Figures 3-6 are radiation patterns obtained from the ridged horn flush mounted in the ground plane both with and without a radant structure at frequencies of 1.0, 1.5, 3.0 and 8.5 GHz. The spacing noted on each pattern is that which resulted in the optimum beamwidth and gain characteristics for that frequency. Figures 7 and 8 are radiation patterns recorded for 1.5 and 3.0 GHz respectively with the ground plane removed from the ridged horn.

The patterns of the radant structure fed by the ridged horn flush mounted in the ground plane at 1.5 GHz (see Fig. 4b) are severely distorted. This distortion is probably due to energy being trapped between the ground plane and the radant structure. This trapped energy then radiates from the edges and the radant is in effect an array of three radiating apertures. As a justification for this reasoning the reader's attention is called to the patterns of the radant shown in Fig. 7b. Here the panel is fed by the ridged horn with the ground plane removed. At 3.0 GHz the patterns of the radant structure when fed by the ridged horn (with or without the

6

TABLE I

Radant and Ridged Horn Pattern Characteristics at 3.0 GHz

Condition	Flush Mounted 18" x 18" Ground Plane		Without Ground Plane	
	θ_{3db}	Side Lobe Level	θ_{3db}	Side Lobe Level
No Radant	40°	-9db	30°	-11db
1/3" Spacing	20°	-11db	17°	-11db
1"	21°	-7db	19°	-7db
1 1/2" Spacing	23°	-7db	19°	-7db

θ_{3db} = half power beamwidth

TABLE II

Radant and Ridged Horn Pattern Characteristics as a Function of Frequency

f MHz	θ_{3db} Without Radant	θ_{3db} Best Condition	Per cent of Reduction
1000	120°	40°	67
1500	73°	Pattern Deteriorates	Not Defined
3000	36°	17°	53°
8500	19°	11°	72°

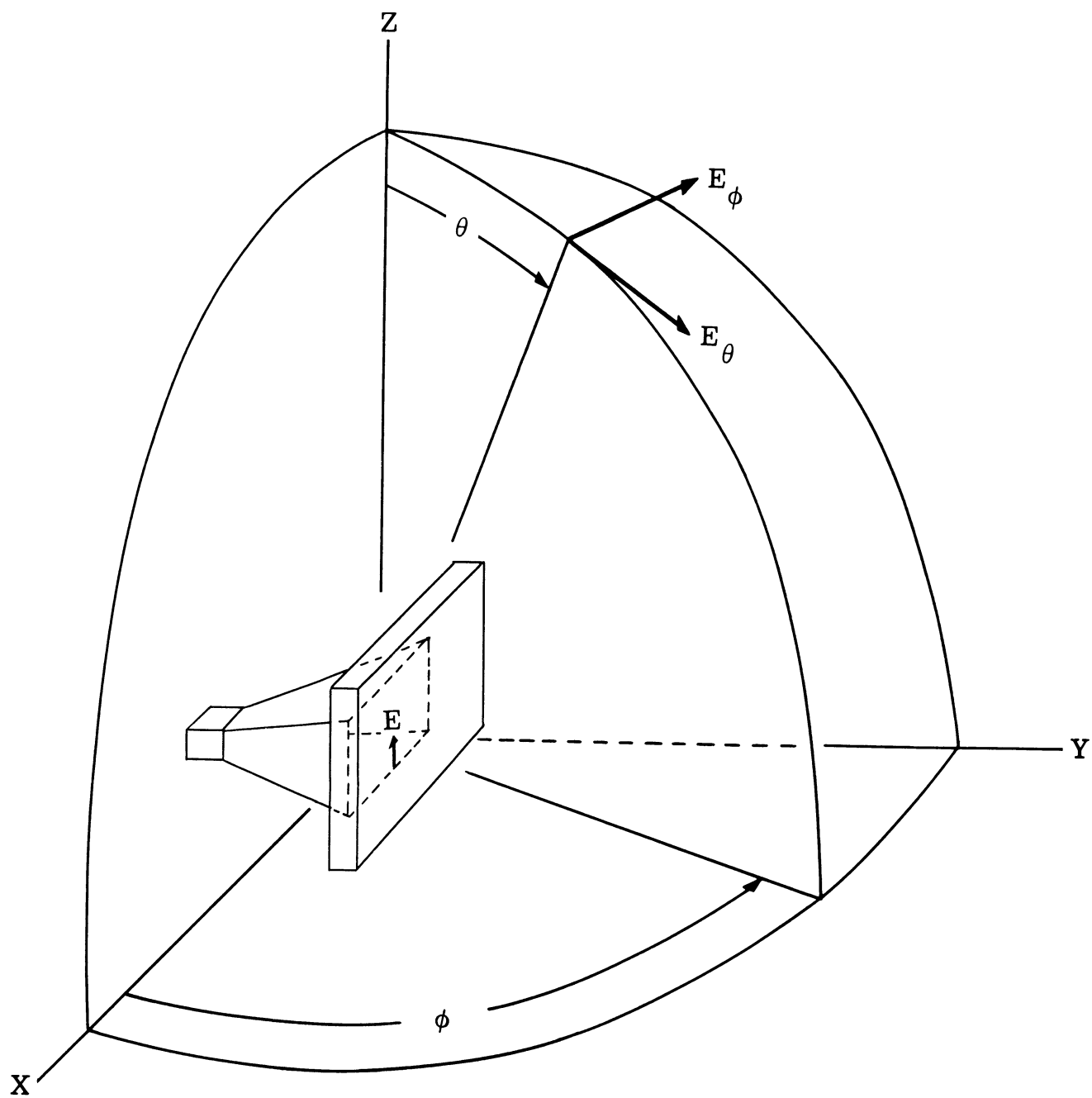No ground plane was used for 3000 MHz and 1500 MHz.

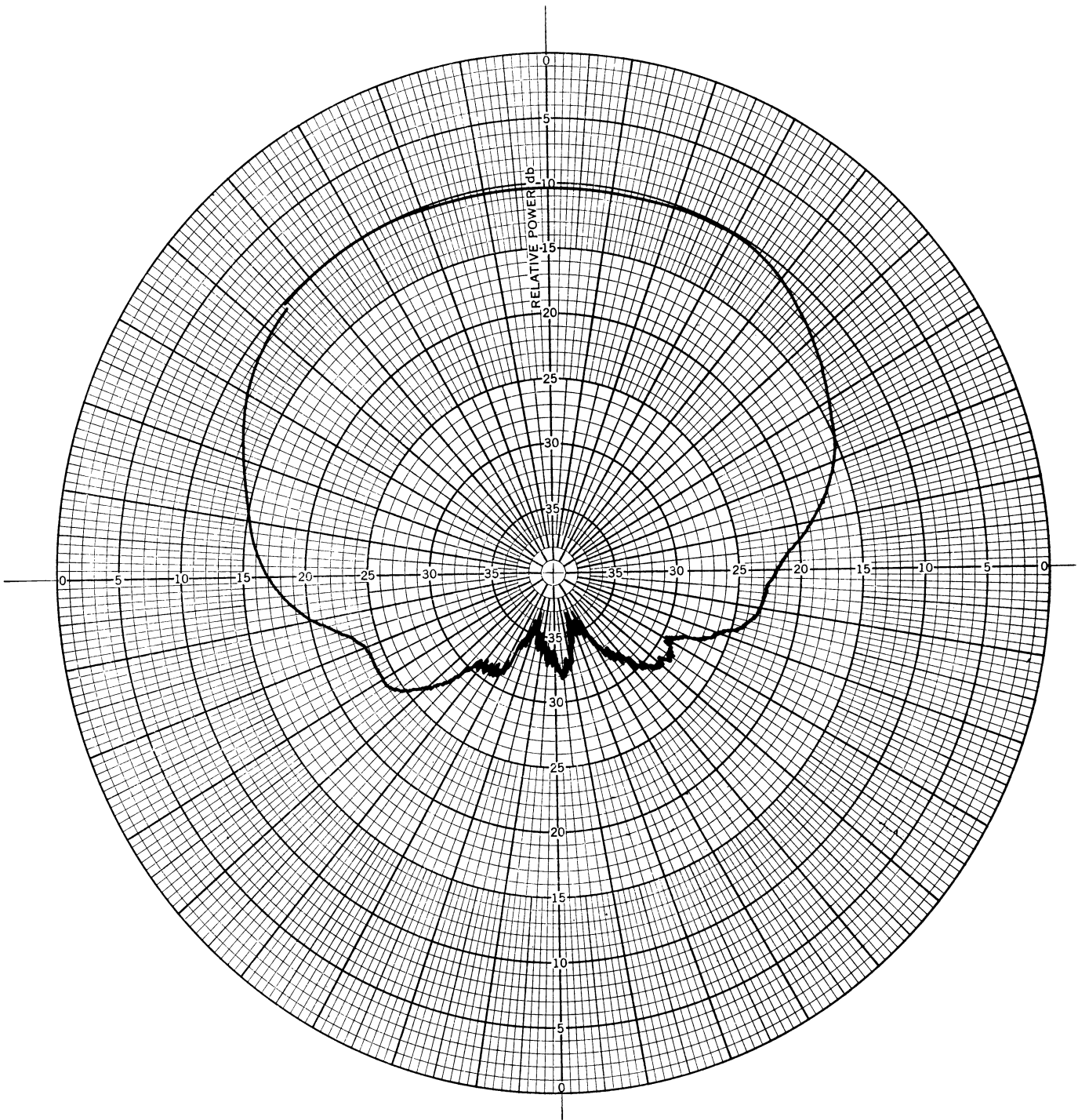FIG. 2: RIDGED HORN AND RADANT COORDINATE SYSTEM

FIG. 3a: E-PLANE PATTERN OF RIDGED HORN IN 18" x 18"
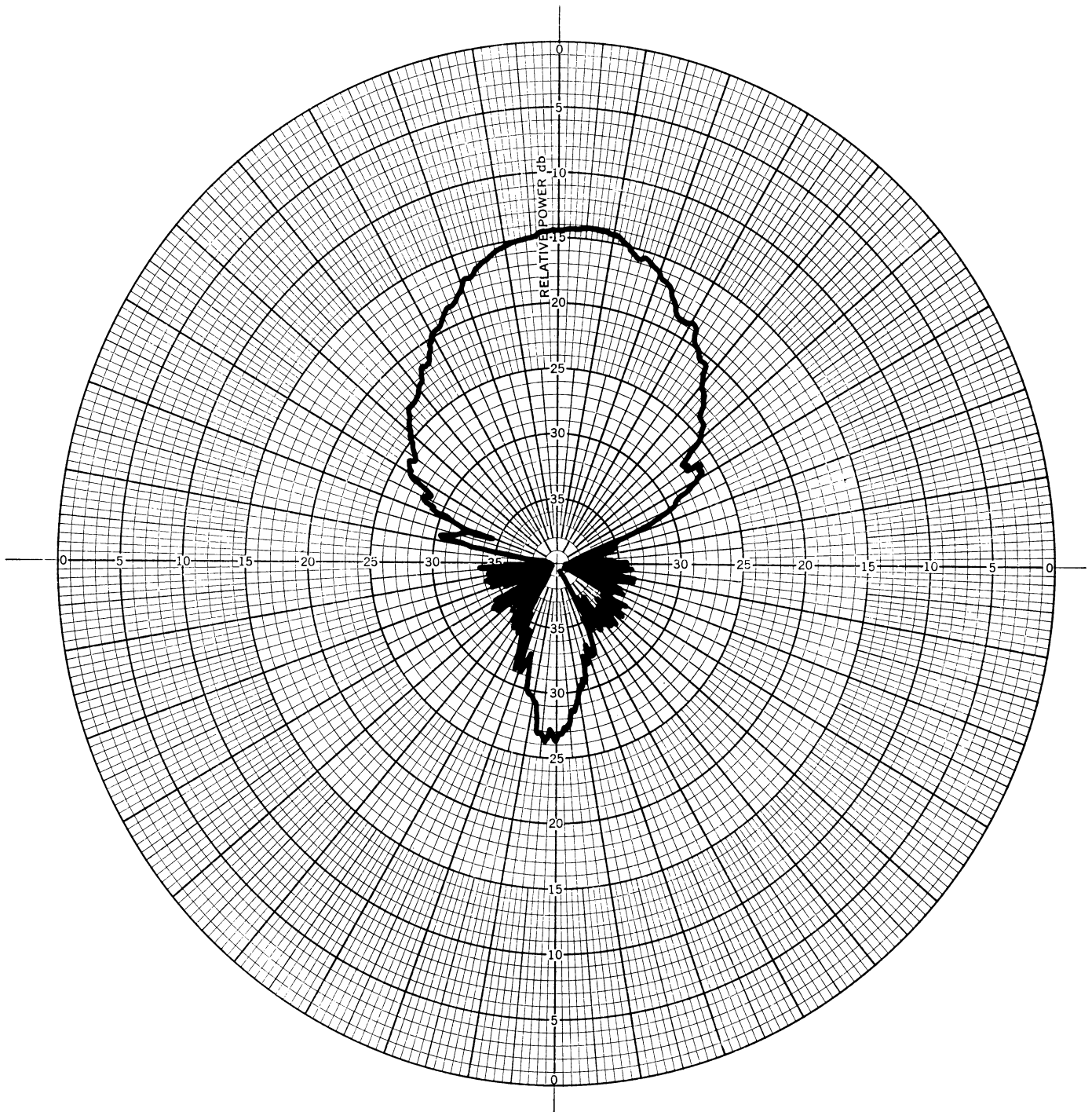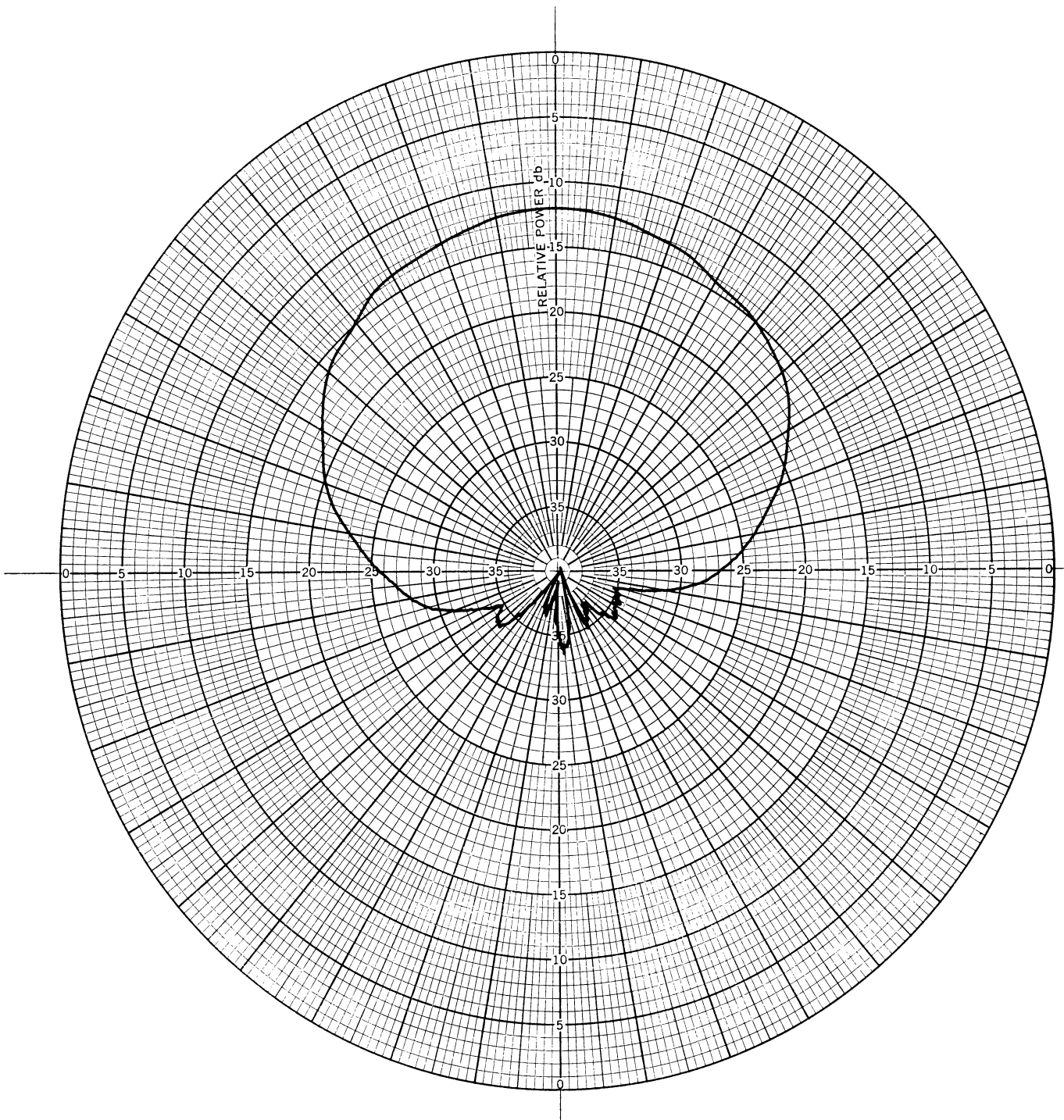GROUND PLANE AT 1.0 GHz (No Radant)

FIG. 3b: E-PLANE PATTERN OF RADANT STRUCTURE WITH RIDGED HORN IN 18" x 18" GROUND PLANE AT 1.0 GHz AND A 1/2" SPACING

FIG. 4a: E-PLANE PATTERN OF RIDGED HORN IN 18" x 18" GROUND PLANE AT 1.5 GHz (No Radant)
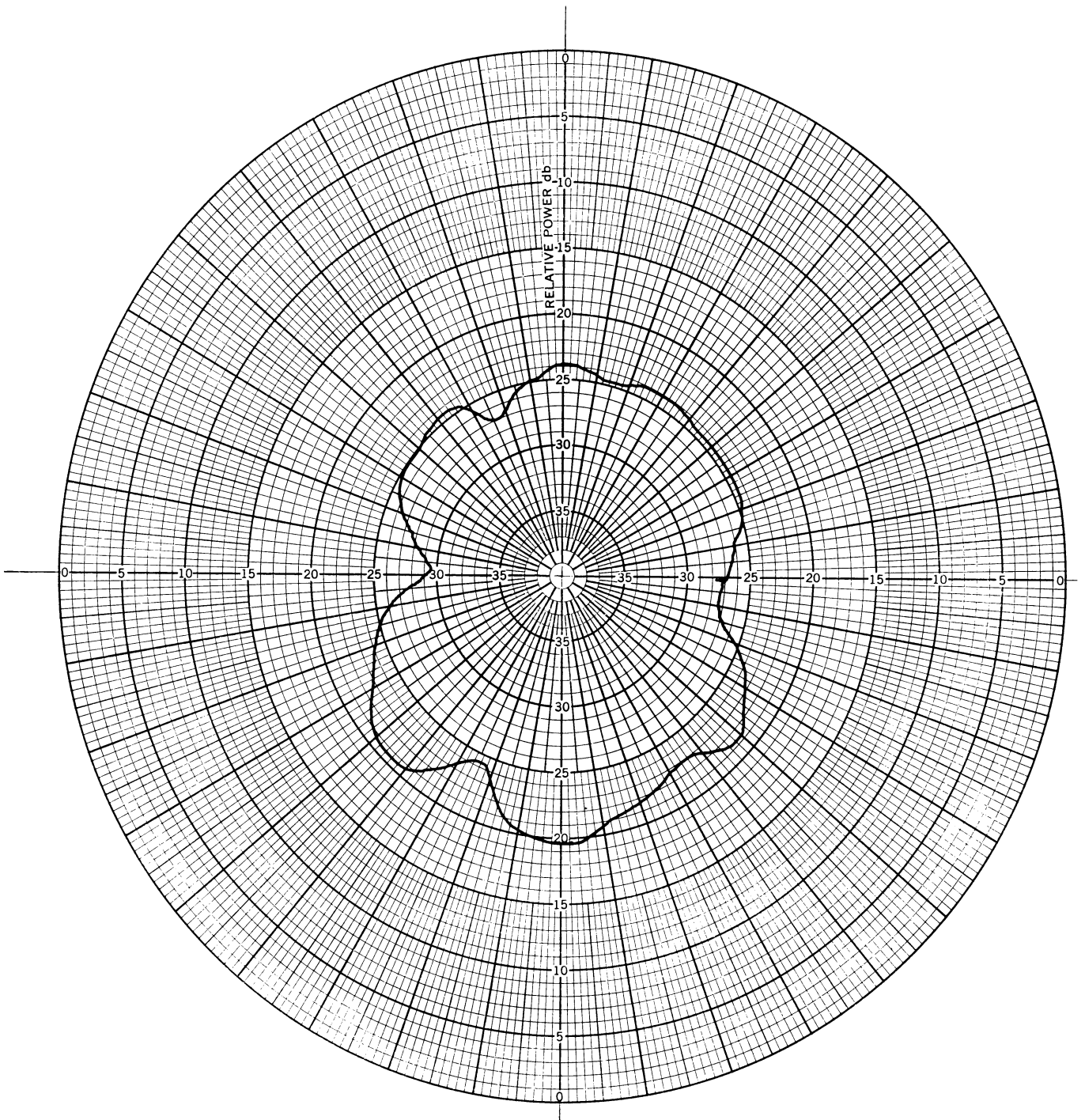
FIG. 4b: E-PLANE PATTERN OF RADANT STRUCTURE WITH
RIDGED HORN IN 18" x 18" GROUND PLANE AT 1.5
GHz AND A 1" SPACING

FIG. 5a: E-PLANE PATTERN OF RIDGED HORN IN 18" x 18"
GROUND PLANE AT 3.0 GHz (No Radant)

FIG. 5b: E-PLANE PATTERN OF RADANT STRUCTURE WITH
RIDGED HORN IN 18" x 18" GROUND PLANE AT 3.0
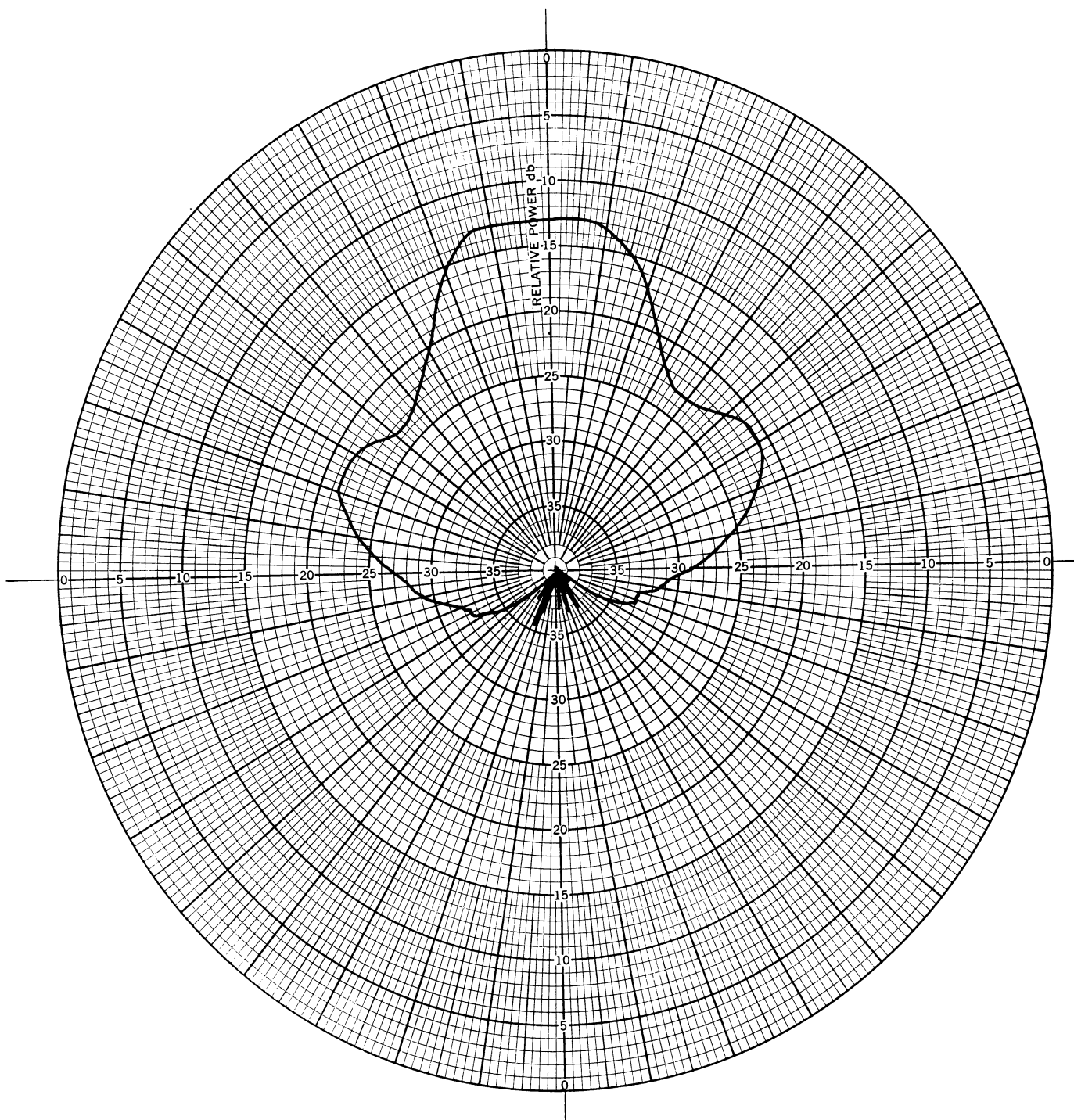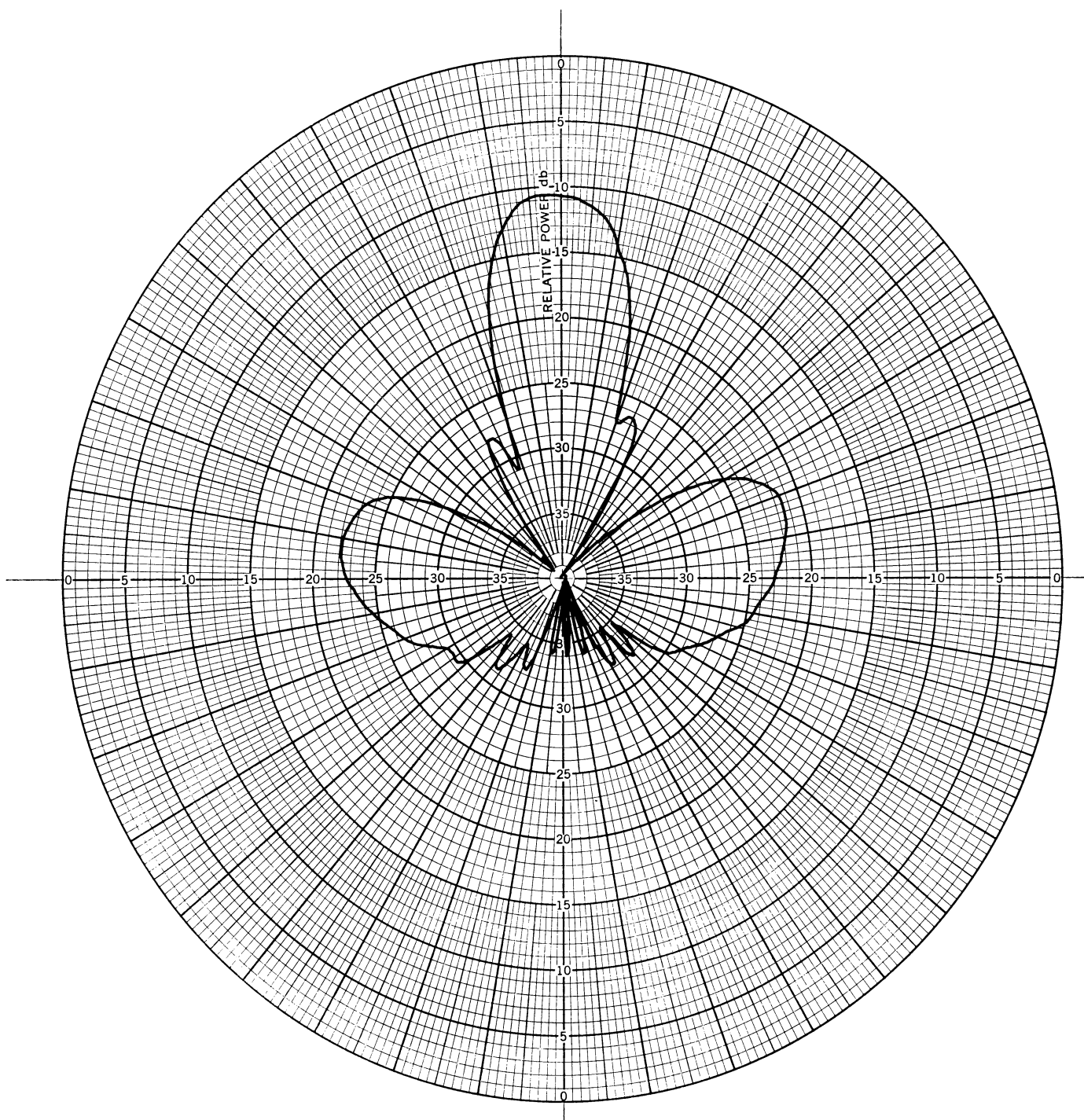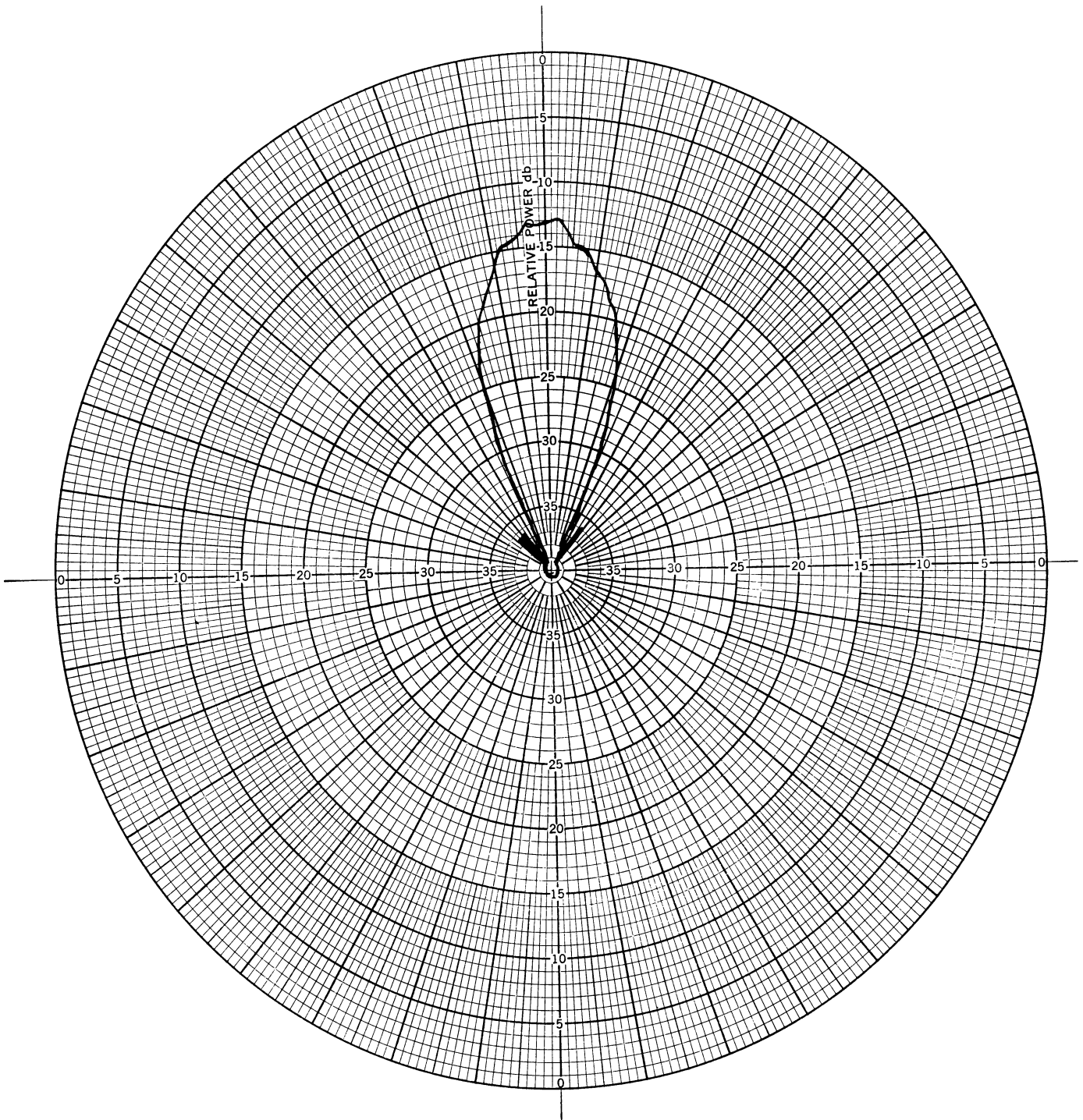GHz AND A 1/2" SPACING

FIG. 6a: E-PLANE PATTERN OF RIDGED HORN IN 18" x 18"
GROUND PLANE AT 8.5 GHz (No Radant)
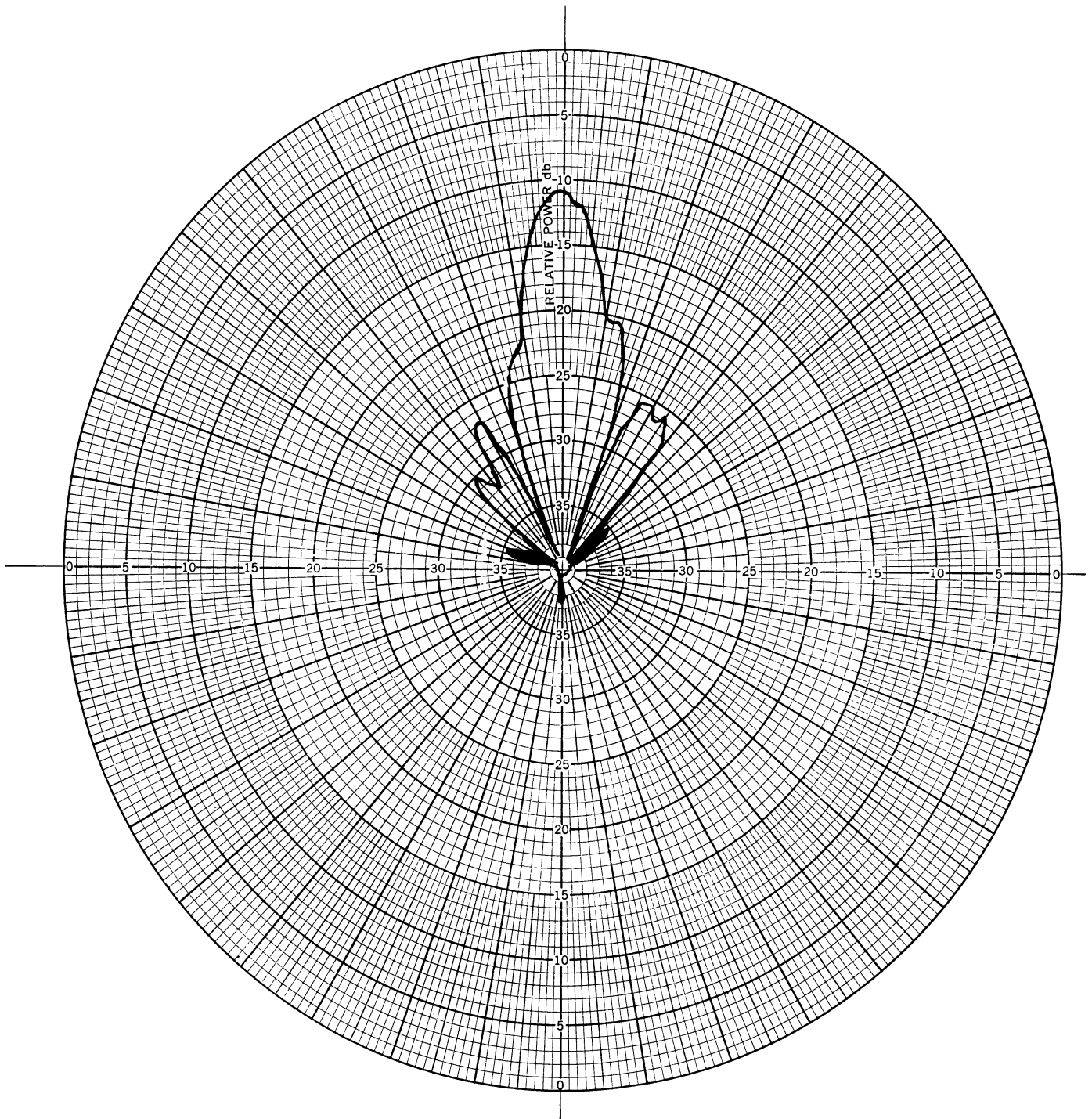
FIG. 6b: E-PLANE PATTERN OF RADANT STRUCTURE WITH
RIDGED HORN IN 18" x 18" GROUND PLANE AT 8.5
GHz AND A 1/4" SPACING

FIG. 7a: E-PLANE PATTERN OF RIDGED HORN AT 1.5 GHz
(No Ground Plane or Radant)
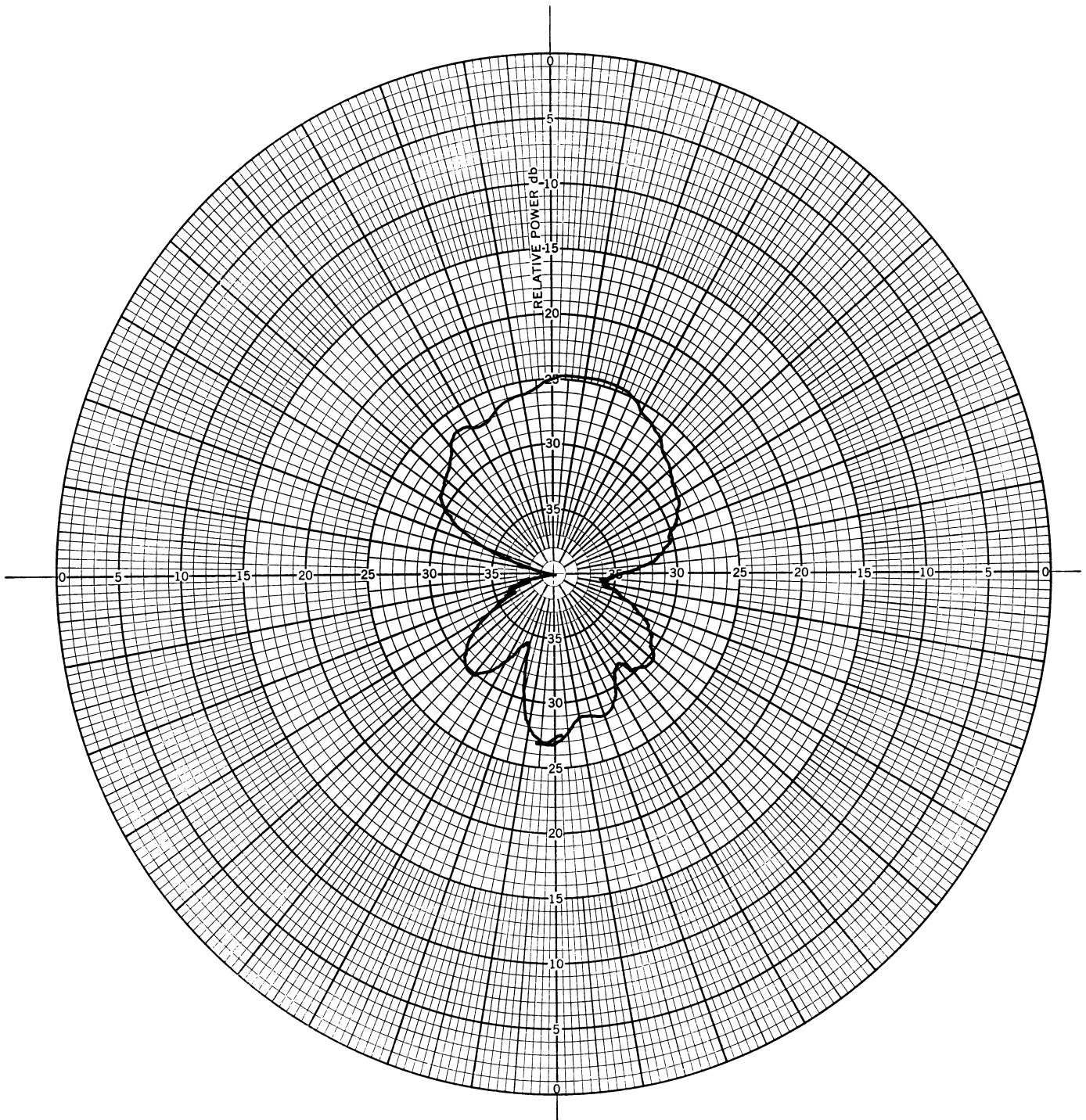
FIG. 7b: E-PLANE PATTERN OF RADANT STRUCTURE WITH RIDGED HORN (No Ground Plane) AT 1.5 GHz (With Radant Touching Horn)
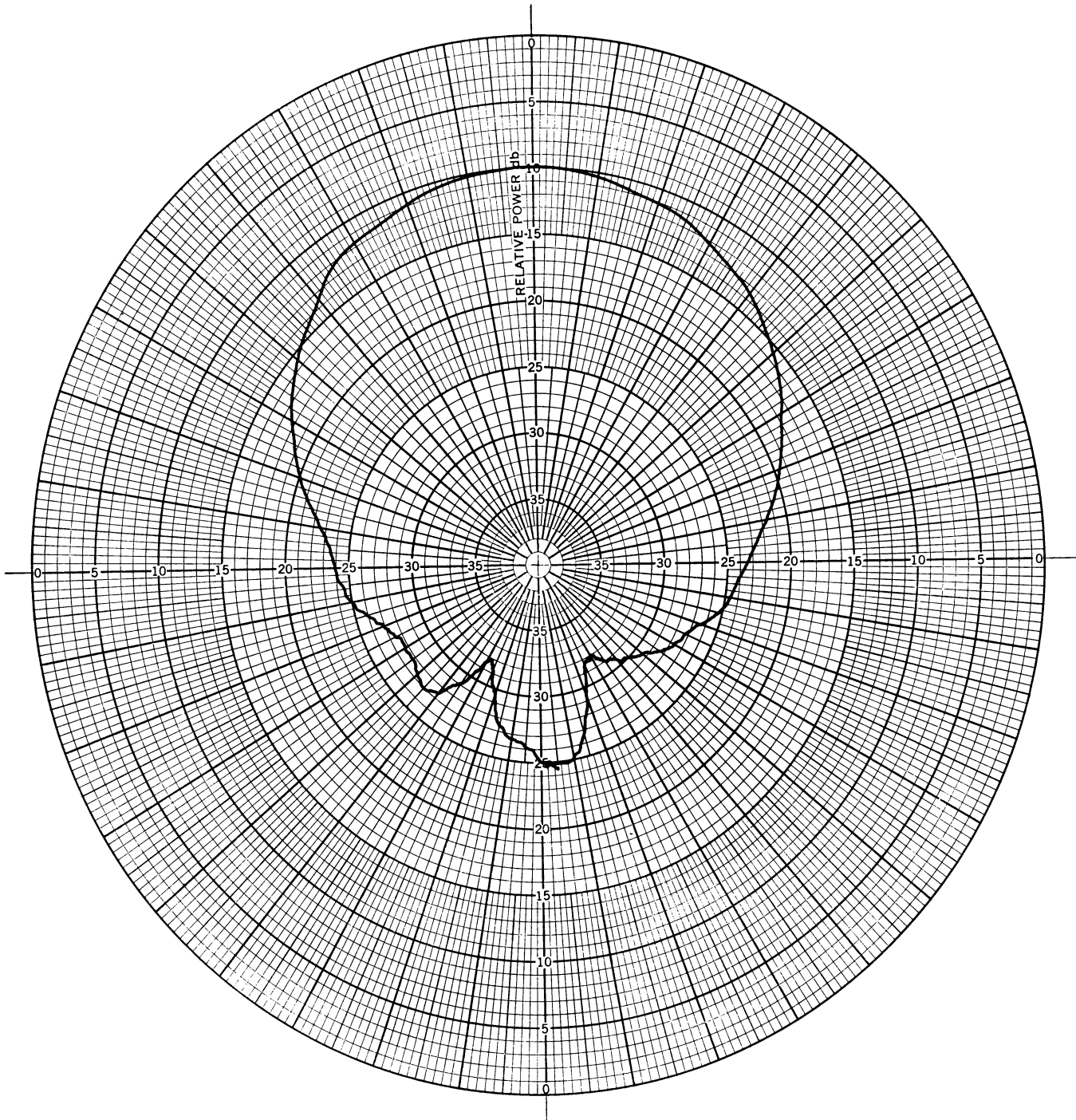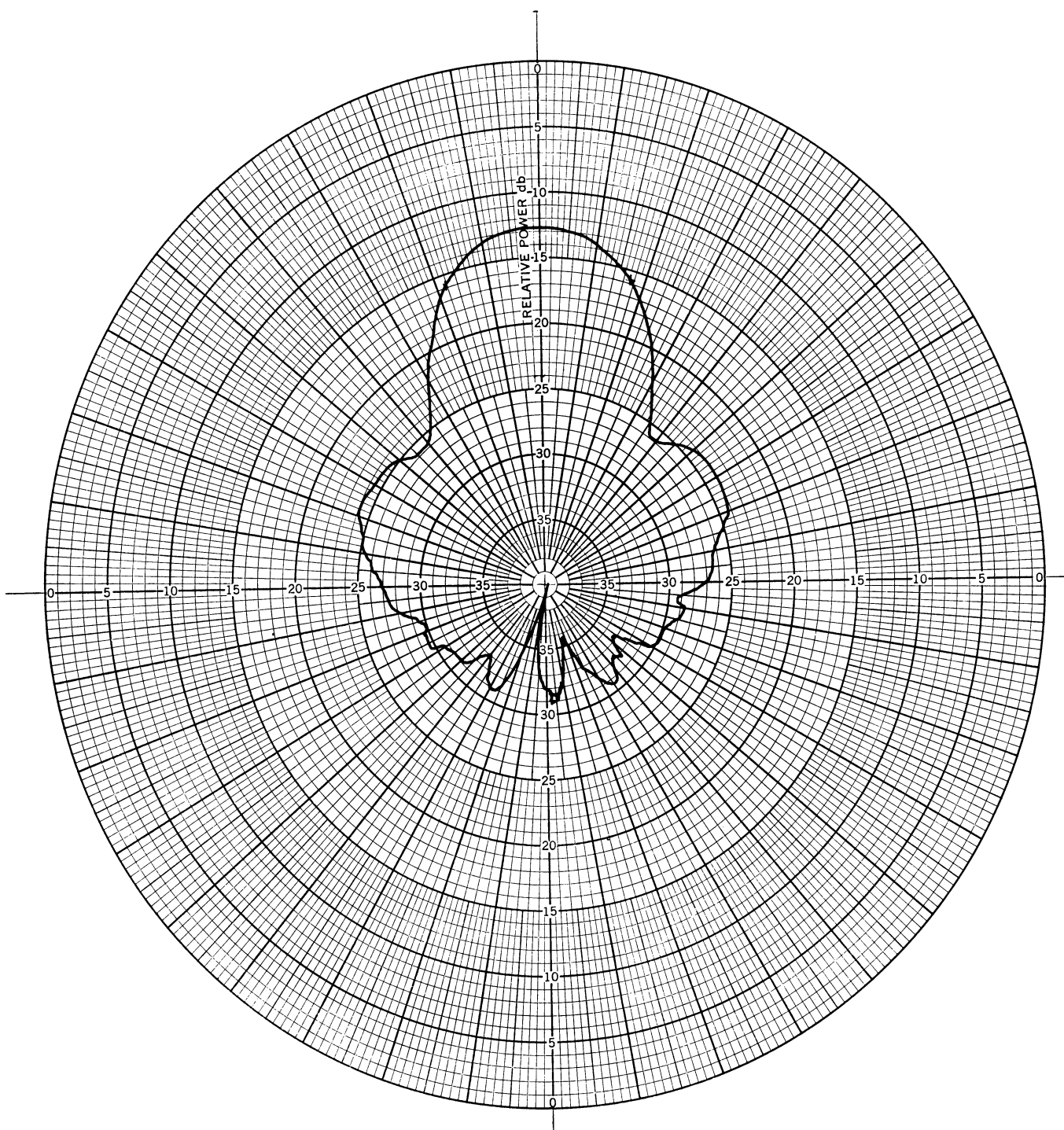
FIG. 8a: E-PLANE PATTERN OF RIDGED HORN AT 3.0 GHz
(No Ground Plane or Radant)
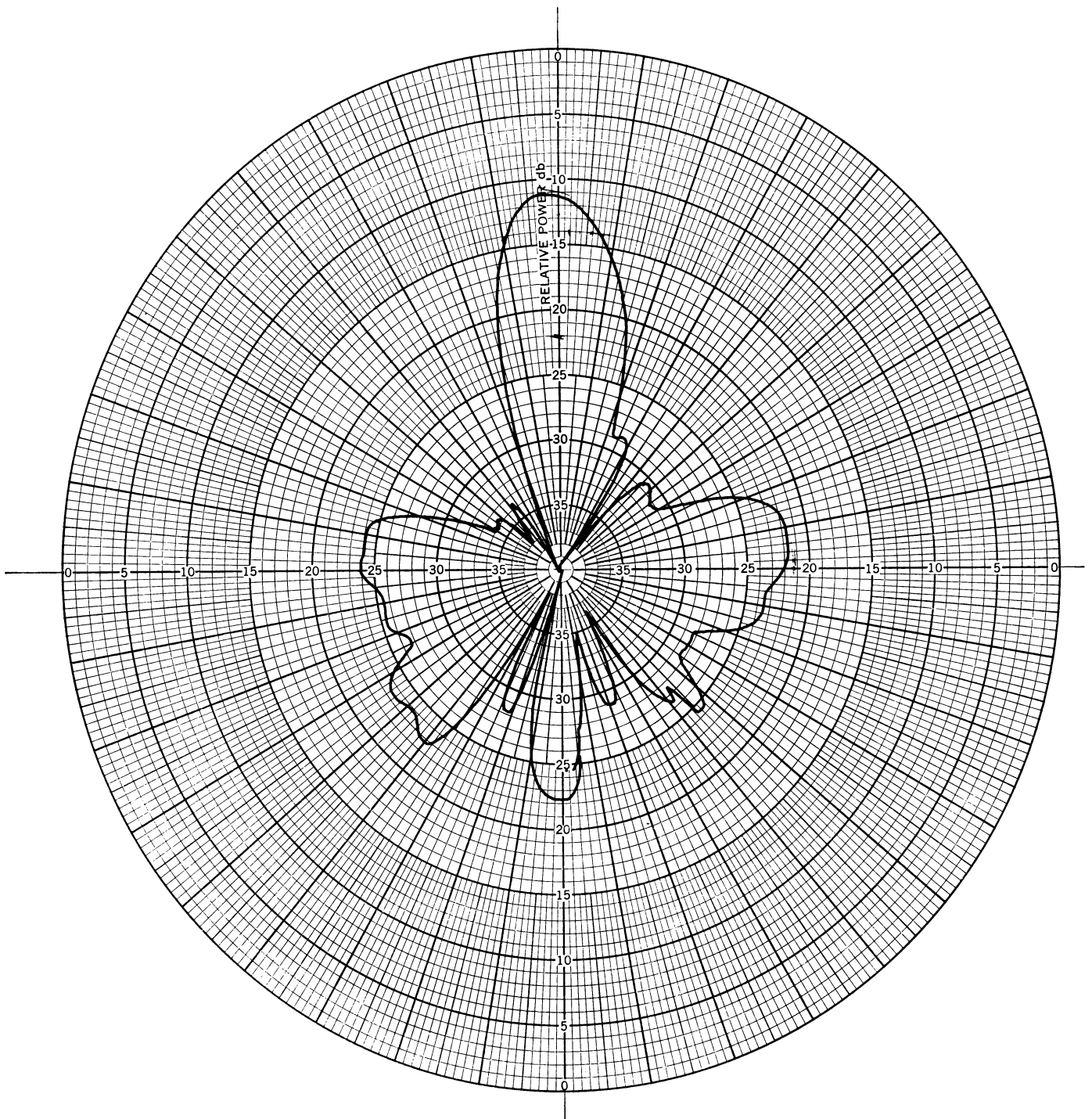
FIG. 8b: E-PLANE PATTERN OF RADANT STRUCTURE WITH
RIDGED HORN (No Ground Plane) AT 3.0 GHz AND A
1/2" SPACING

ground plane) appear to be optimum for a spacing of one-half inch. These patterns further show a 50 per cent reduction in the half power beamwidth when using the radant structure. A similar reduction in half power beamwidth was noted in the second Interim for the radant fed by the ridged horn at 8.5 GHz. There it will be recalled the half power beamwidth was 19° without the radant and 11° with the radant.

III

RADANT STRUCTURE EXCITED BY HALF WAVE DIPOLE

Because of the well defined radiation pattern of the dipole and the ease with which it can be represented mathematically, a series of experiments were performed with the radant fed by a half wave dipoles. Other significant features of the half wave dipole are its simplicity of construction and its low cost in comparison with the ferrite filled slot. This study was conducted using four dipoles resonant at the following frequencies: 0.36, 0.75, 1.5 and 3.0 GHz. Both E and H-plane patterns were recorded following the coordinate system of Fig. 9. The dipoles were oriented to provide normal incidence with the E-field parallel to the plane of the loop element as shown in Fig. 10. The spacing between the dipoles and radant structure was a variable which was adjusted in finite increments.

3.1 Radant Excited by Half-Wave Dipoles at 0.36 GHz

At 0.36 GHz the radant structure is approximately 0.56λ square and the loop perimeter is approximately 0.145λ and is thus an electrically small loop. Electrically small loops are defined as having a uniform surface current distribution around their perimeter, a desirable feature for theoretical analysis. The E and H-plane radiation patterns for the half-wave dipole (less the radant) are shown in Fig. 11 and 12. Figure 13 and 14 shows the E and H-plane patterns for the dipole with the radant structure; the radant-dipole spacing is three inches. It is interesting to note that the pattern of Fig. 13 (E-plane pattern) has a half power beamwidth which has been reduced approximately 8° as compared to the pattern of Fig. 11. Further the pattern of Fig. 14 is no longer omnidirectional but has a 3db improvement in the forward directivity as compared to Fig. 12. Additional data that has been obtained suggests that the directivity of the radant increases as the spacing between the radant structure and dipole increases.

FIG. 9: DIPOLE COORDINATE SYSTEM

FIG. 10: RADANT WITH DIPOLE FEED

FIG. 11: E-PLANE PATTERN OF 0.36 GHz DIPOLE
(No Radant)

FIG. 12: H-PLANE PATTERN OF 0.36 GHz DIPOLE
(No Radant)
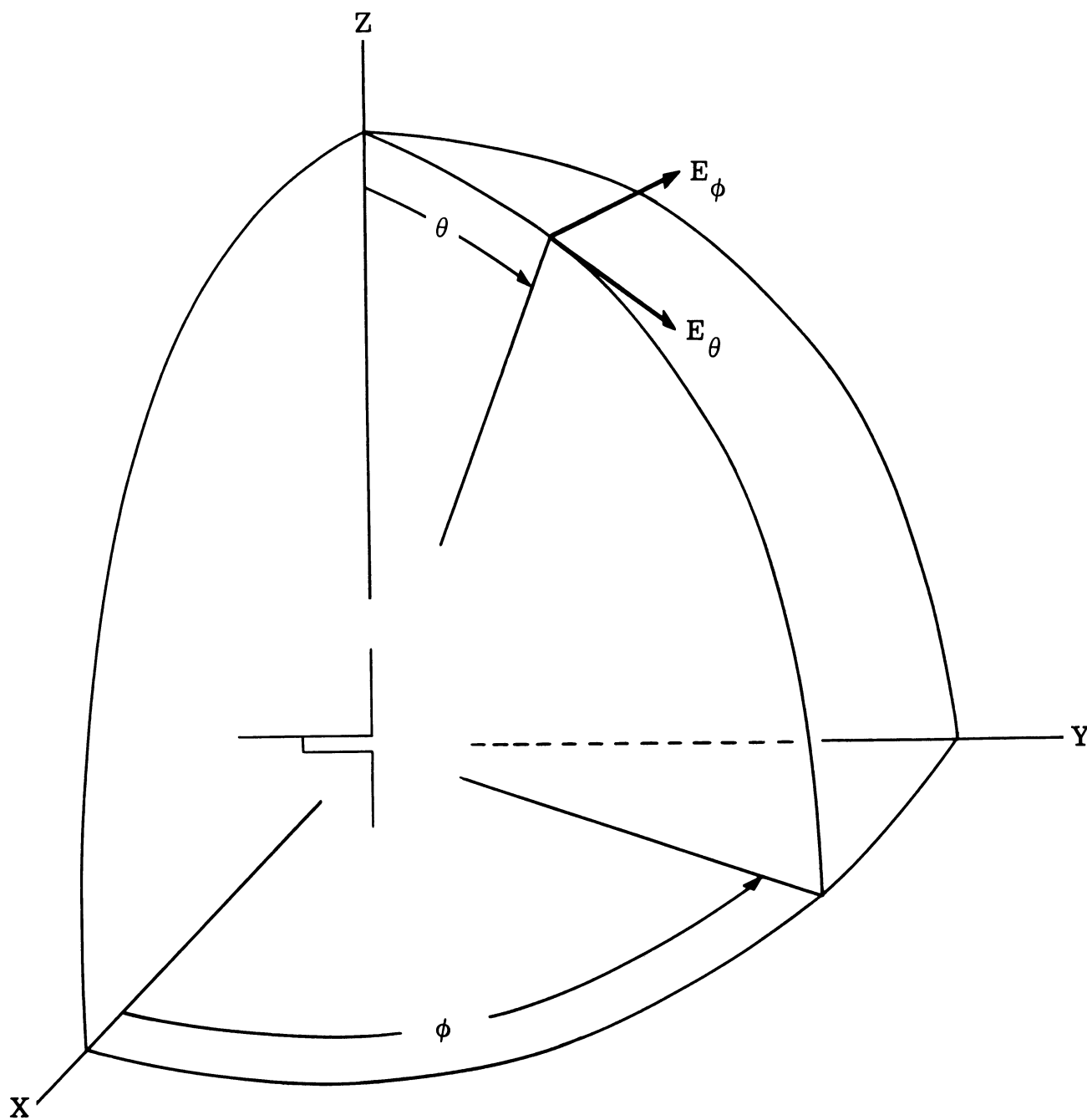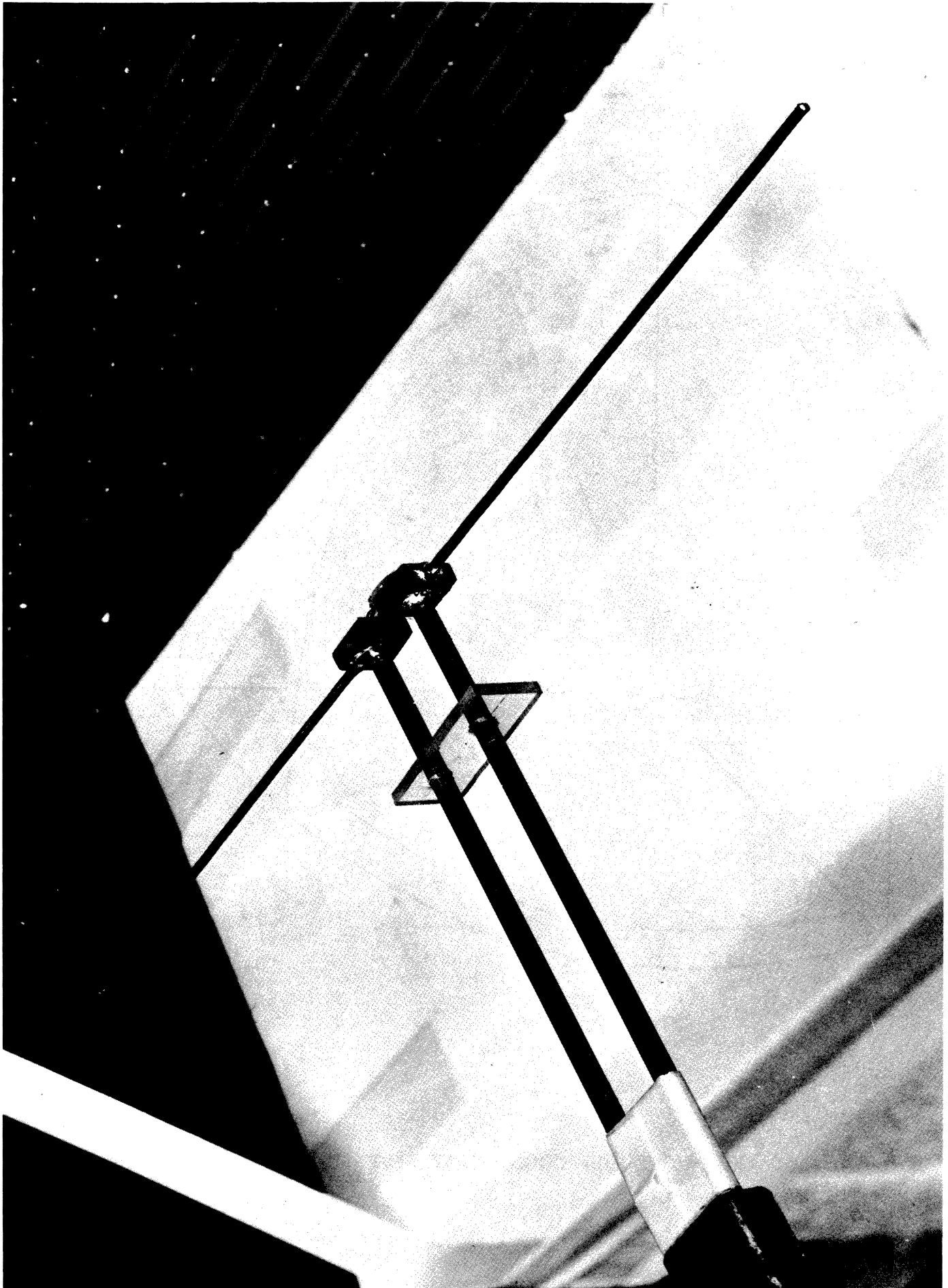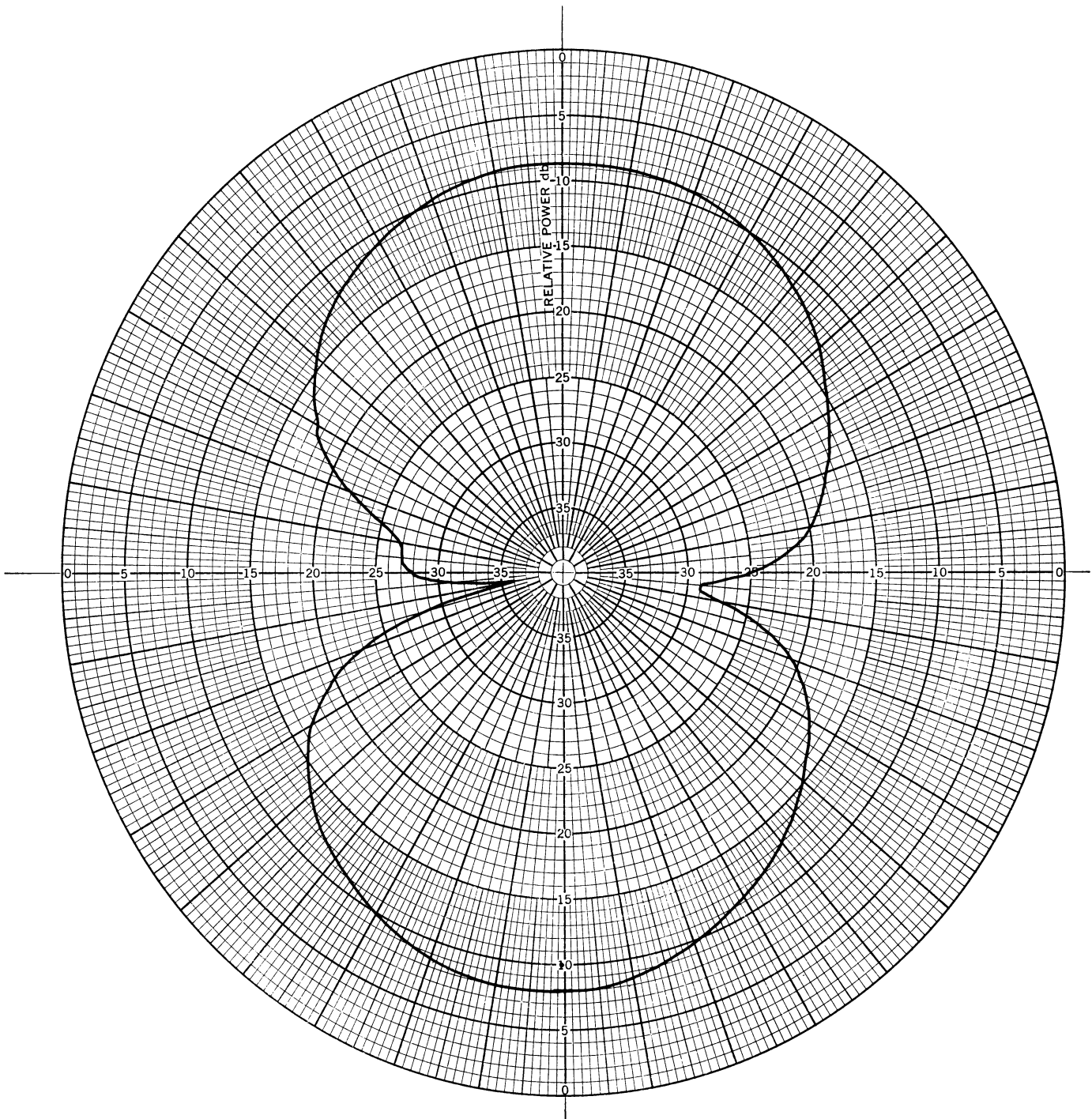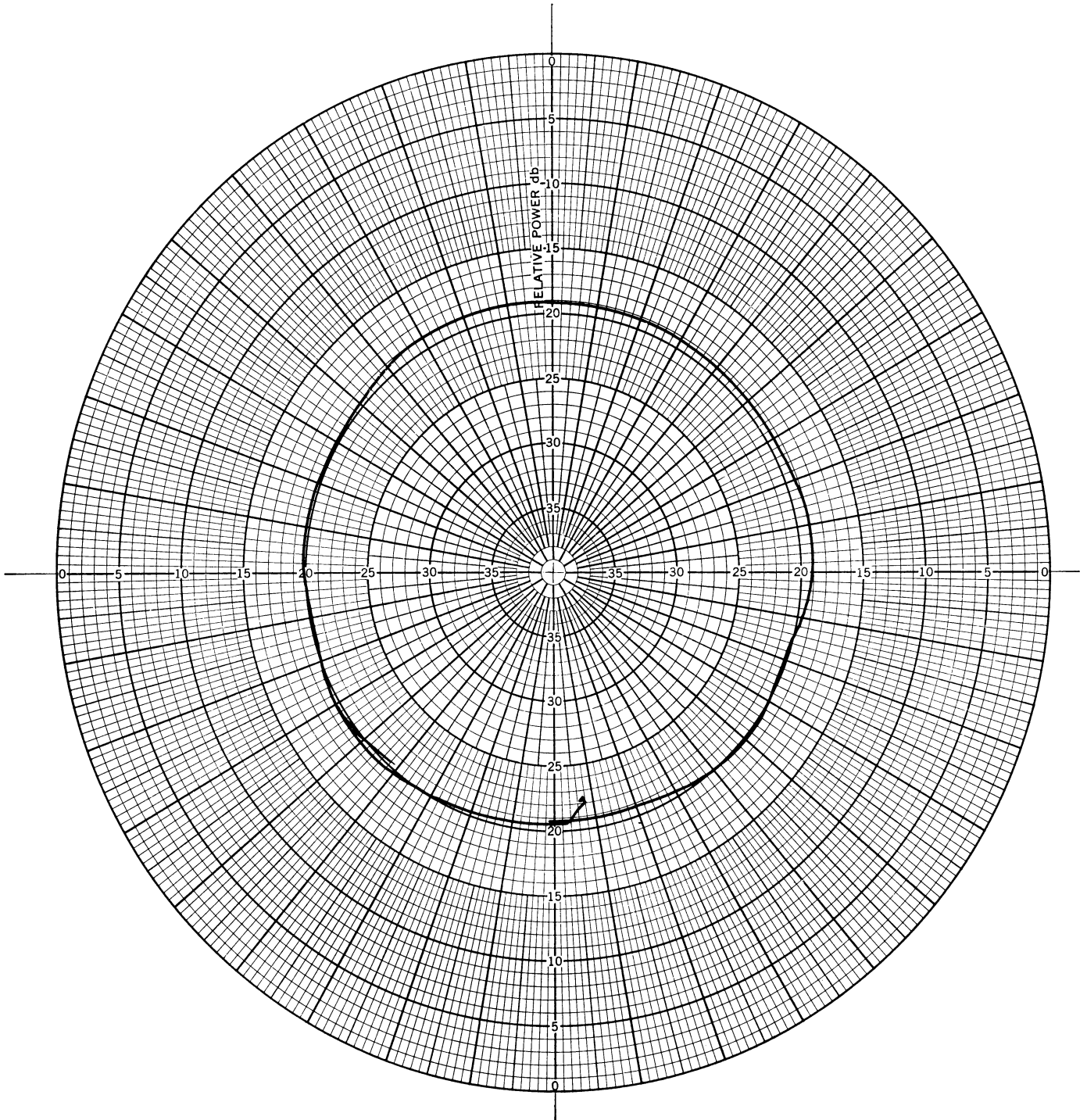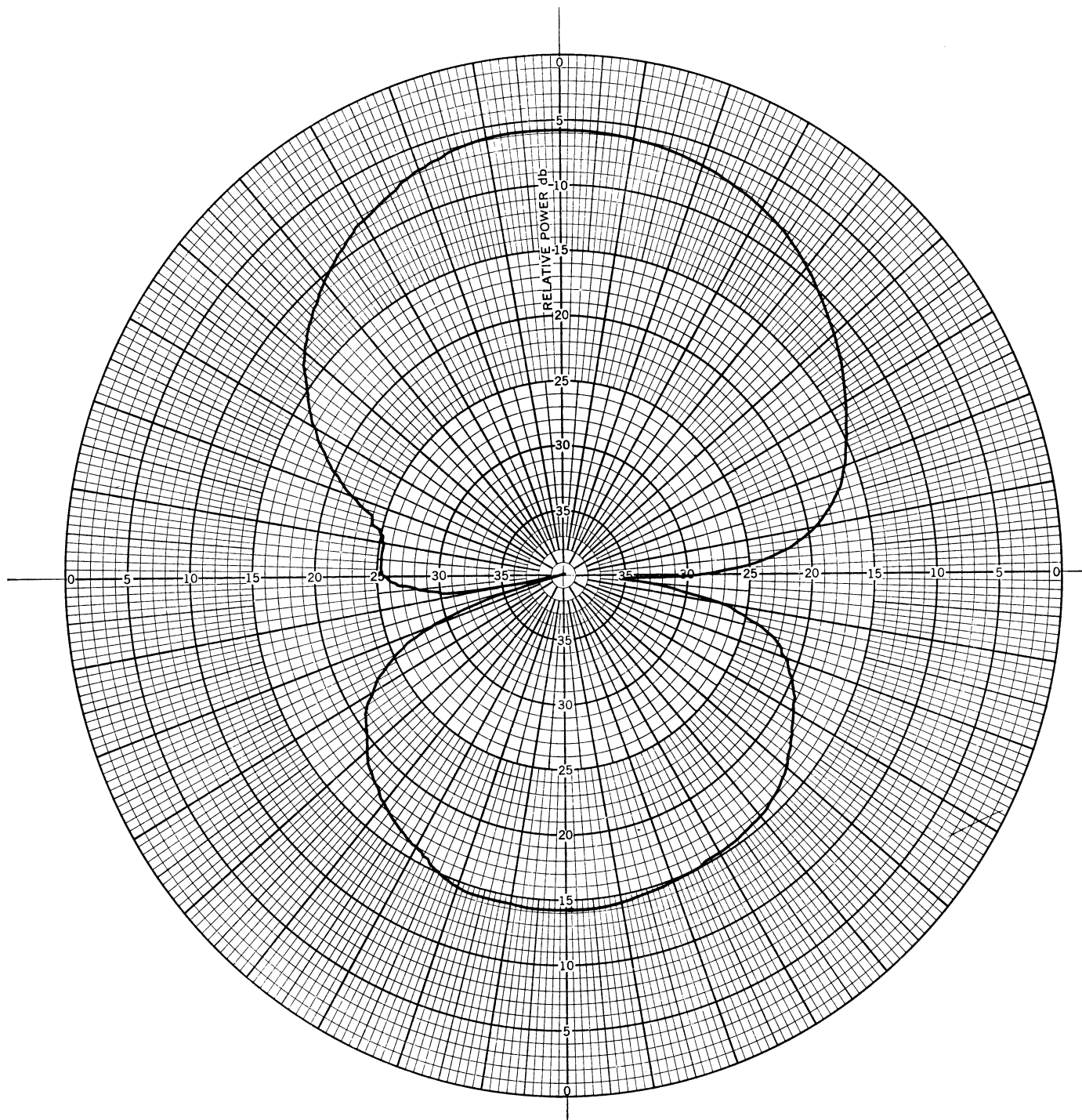
FIG. 13: E-PLANE PATTERN OF RADANT STRUCTURE
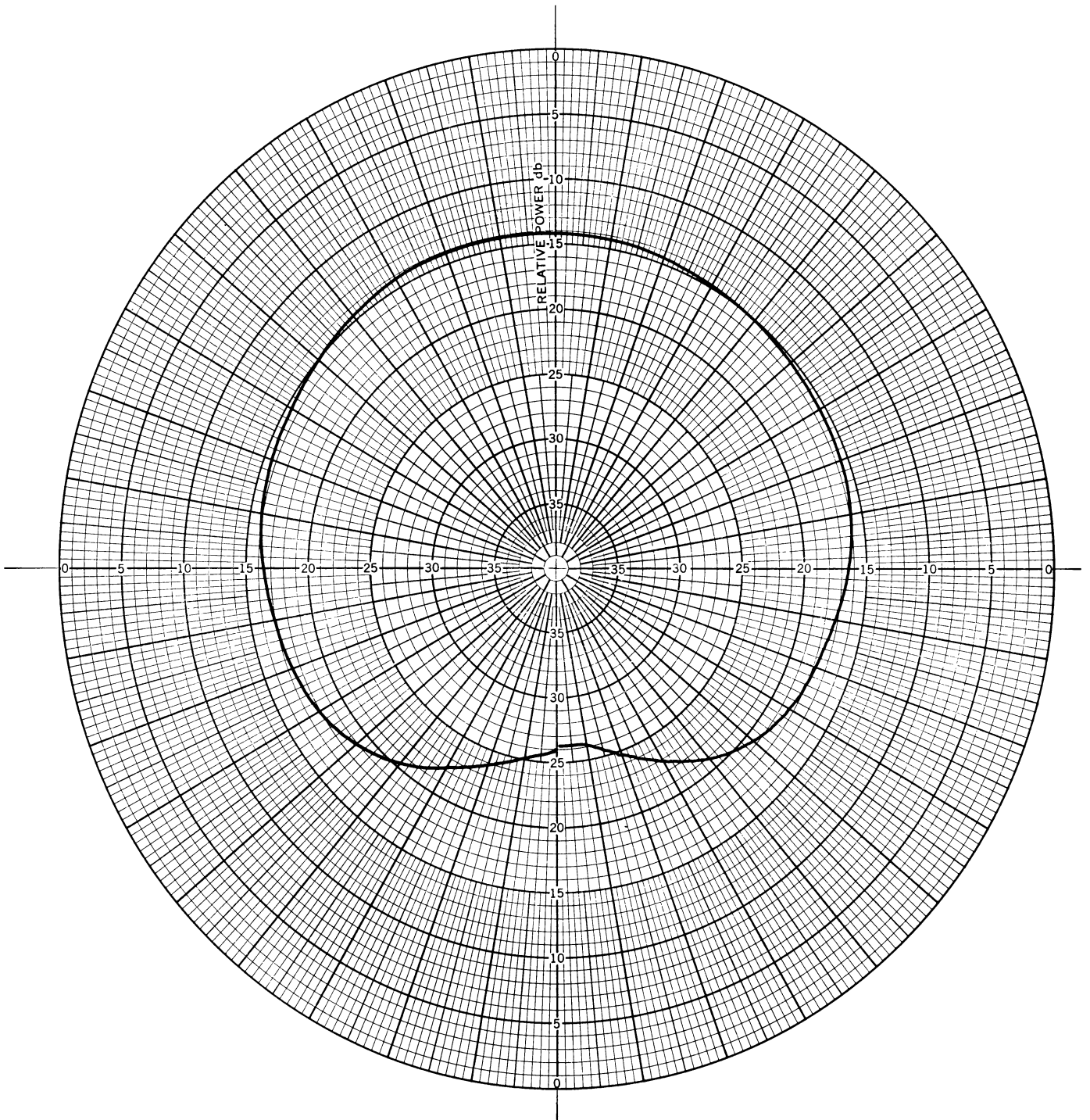WITH 0.36 GHz DIPOLE AND 3" SPACING

FIG. 14: H-PLANE PATTERN OF RADANT STRUCTURE WITH
0.36 GHz DIPOLE AND 3" SPACING

3.2 Radant Excited by a Half-Wave Dipole at 0.75 GHz

At 0.75 GHz the radant structure is approximately 1.14λ square and the loop perimeter is approximately 0.30λ, no longer to be considered electrically small. The E and H-plane patterns for the dipole less the radant are shown in Fig. 15 and 16 respectively and with the radant in Fig. 17 and 18 respectively. Employing a half inch spacing between the radant structure and dipole the E-plane half power beamwidth was reduced approximately 60° as compared to the dipole with the radant. However, the H-plane pattern (for the half inch spacing) exhibits maximum radiation in the direction tangential to the structure. Additional data was collected for larger spacings (see Fig. 19 and 20 for 3 inch spacing) and it was found that the E-plane half power beamwidth increased as a function of spacing. For these larger spacings the H-plane pattern had a maximum in a direction normal to the radant structure in both the front and back half planes. A discouraging feature was that the lobe in the back half plane was 7 db larger than the lobe in the front half plane.

3.3 Radant Excited by a Half-Wave Dipole at 1.5 GHz

At 1.5 GHz the radant structure is approximately 2.28λ square and the loop perimeter is approximately 0.60λ. The E and H-plane patterns for the dipole less the radant structure are shown in Fig. 21 and 22 respectively. Patterns with the radant structure are shown in Fig. 23 - 26 for both E and H-plane cuts and two spacings (3/16 and 2 inches). In general it may be concluded that for small spacings, and in the E-plane, maximum radiation occurs in the forward half plane and as the spacing increases radiation maximizes in the back half plane. In the H-plane it was noted that radiation was tangential to the structure for small spacings and became normal to the surface for large spacings with maximum radiation in the back half plane.

3.4 Radant Excited by a Half-Wave Dipole at 3.0

At 3.0 GHz the radant structure is approximately 4.56λ square and the loop

FIG. 15: E-PLANE PATTERN OF 0.75 GHz DIPOLE
(No Radant)

FIG. 16: H-PLANE PATTERN OF 0.75 GHz DIPOLE
(No Radant)
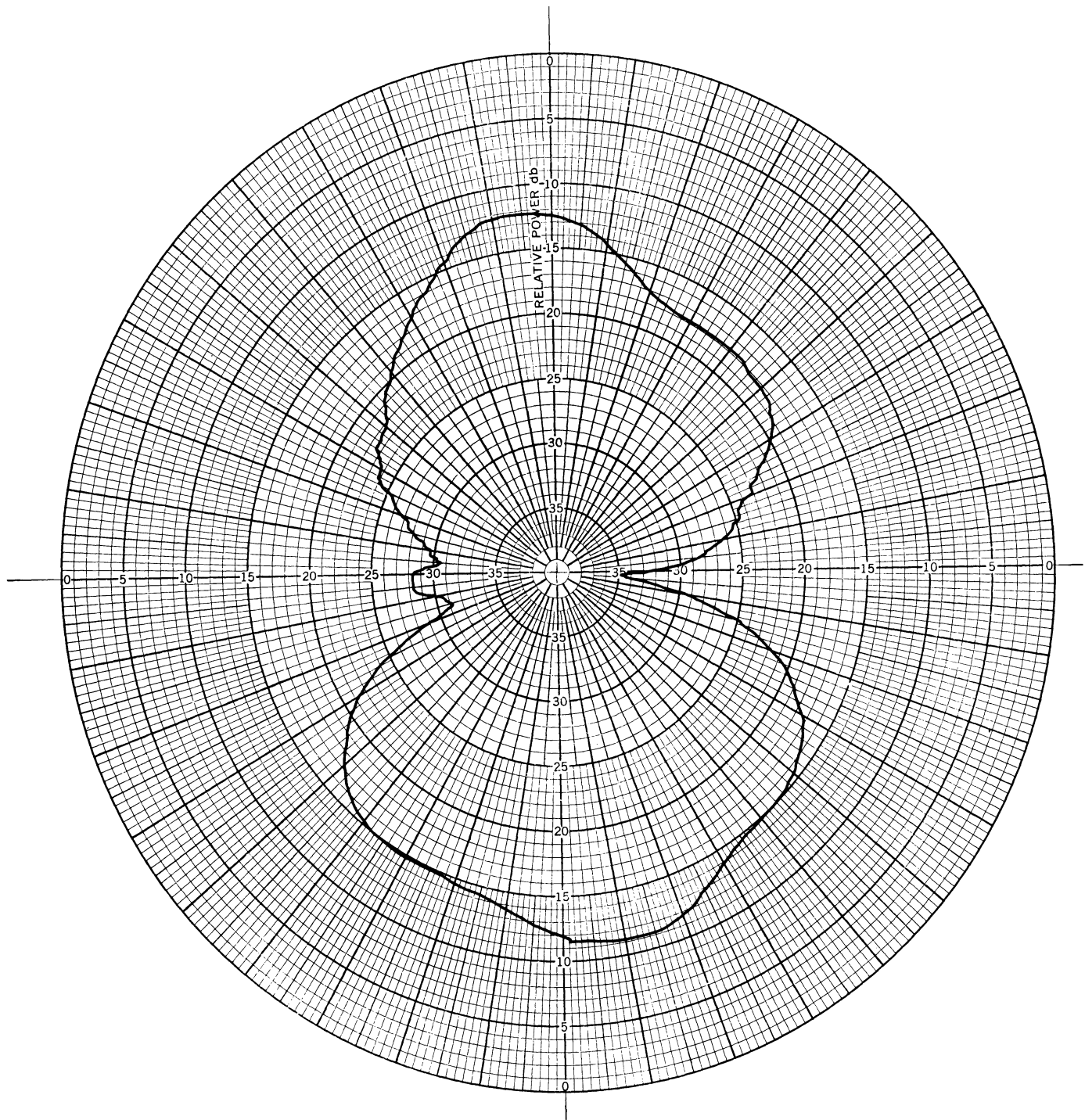
FIG. 17:   E-PLANE PATTERN OF RADANT WITH 0.75 GHz
DIPOLE AND 1/2" SPACING

FIG. 18: H-PLANE PATTERN OF RADANT WITH 0.75 GHz
DIPOLE AND 1/2" SPACING
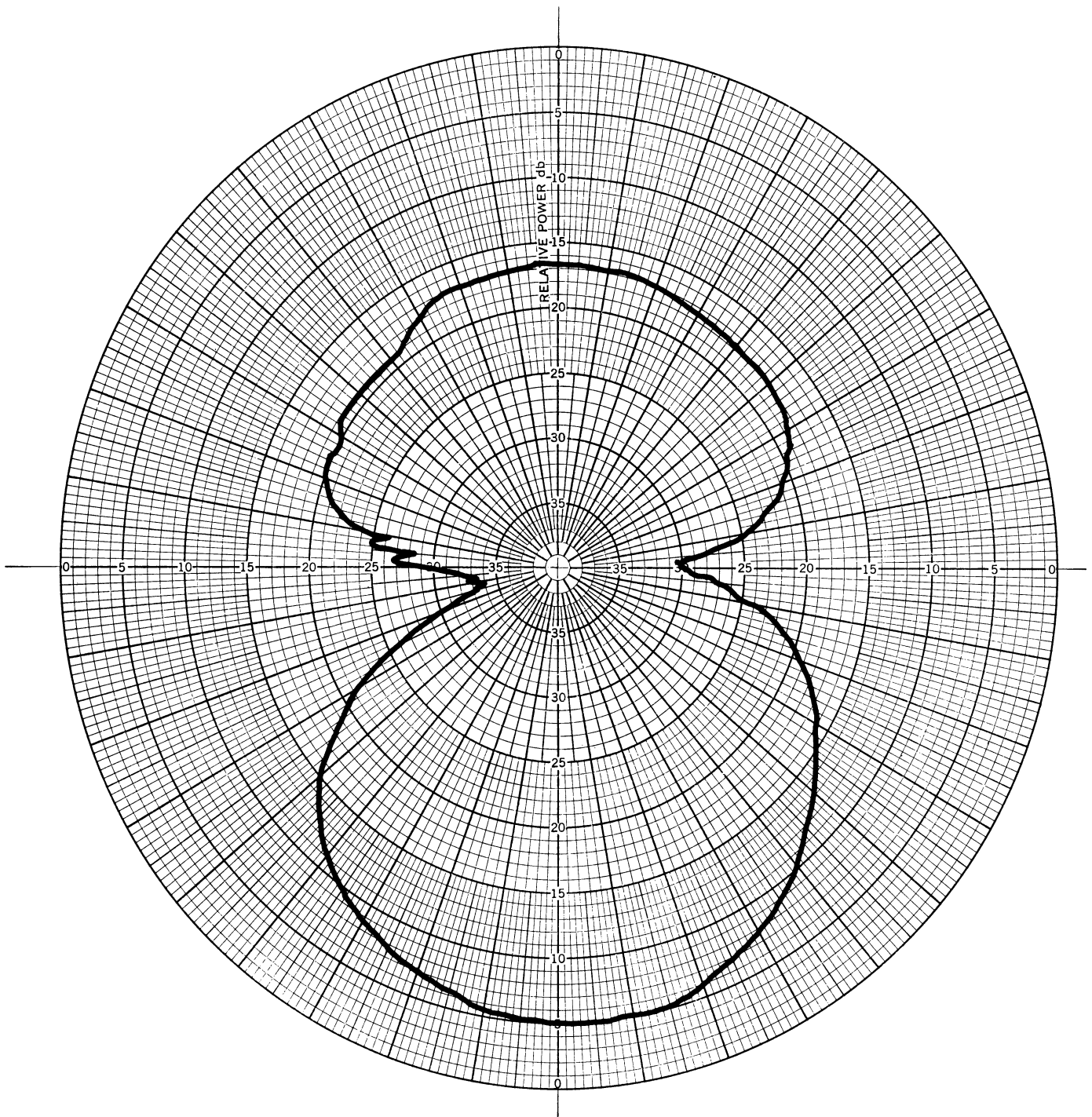
FIG. 19: E-PLANE PATTERN OF RADANT WITH 0.75 GHz
DIPOLE AND 3" SPACING
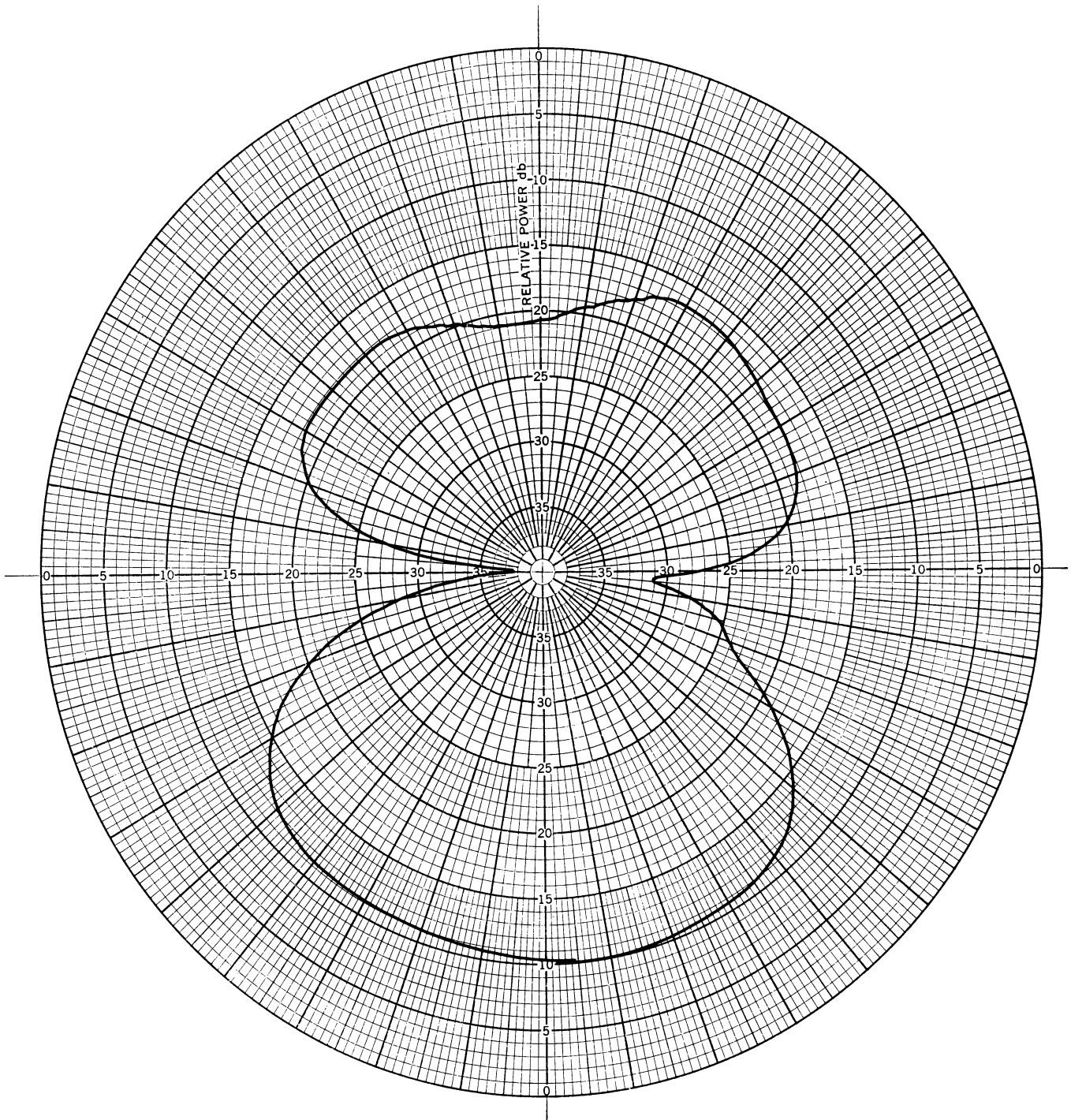
FIG. 20: H-PLANE PATTERN OF RADANT WITH A 0.75 GHz
DIPOLE AND 3" SPACING
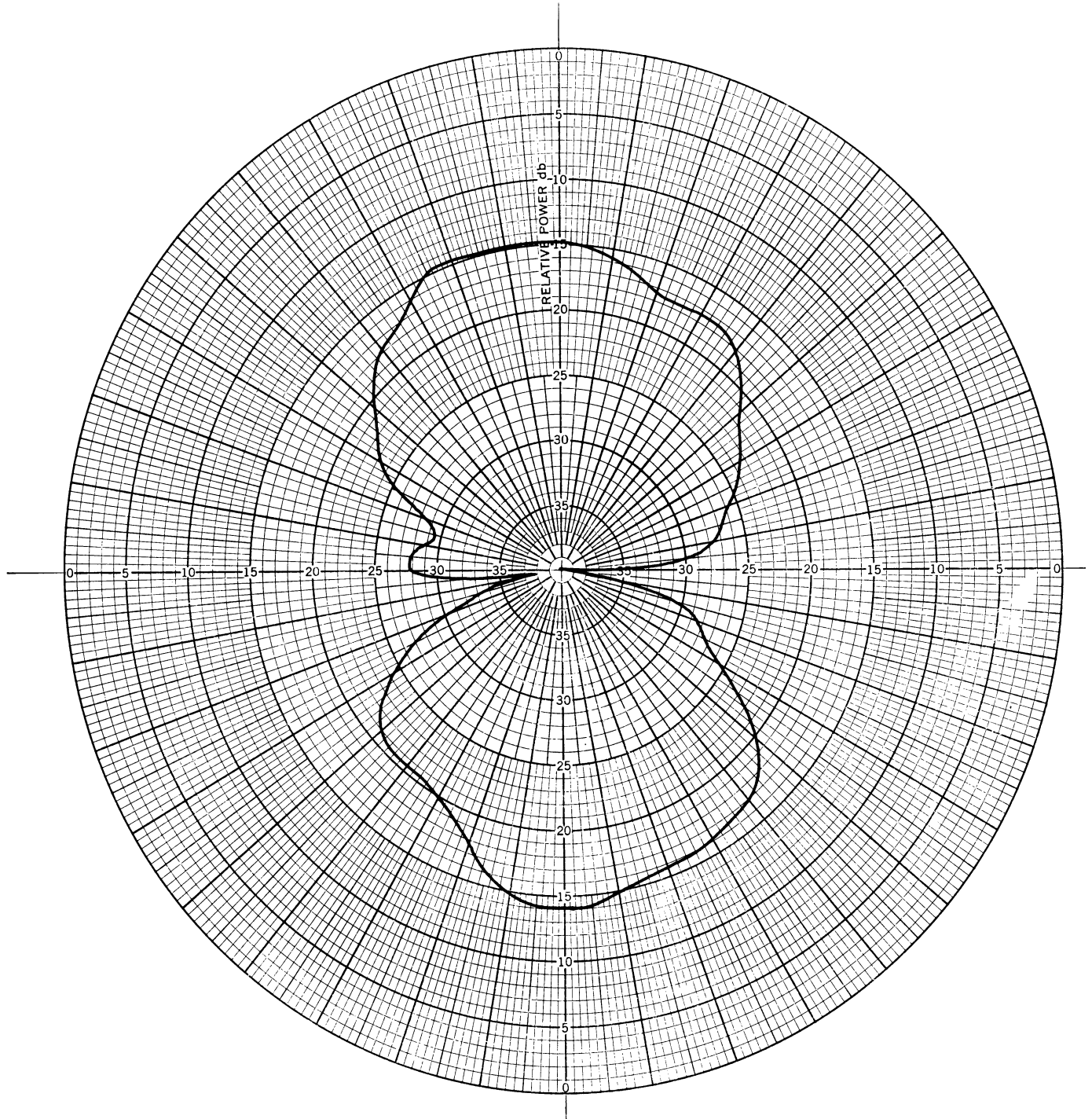
FIG. 21: E-PLANE PATTERN OF 1.5 GHz DIPOLE (No Radant)
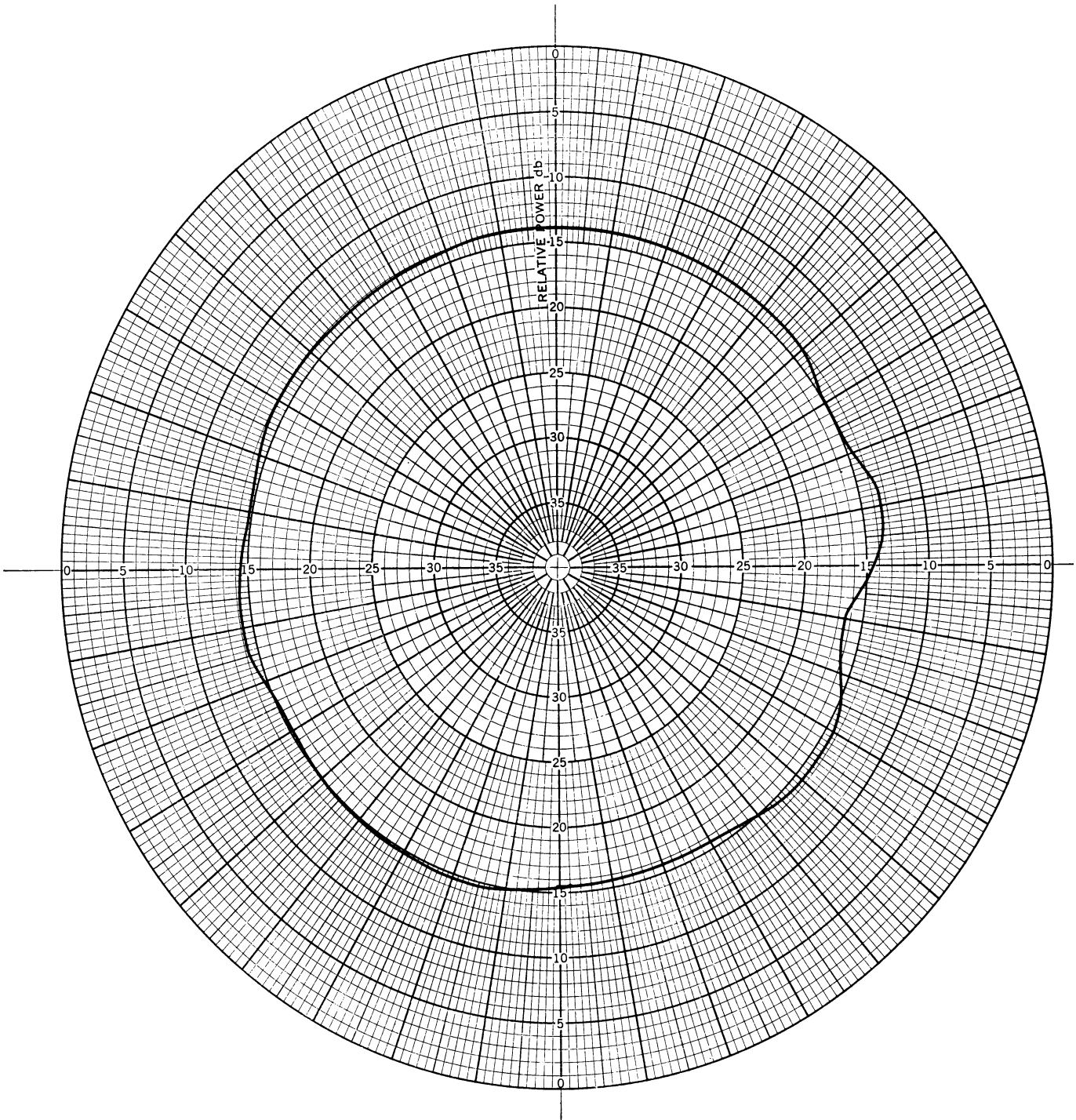
FIG. 22: H-PLANE PATTERN OF 1.5 GHz DIPOLE (No Radant)
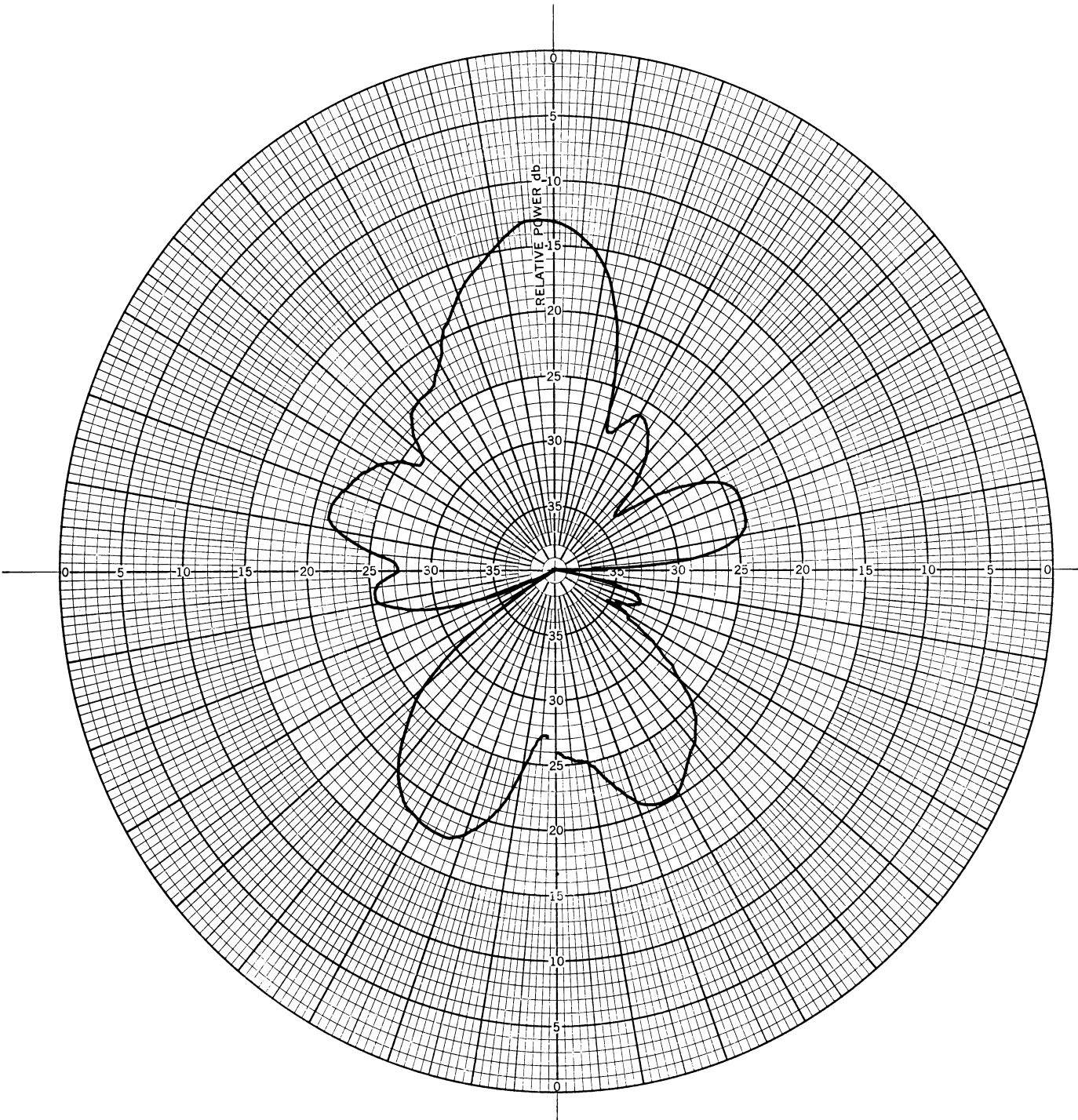
FIG. 23: E-PLANE PATTERN OF RADANT WITH 1.5 GHz
DIPOLE AND 3/16" SPACING
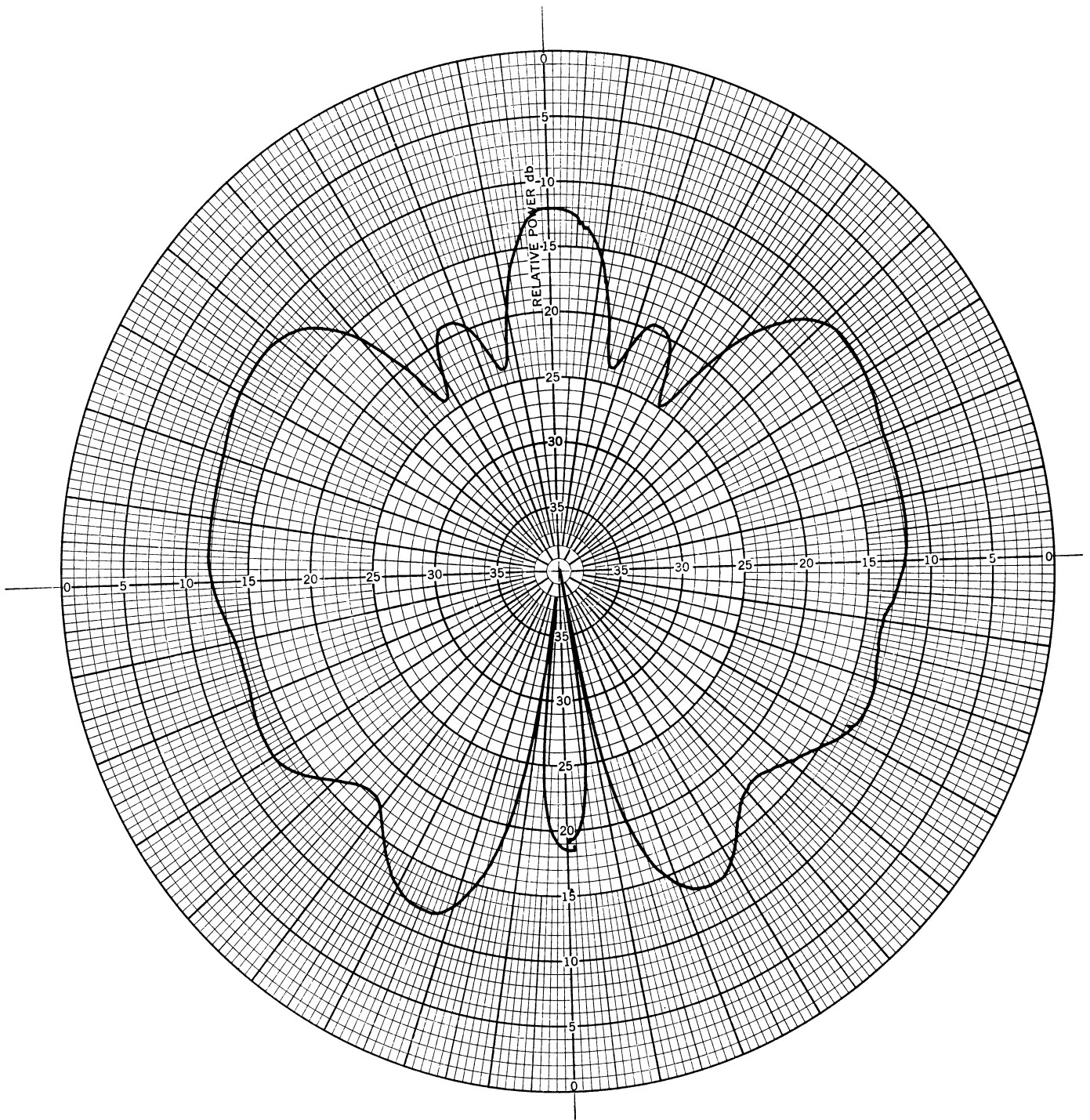
FIG. 24: H-PLANE PATTERN OF RADANT WITH 1.5 GHz
DIPOLE AND 3/16" SPACING
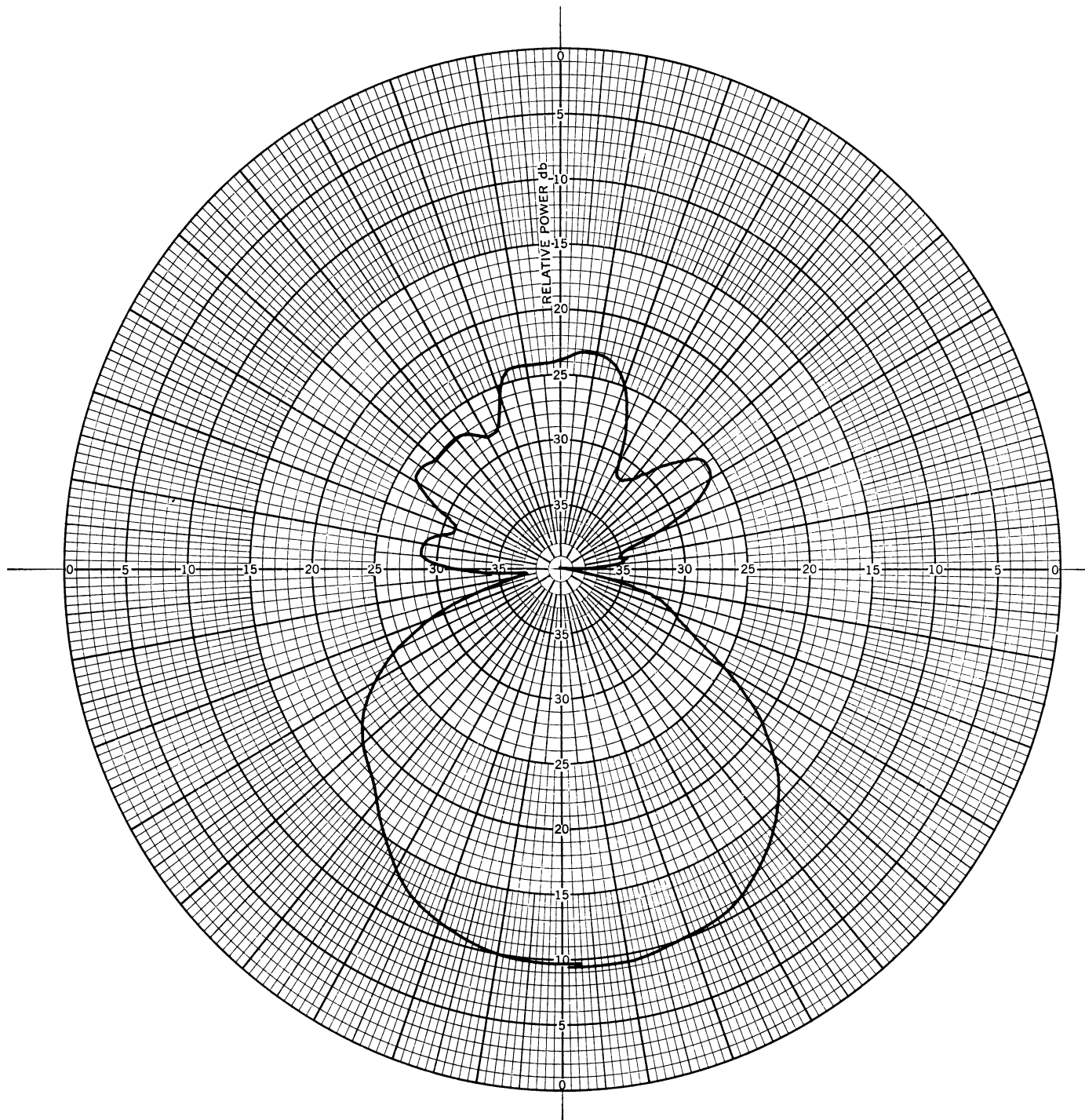
FIG. 25: E-PLANE PATTERN OF RADANT WITH 1.5 GHz
DIPOLE AND 2" SPACING
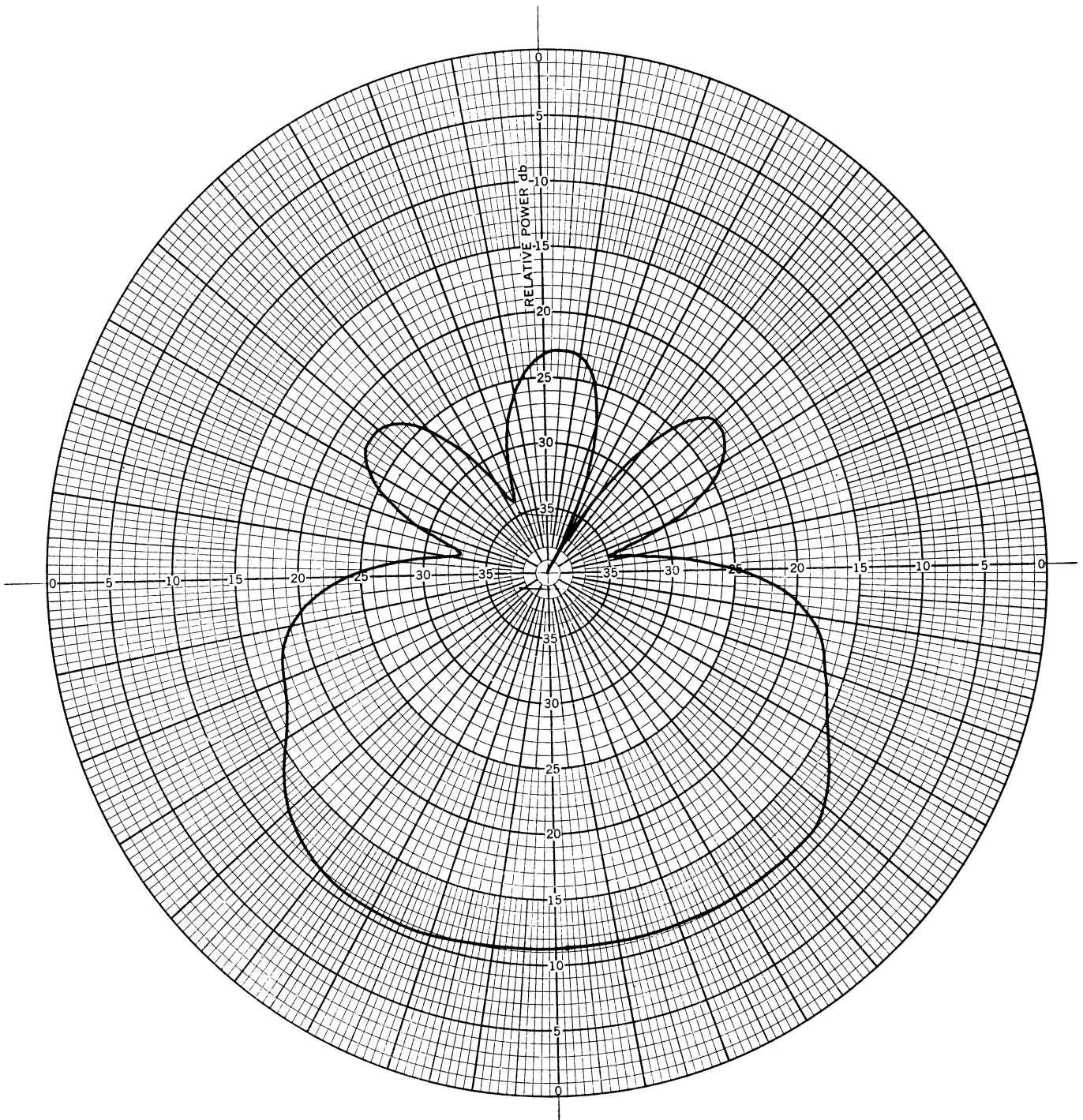
FIG. 26: H-PLANE PATTERN OF RADANT WITH 1.5 GHz
DIPOLE AND 2" SPACING

perimeter is approximately 1.20λ. Patterns for the dipole less the radant structure are shown in Fig. 27 and 28 and with the structure (for a 2 inch spacing) in Fig. 29 and 30. At this frequency radiation in the direction tangent to the radant surface was not observed for H-plane polarization and in general the E and H-plane patterns have deteriorated considerably and the back lobes tend to exceed the forward lobe through the radant.

3.5 Cross Polarization Measurements

Cross polarization measurements were made by rotating the transmitting antenna about the axis of its major lobe. The data of Table III shows that as the frequency is increased the amount of cross polarization also increases such that the isolation between the two polarization components is only 17 db at 3 GHz. The cross polarization isolation of the dipole (less the radant structure) was measured at each frequency and was found to be at least 35 db.

TABLE III

Cross Polarization

Frequency (GHz)	Cross Polarization Level db
0.36	-32
0.75	-30
1.5	-24
3.0	-17

3.6 Conclusions on the Use of the Dipole as a Primary Feed

From the data presented in the preceeding section it can be seen that the radant structure tends to improve the directivity of the dipole at the lower
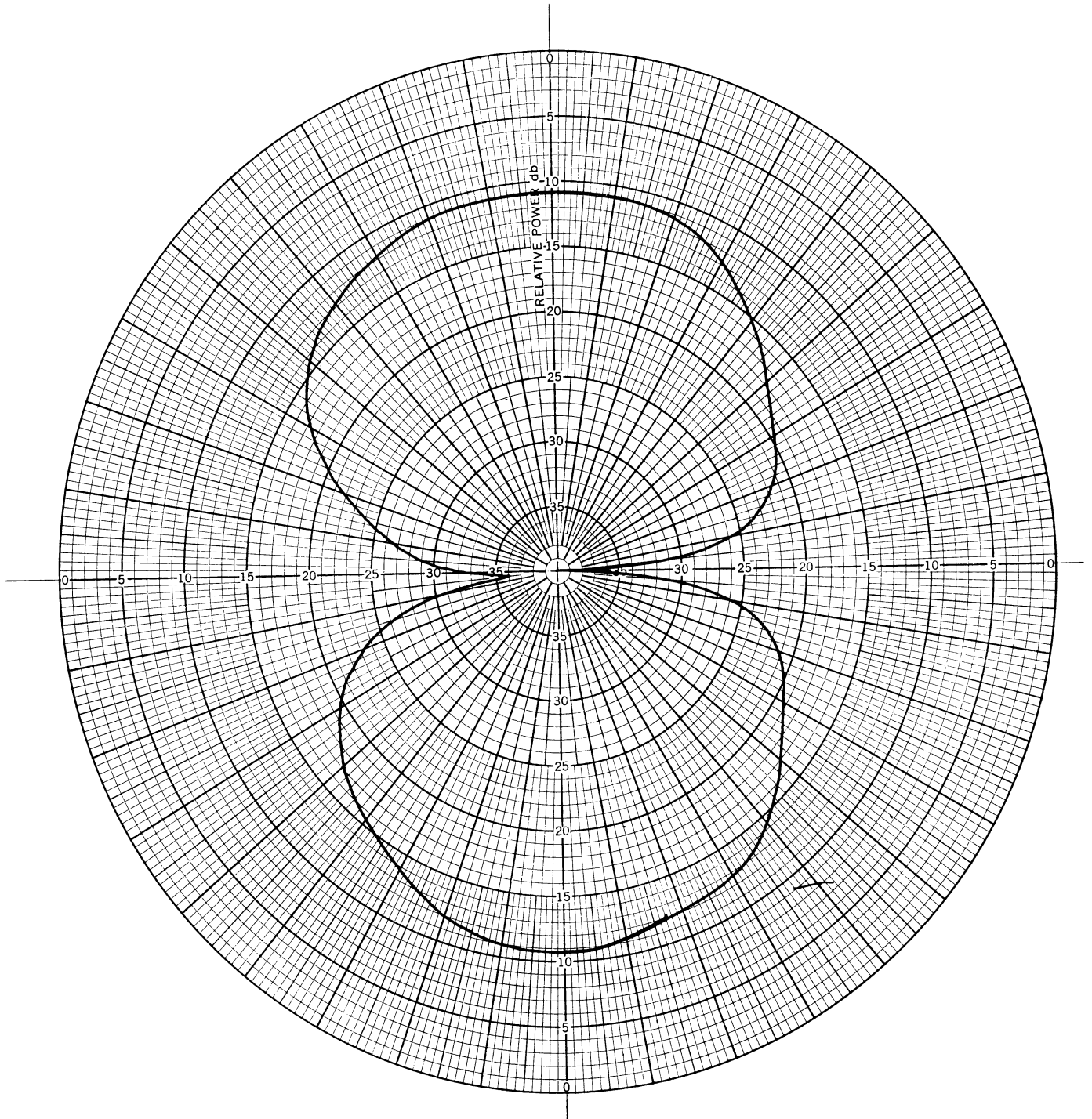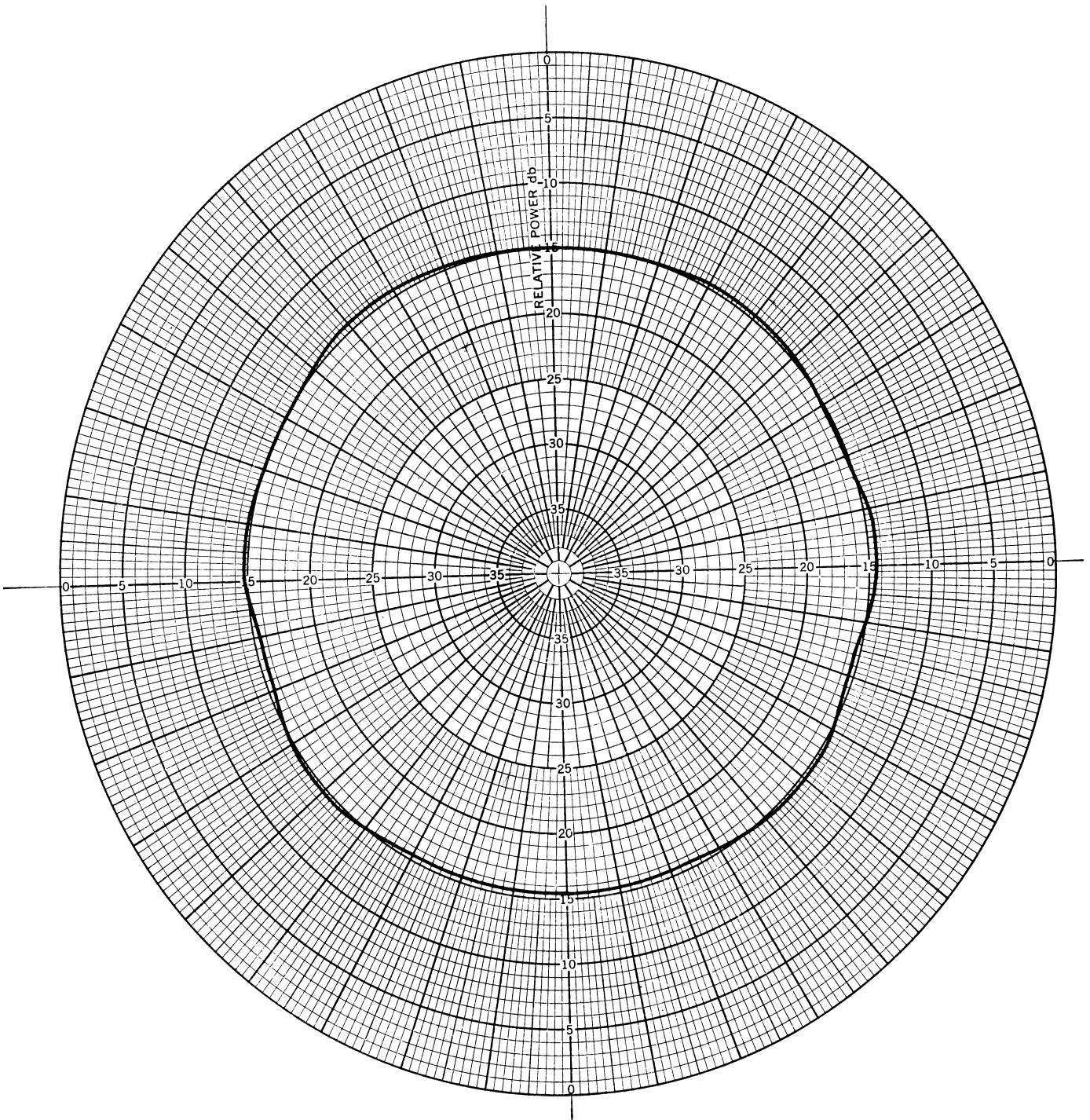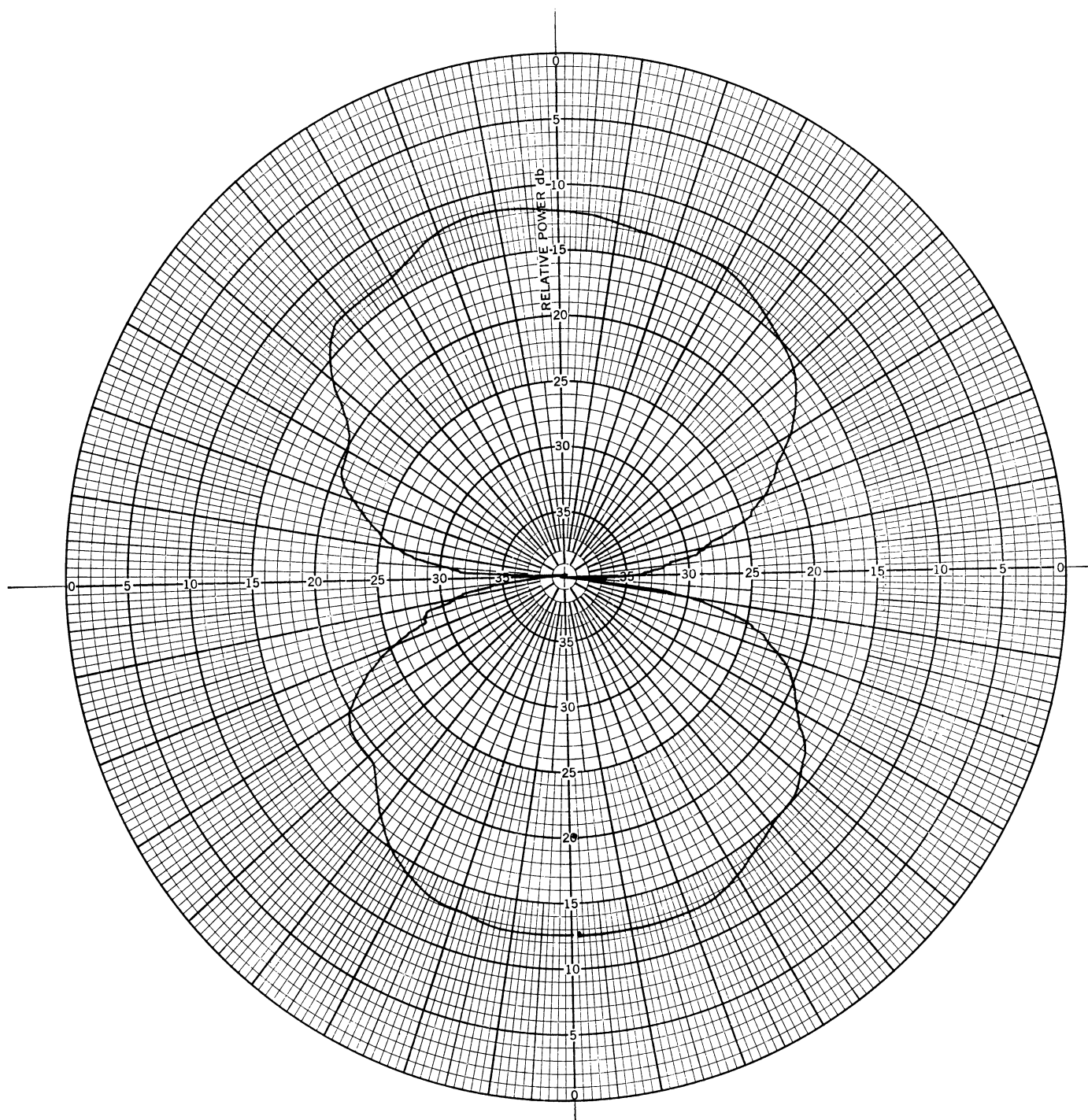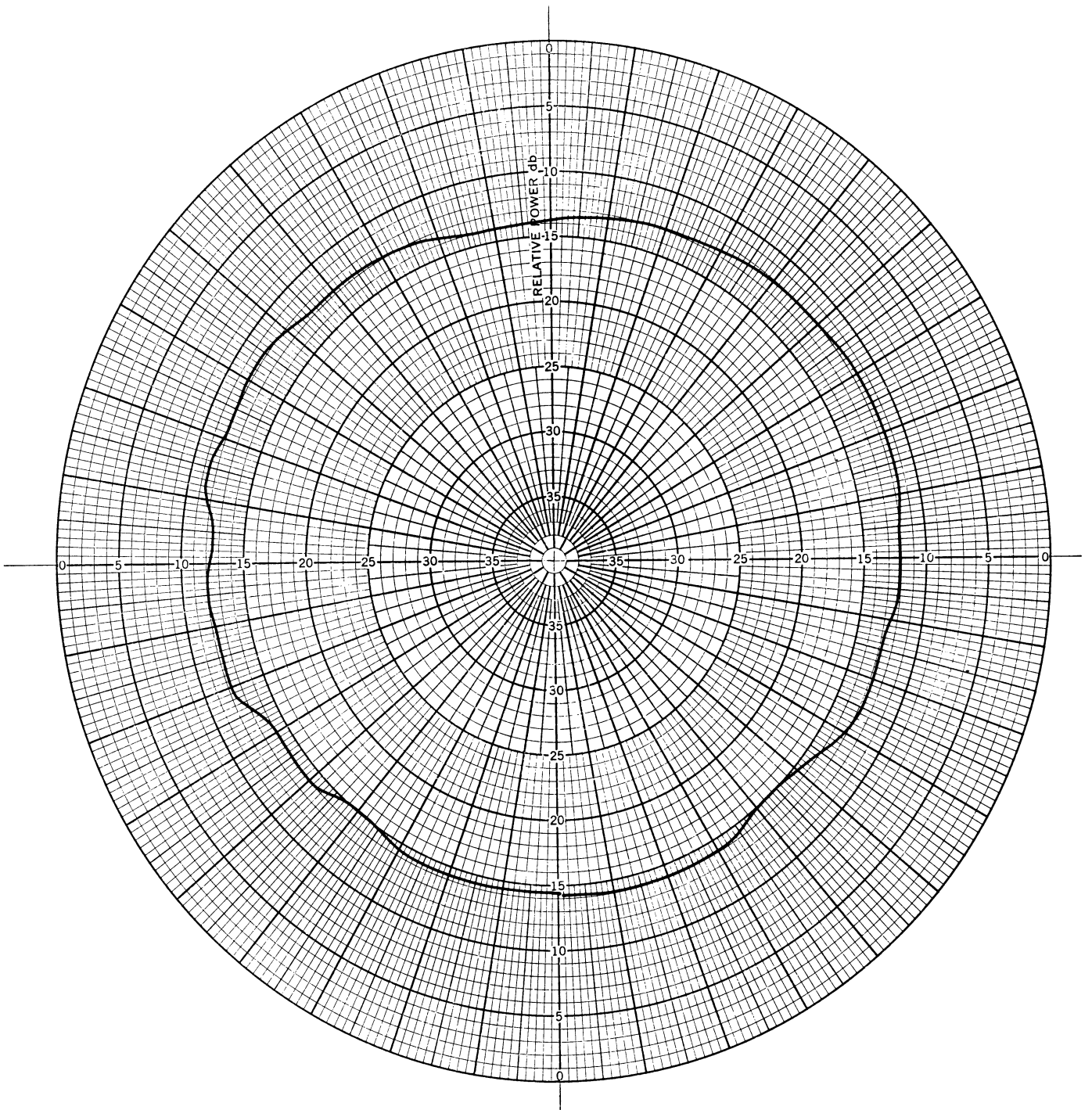
FIG. 27: E-PLANE PATTERN OF 3.0 GHz DIPOLE (No Radant)

FIG. 28: H-PLANE PATTERN OF 3.0 GHz DIPOLE (No Radant)

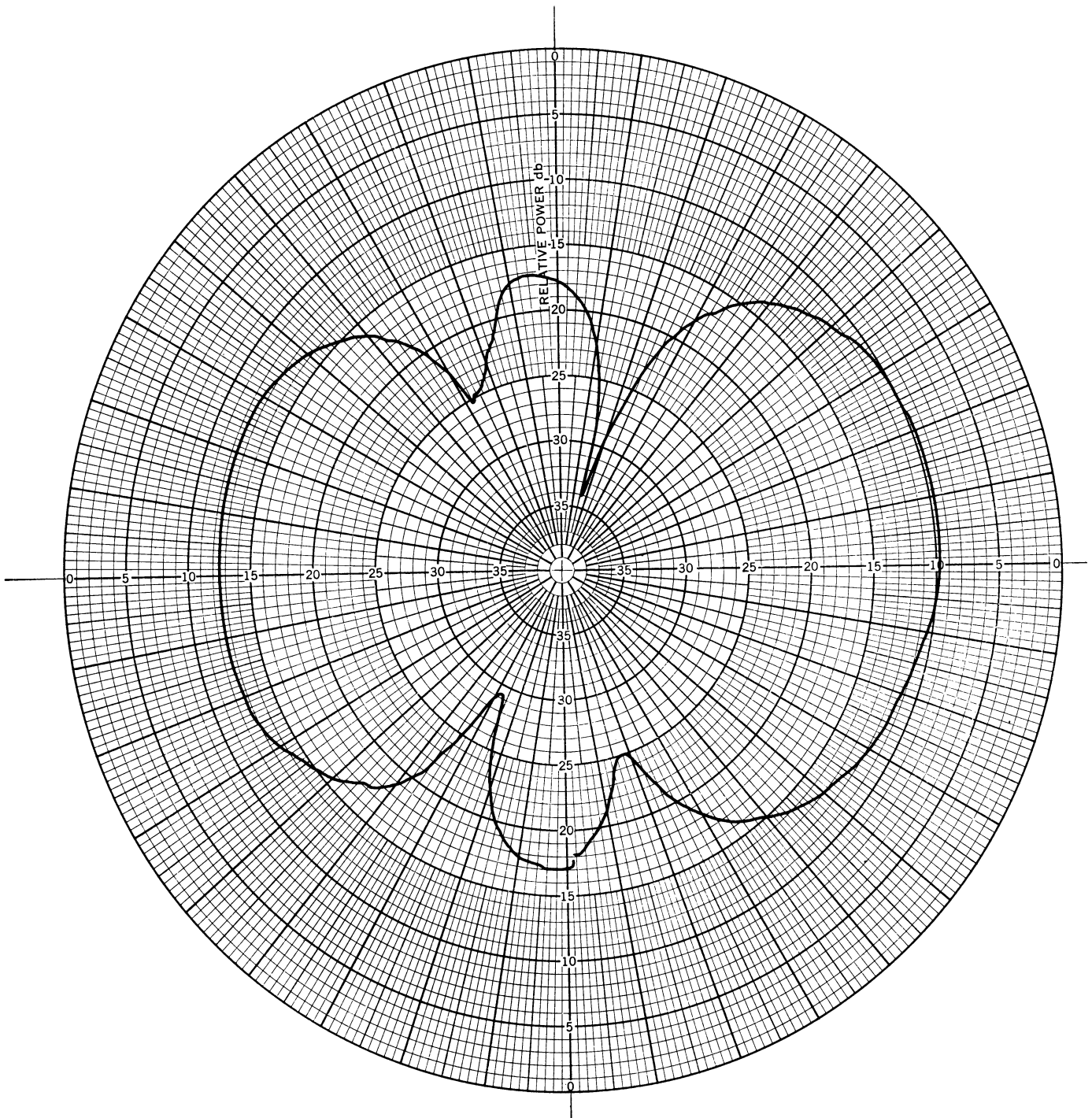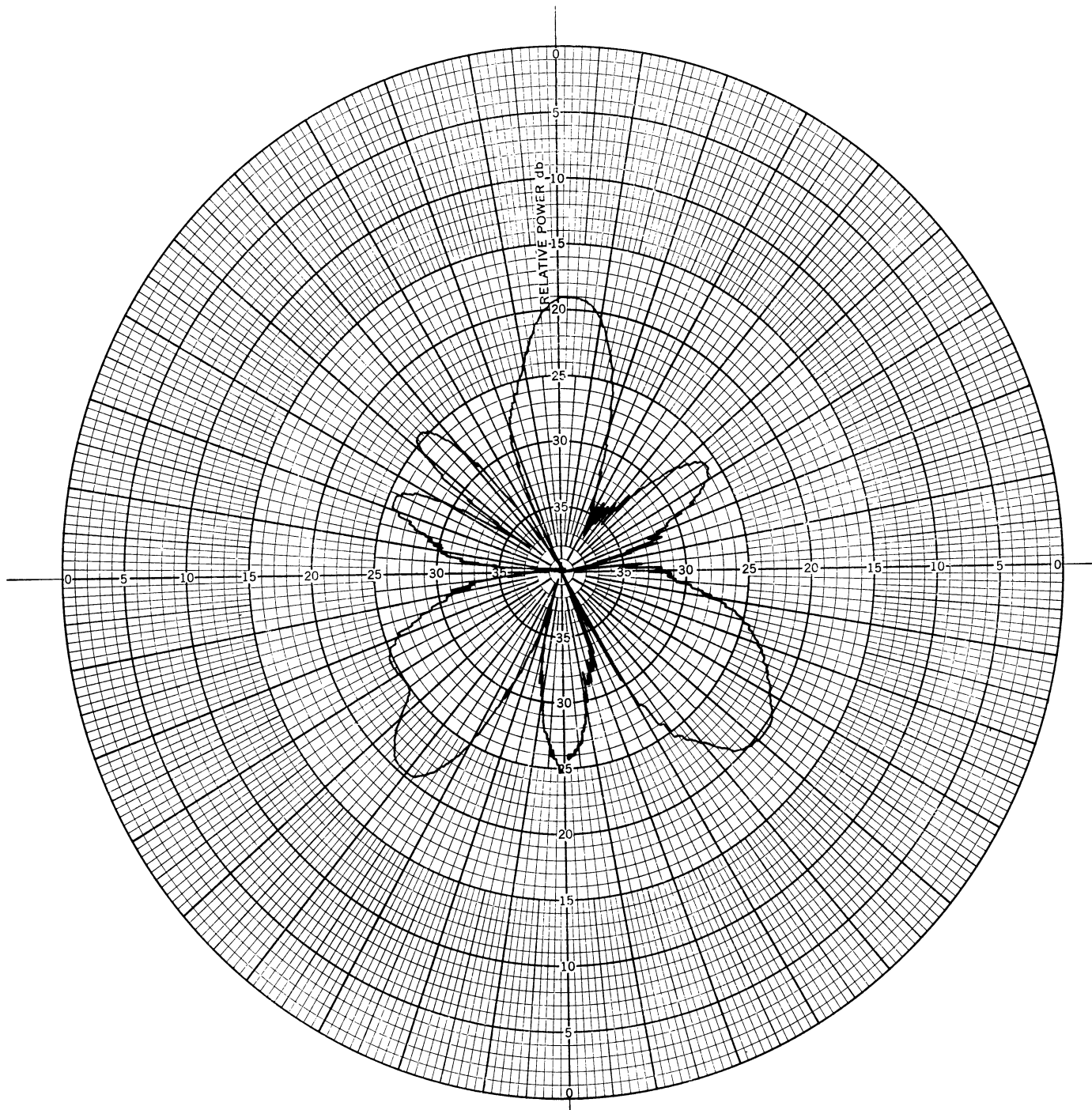FIG. 29: E-PLANE PATTERN OF RADANT WITH 3.0 GHz
DIPOLE AND 2" SPACING
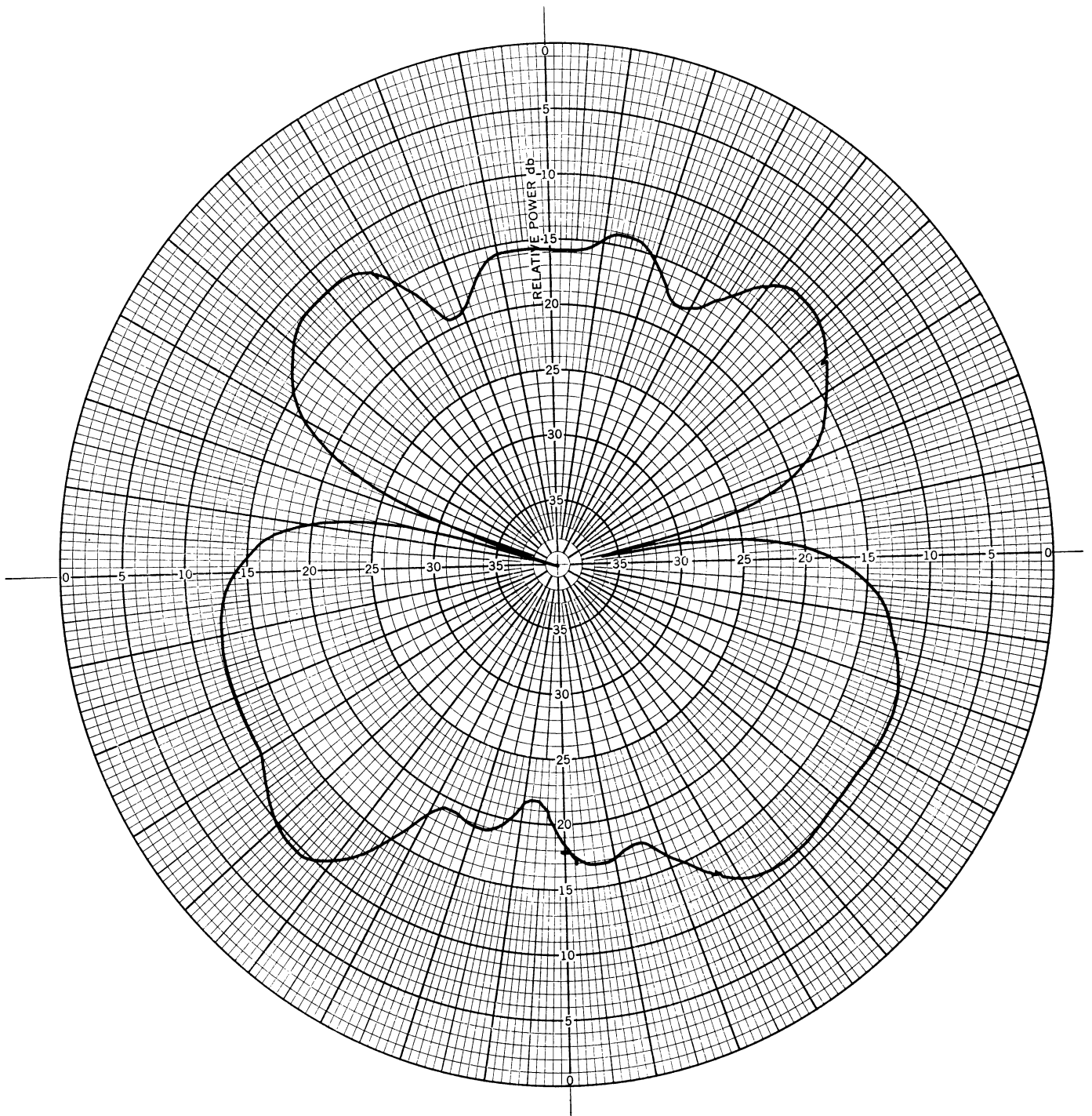
FIG. 30:   H-PLANE PATTERN OF RADANT WITH 3.0 GHz
DIPOLE AND 2" SPACING

frequencies; at the higher frequencies, however, the addition of the radant may produce a distorted or unusable pattern. Thus, its use is limited to those frequencies where the thickness and loop perimeter of the radant structure are electrically small. At those frequencies where the loop perimeter is electrically large the radiation characteristics of the loop are not well defined, i.e., it has a multi lobe characteristic. The break up in the pattern at the higher frequencies is caused, no doubt, by the out of phase currents on the loop perimeter.

IV

RADANT STRUCTURE AS A PRIMARY SOURCE

Consideration has been given determining the feasibility of using the radant structure as a primary source as a means to better understand its behavior. To employ the radant structure as a primary source, only one of the loops was active and the remaining loops of the array were parasitically excited. The resulting radiation pattern should then give an indication of the amount of coupling between the loops. The active loop was located in the central region of the structure and excited through a quarter wave balun from a 50 ohm coaxial system. Although the quarter wave balun used provides a simple transformation from an unbalanced to a balanced system, it is limited for mechnical reasons to frequencies less than 3.0 GHz.

The balun used as a part of this study consists of a $\lambda/4$ length of two transmission lines shown in Fig. 31 where it will be noted that the 50 ohm coax is fed through one leg of the two wire system. This type of balun is limited in bandwidth, therefore to investigate the electrical characteristics of the self-excited radant, it was necessary to adjust the shorting strap of the two wire system shown in Fig. 31 such that it was $\lambda/4$ from the feed point. A balun of this configuration tends to radiate because the currents flowing on the two wire system are of opposite polarity and the wires are separated a finite distance. If the wire spacing is an appreciable part of a wavelength ($>\lambda/10$) radiation will occur causing unwanted lobes in the radant radiation patterns.

With the balun properly adjusted and connected to a single loop patterns were obtained in both the E and H-plane. The loop was similar in construction to those of the radant structure. For these measurements the balun was oriented such that it was in the plane of the loop as shown in Fig. 31. E-plane patterns measured for this configuration are shown in Fig. 32, 33 and 34 at 2.5, 3.0 and 3.5 GHz as noted
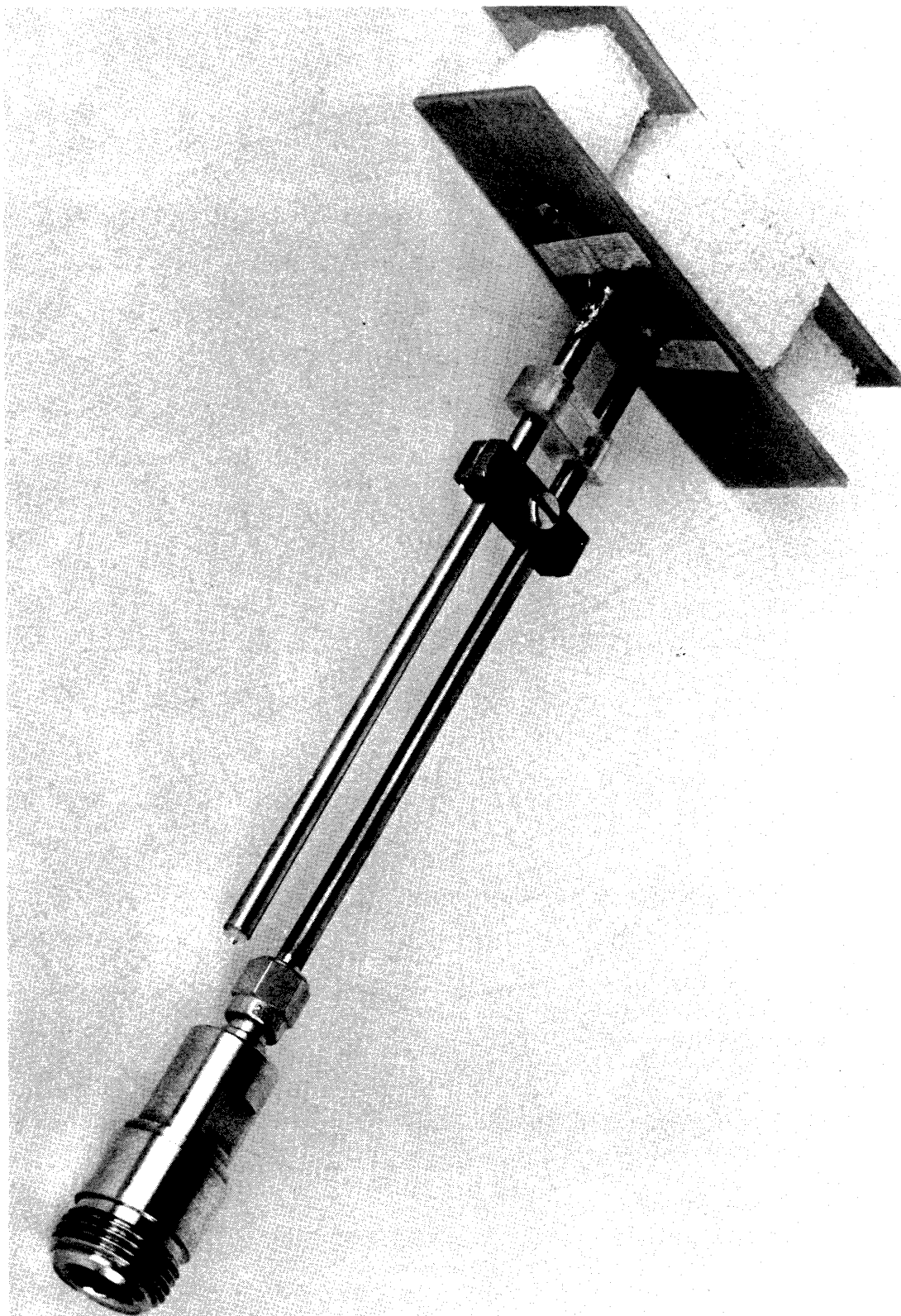
FIG. 31: SINGLE RADANT LOOP AND BALUN
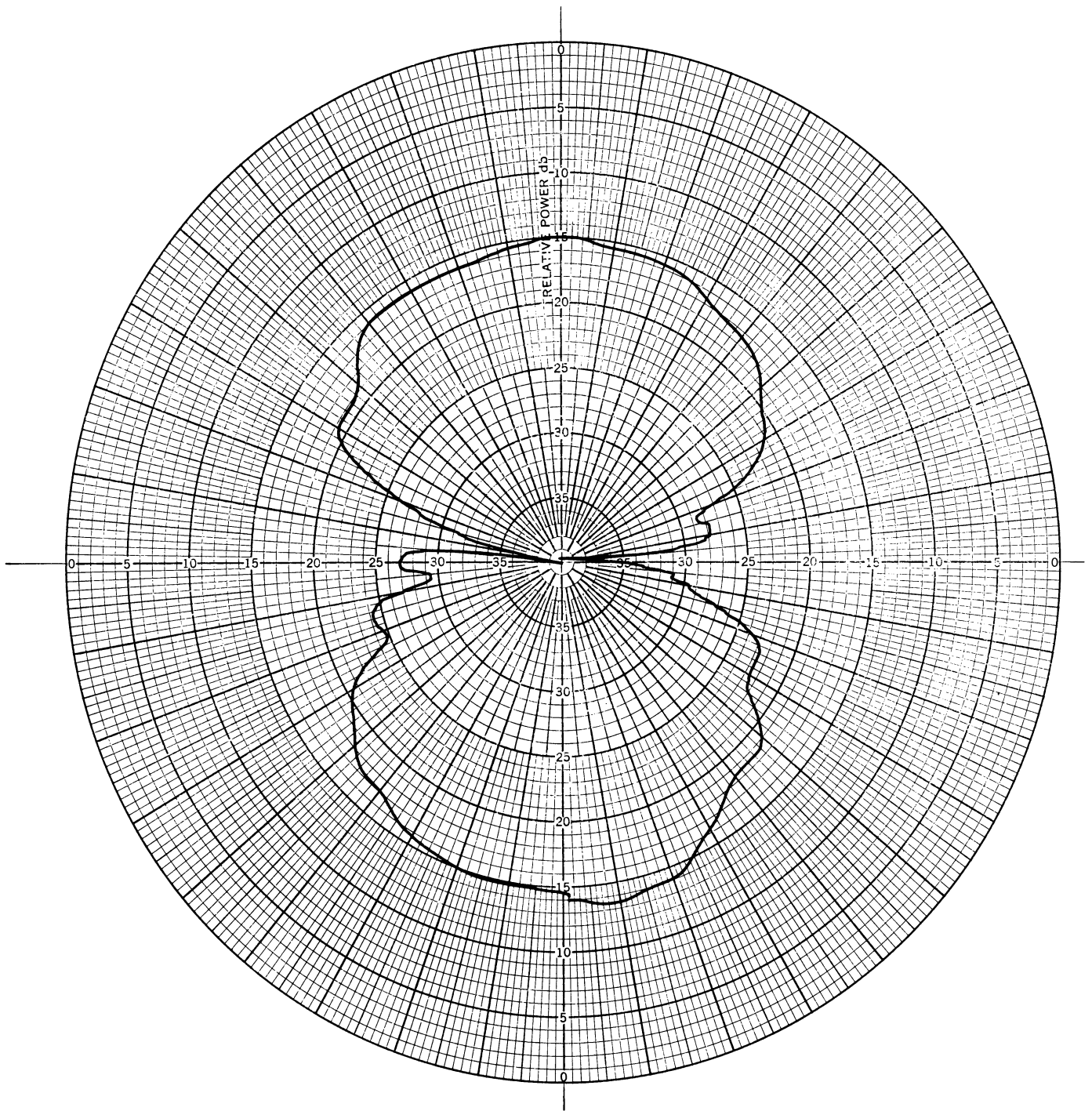
FIG. 32: E-PLANE PATTERN OF SINGLE RADANT LOOP AT
2. 5 GHz
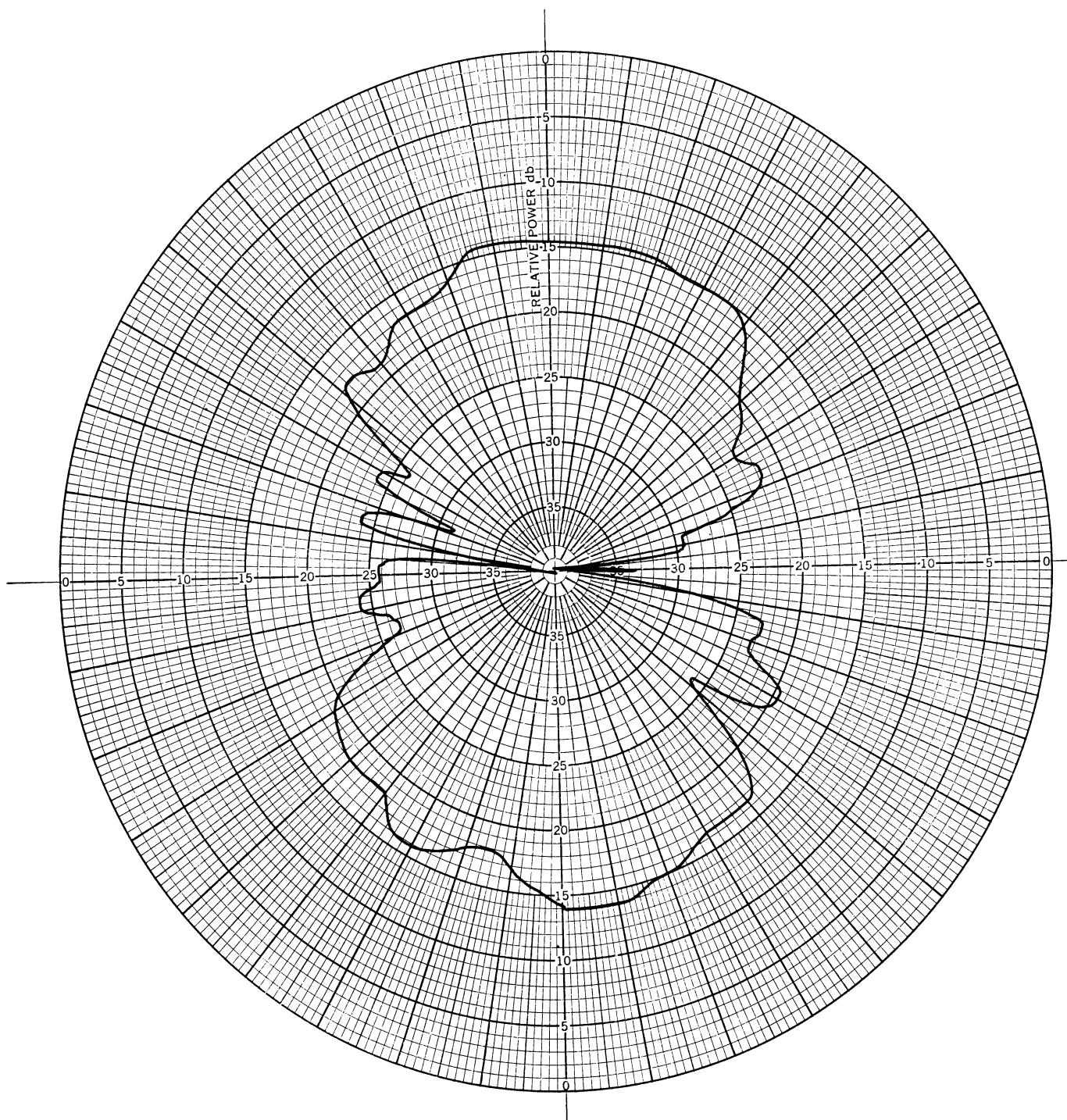
FIG. 33: E-PLANE PATTERN OF A SINGLE RADANT LOOP AT
3.0 GHz
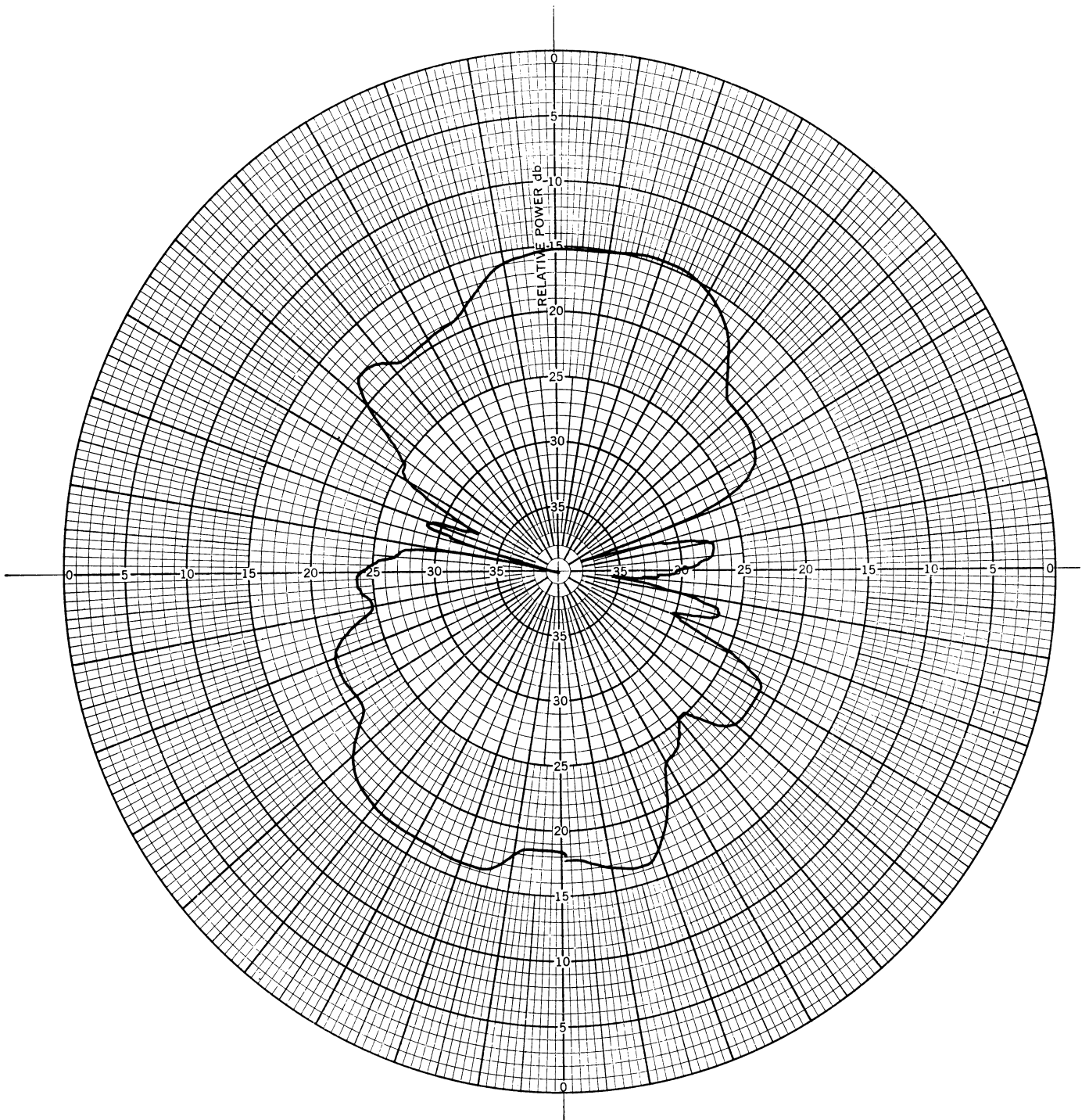
FIG. 34: E-PLANE PATTERN OF A SINGLE RADANT LOOP
AT 3.5 GHz

in the figures. H-plane patterns were taken also and were found to be essentially omnidirectional. The radiation characteristics are typical of electrically small loop antennas, however, at frequencies of 3.0 GHz and above the patterns break up as would be expected for electrically large loop antennas. In addition to the above pattern data cross polarized data was obtained. At frequencies above 2.5 GHz the cross polarization component was within 10 db of the excited component. The cause for the high cross polarized data is assumed to be due to 1) the balun, and 2) the electrically large size of the loop.

Since the data for the single loop was found to be limited to frequencies below 2.5 GHz, the study of the radant (as a primary structure source) was restricted to this frequency range. To conduct this study the balun was connected to one of the loops in the central portion of the array as shown in Fig. 35. It was assumed that the remaining loops of the array would be parasitically coupled to the active loop. It was felt that loops in close proximity to the active loop would be more tightly coupled than the others. Following this presumption the aperture distribution would have a natural taper. However, little was known as to the aperture phase distribution. Because of the complexity of the problem it was felt that a better insight could be obtained from experimental rather than theoretical data.

Patterns obtained at 2.5 GHz are shown in Fig. 36 and 37 for the E and H planes respectively. The multi-lobe characteristics of the structure indicates an out of phase condition for those parts of the structure that are excited. Other tests were made involving variations in frequency or feed arrangement but no satisfactory patterns were obtained.

Due to the difficulties of obtaining clean excitation of one loop and the complexity of the patterns obtained with the self-fed radant structure it did not appear feasable to continue this phase of the investigation. It seemed unlikely that further measurements of this would add to the knowledge of the radant behavior.
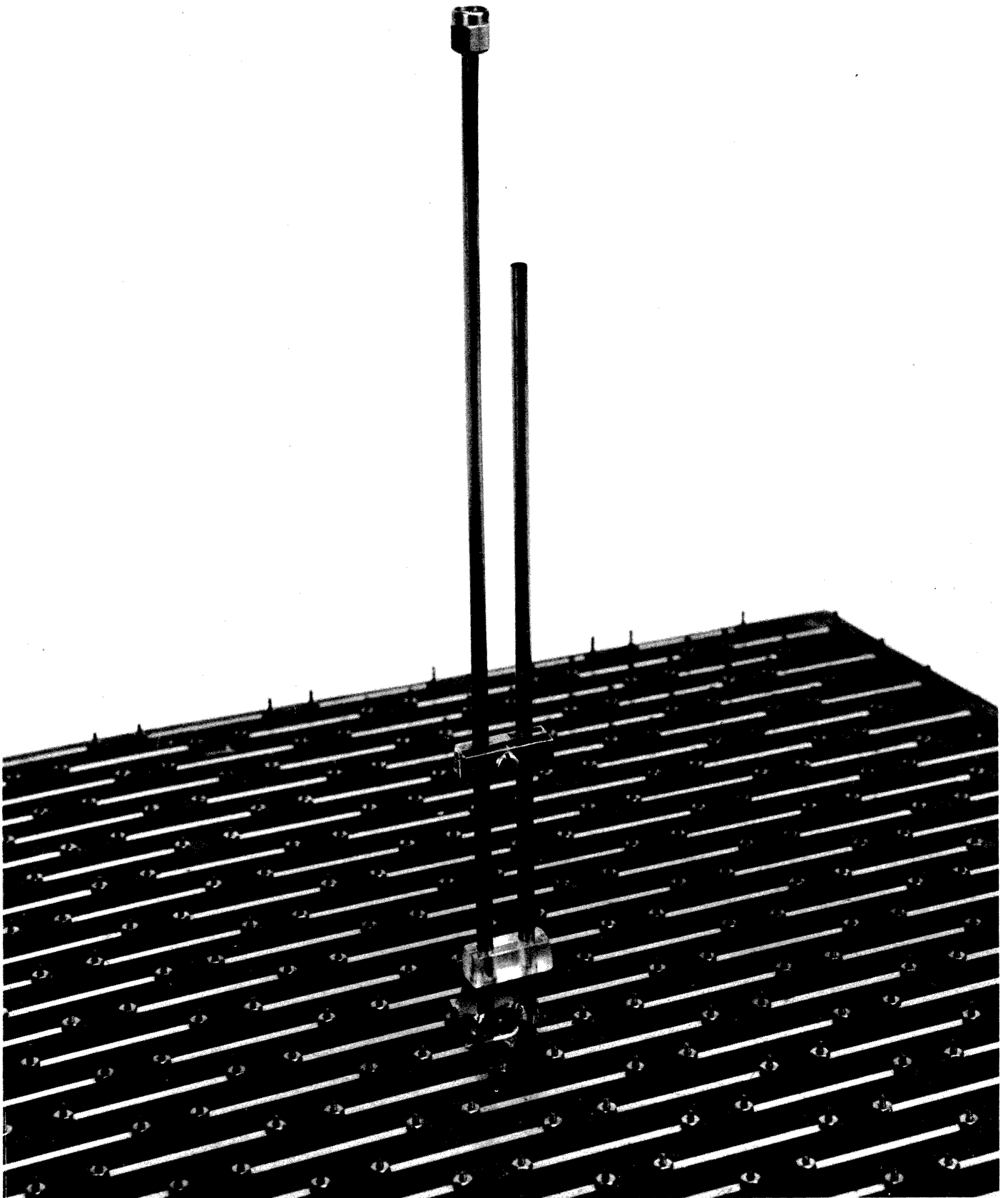
FIG. 35: SELF-EXCITED RADANT STRUCTURE
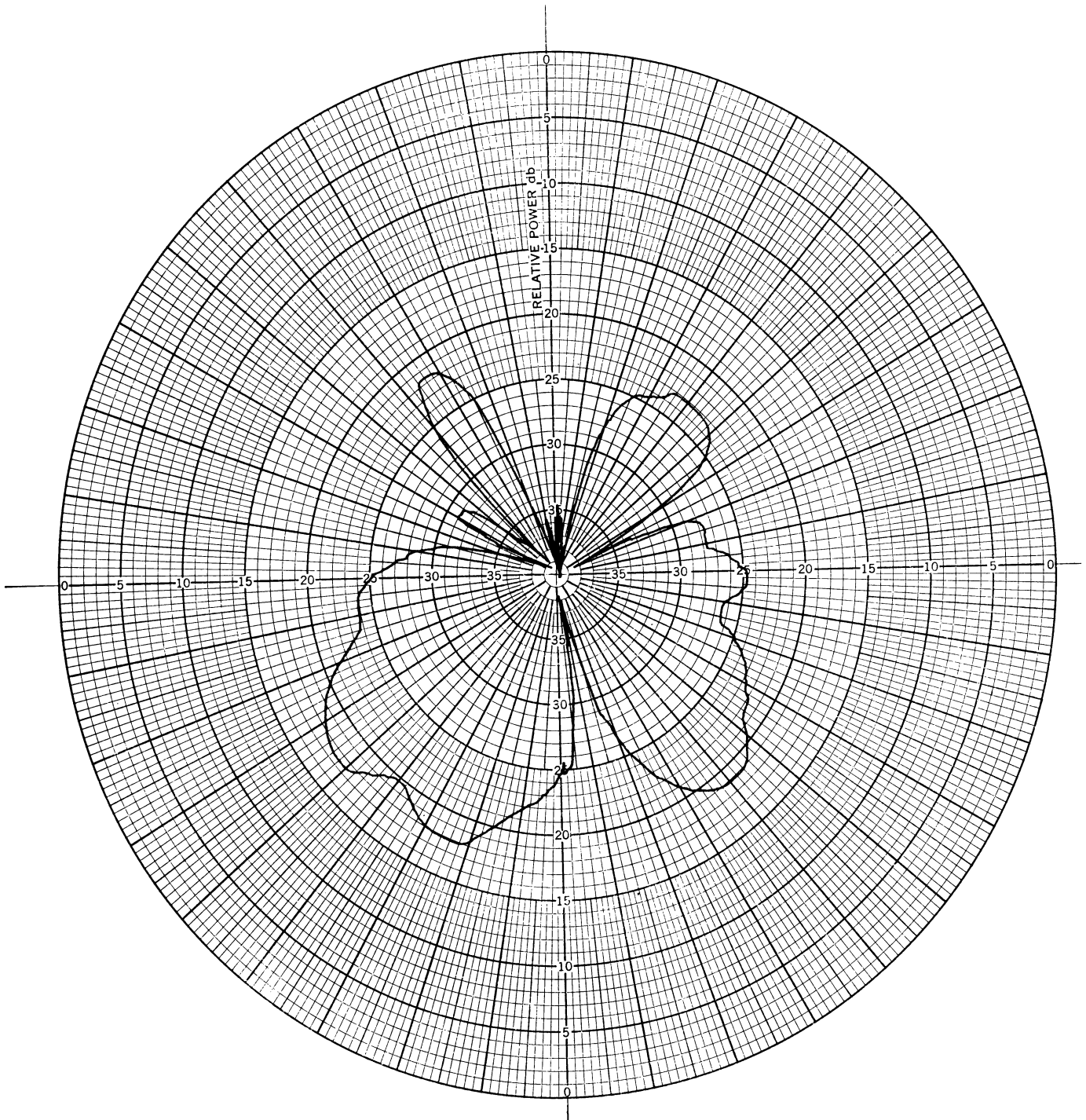
FIG. 36:   E-PLANE PATTERN OF A SELF-ESCITED RADANT
AT 2.5 GHz

FIG. 37: H-PLANE PATTERN OF A SELF-EXCITED RADANT
AT 2.5 GHz

V
TRANSMISSION THROUGH AN ISOTROPIC DIELECTRIC PANEL

A theoretical study of an anisotropic panel of conducting discs was reported in the first Interim (Tai, et al 1965). The purpose of this study was to obtain a better understanding of the transmission coefficient of the loop radant structure (supplied by Avionics Laboratory). From this study it was concluded that to verify the theoretical analysis, it would be desirable to investigate an isotropic dielectric panel since the transmission coefficients of the isotropic panel could be readily measured using relatively simple sources to excite it.

Experimental data was collected employing a 51" x 51" x 2" plexiglass sheet at 0.34 and 0.75 GHz. To excite the plexiglass sheet half wave dipoles were employed. Preliminary results obtained for the plexiglass sheet showed the supporting wood structure (Fig. 38) was causing undesired undulations in the far-field radiation pattern. To overcome the effects of the supporting structure a smaller plexiglass sheet 12" x 12" x d" thick was employed for some of the measurements. The "d" dimension of the smaller panel was varied to obtain transmission characteristics as a function of thicknesses of plexiglass. In the theoretical analysis the incident field was normal to the plane of the plexiglass and its dielectric constant was assumed to be 2.76. Employing these conditions both theoretical and experimental pattern data was collected and compared. The theoretical pattern data was calculated employing the following expression:

$$T = \frac{1}{1 + \left(\dfrac{2r\sin x}{1-r^2}\right)^2}$$

$$T = \frac{1}{1 + \left[\dfrac{2+\sin x}{1-t^2}\right]^2}$$
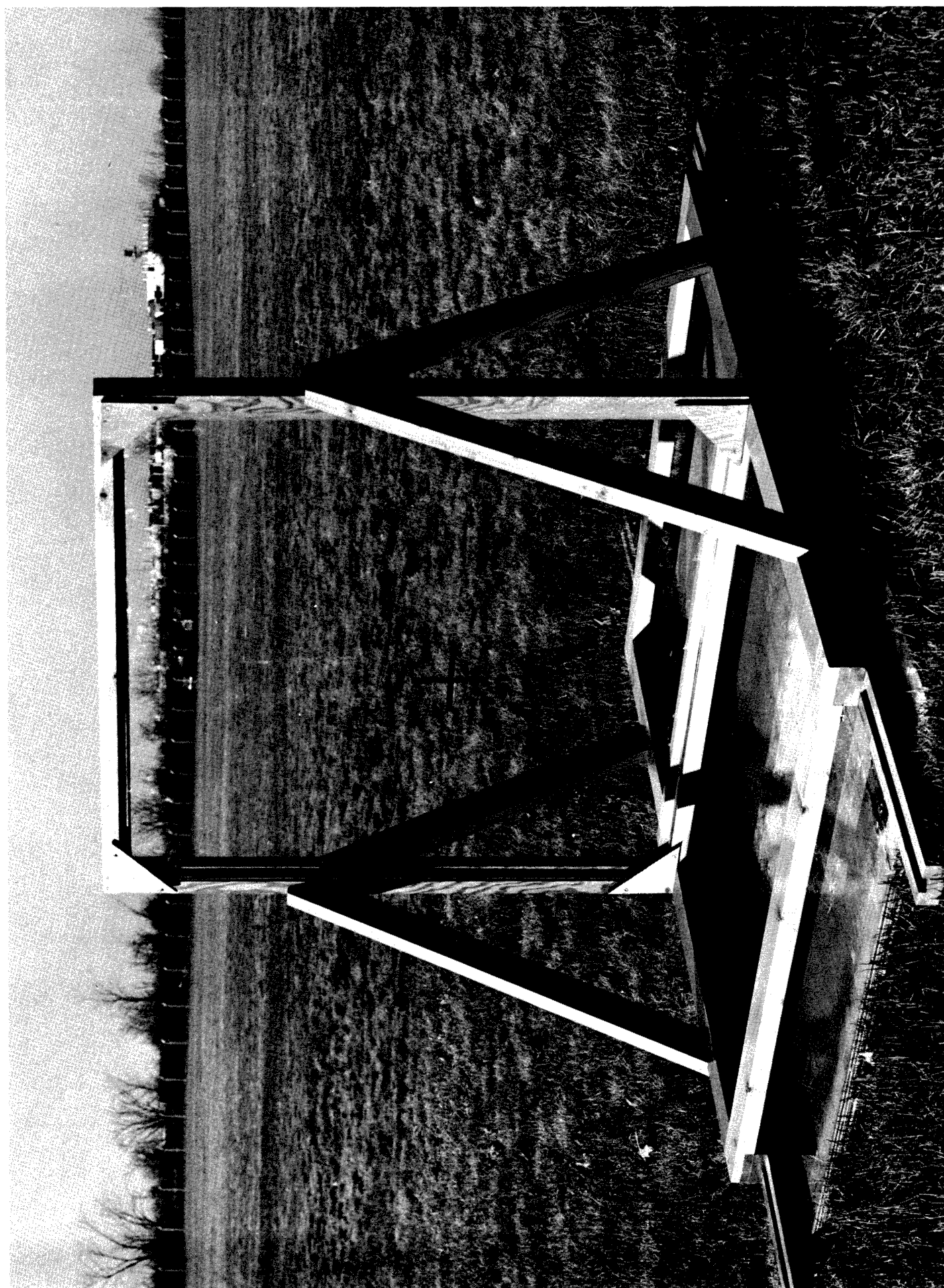
FIG. 38: ISOTROPIC DIELECTRIC PANEL

where

$$x = x_o \sqrt{k - \sin^2\theta}$$

$$r = \frac{\cos\theta - \sqrt{k - \sin^2\theta}}{\cos\theta + \sqrt{k - \sin^2\theta}}$$

$$t = \frac{k\cos\theta - \sqrt{k - \sin^2\theta}}{k\cos\theta - \sqrt{k - \sin^2\theta}}$$

x_o = thickness of dielectric in radians
    in terms of wavelength in air

k = relative dielectric constant

The geometry of the panel is shown in Fig. 39 where θ_a is the limiting angle. Since the dielectric sheet is square the angle θ_a will be equal for the E and H planes. Since the theoretical analysis was based on an isotropic source, experimental data was collected only for the H plane of the dipole. To compare the theoretical pattern with the experimental data the precedure outlined below was followed.

1) An H-plane pattern of a resonant dipole alone was measured at the frequency of interest.

2) Step (1) was repeated with the plexiglass.

3) A far-field pattern was calculated using the above expressions.

4) The results of (3) were multiplied by the pattern of (1).

5) The results of (4) were then compared with (2).
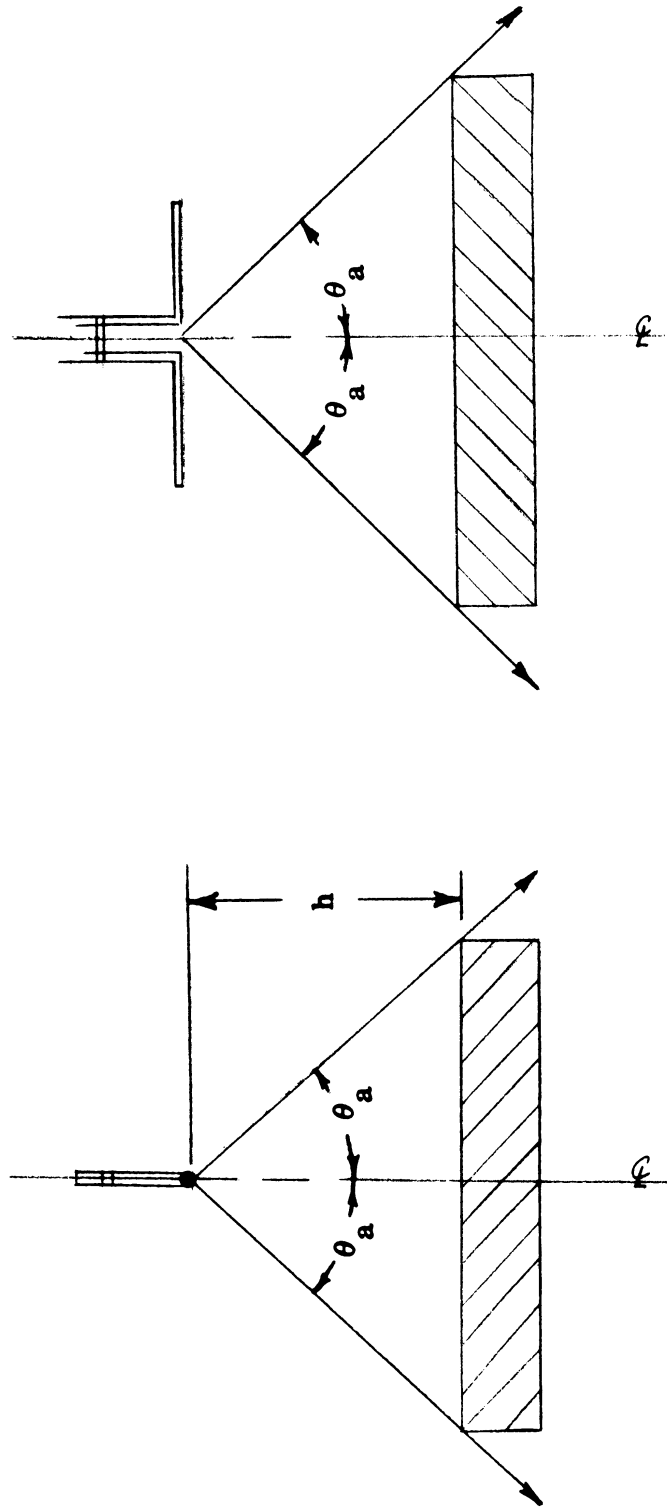
FIG. 39: DIMENSIONAL PARAMETER OF A DIELECTRIC PANEL

Typical results of the comparison between the theoretical and experimental data are shown in Figs. 40 for 0.34 GHz, Fig. 41 and 42 for 0.75 GHz and Fig. 43 and 44 for 3.0 GHz. The 50" x 50" panel was used for the first two frequencies and the 12" x 12" panel was used for the 3.0 GHz measurements. The spacing between the dipole and plexiglass sheet is a variable that must be taken into account in view of the pattern variations that are noted at 0.75 GHz, since the angle θ_a is a function of the spacing.

7300-1-F

$k = 2.76$

$x_o = 0.364$

$\theta_a = 87.2^o$
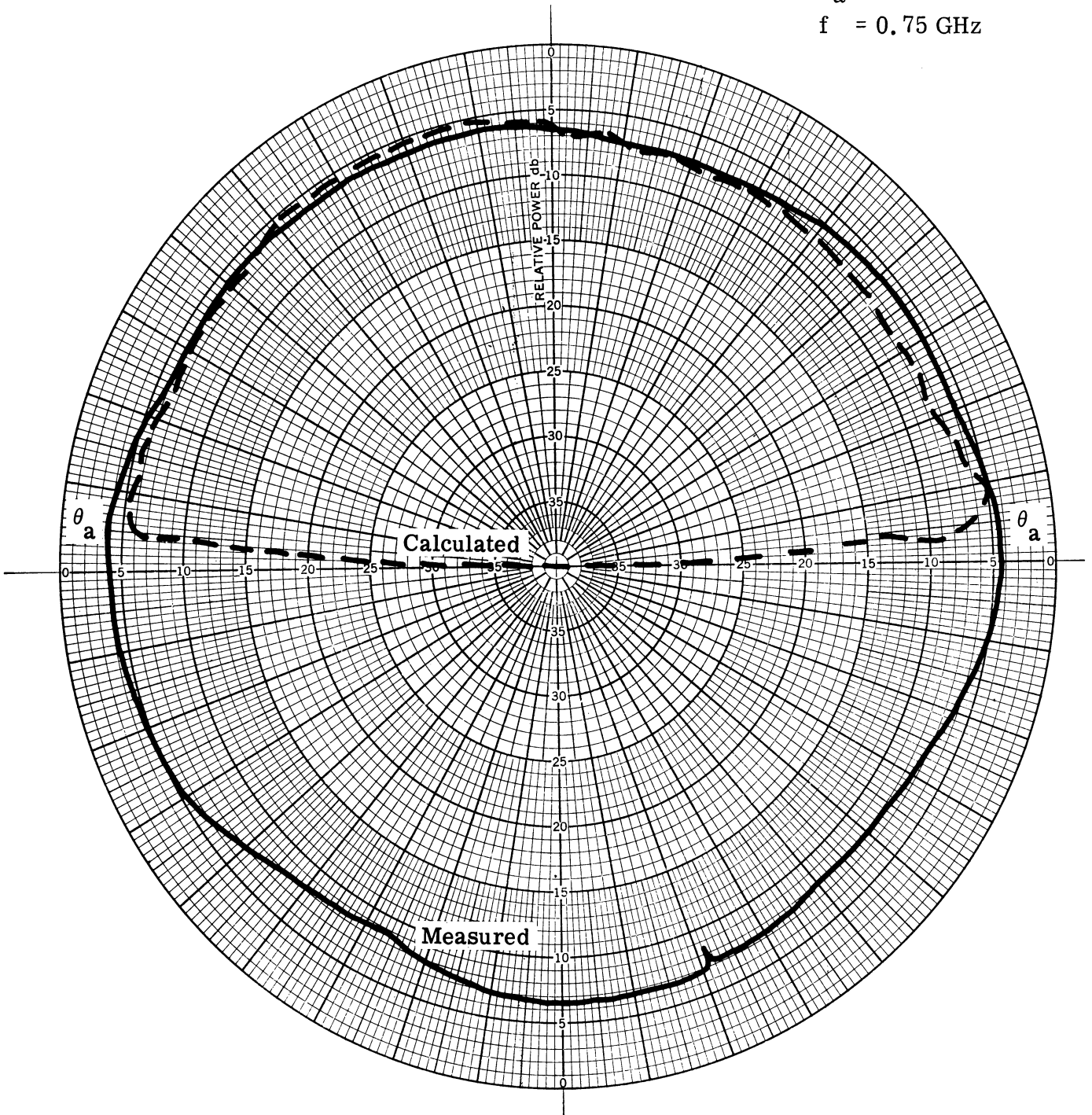
$f = 0.75$ GHz

FIG. 40: H-PLANE MEASURED AND THEORETICAL PATTERNS FOR AN ISOTROPIC PANEL

7300-1-F

k = 2.76

x$_o$ = 0.364

θ_a = 87.2^o
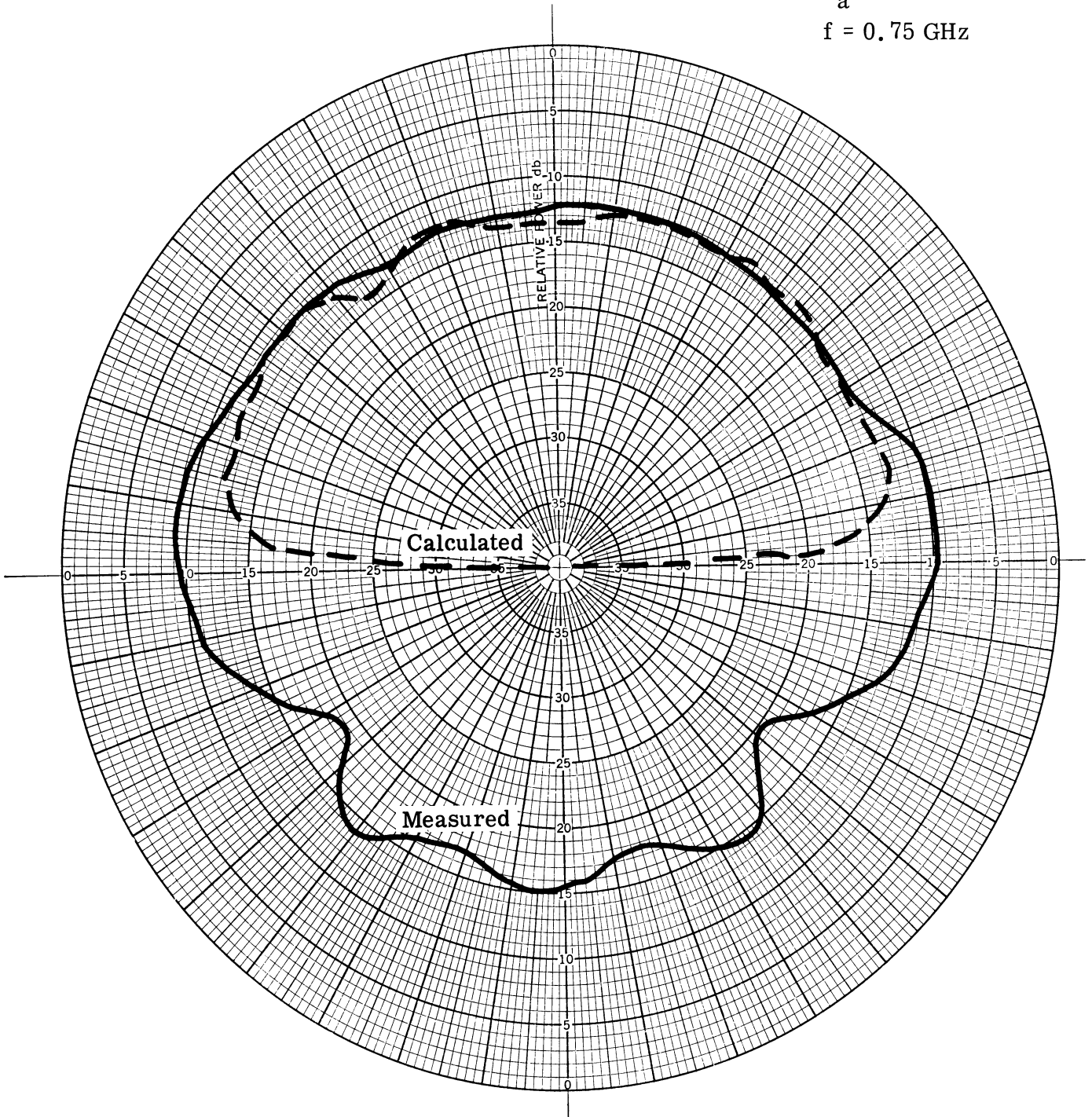
f = 0.75 GHz

FIG. 41: H-PLANE THEORETICAL AND MEASURED PATTERNS FOR AN ISOTROPIC PANEL

7300-1-F

$k = 2.76$

$x_o = 0.364$

$\theta_a = 84.5^o$

$f = 0.75$ GHz
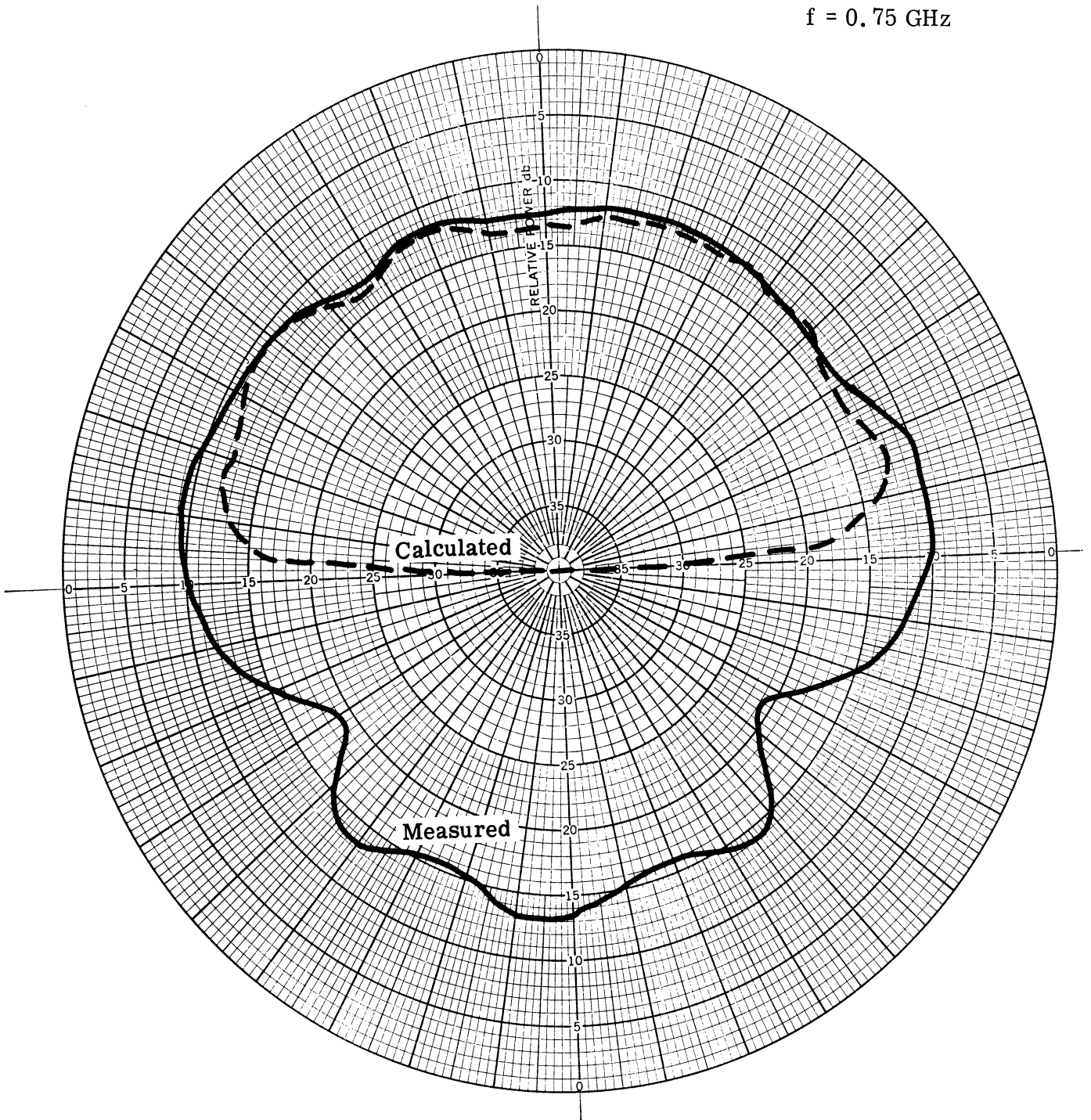
FIG. 42: H-PLANE THEORETICAL AND MEASURED PATTERNS FOR AN ISOTROPIC PANEL

7300-1-F

k = 2.76

x_o = 3.06

θ_a = 80.5°
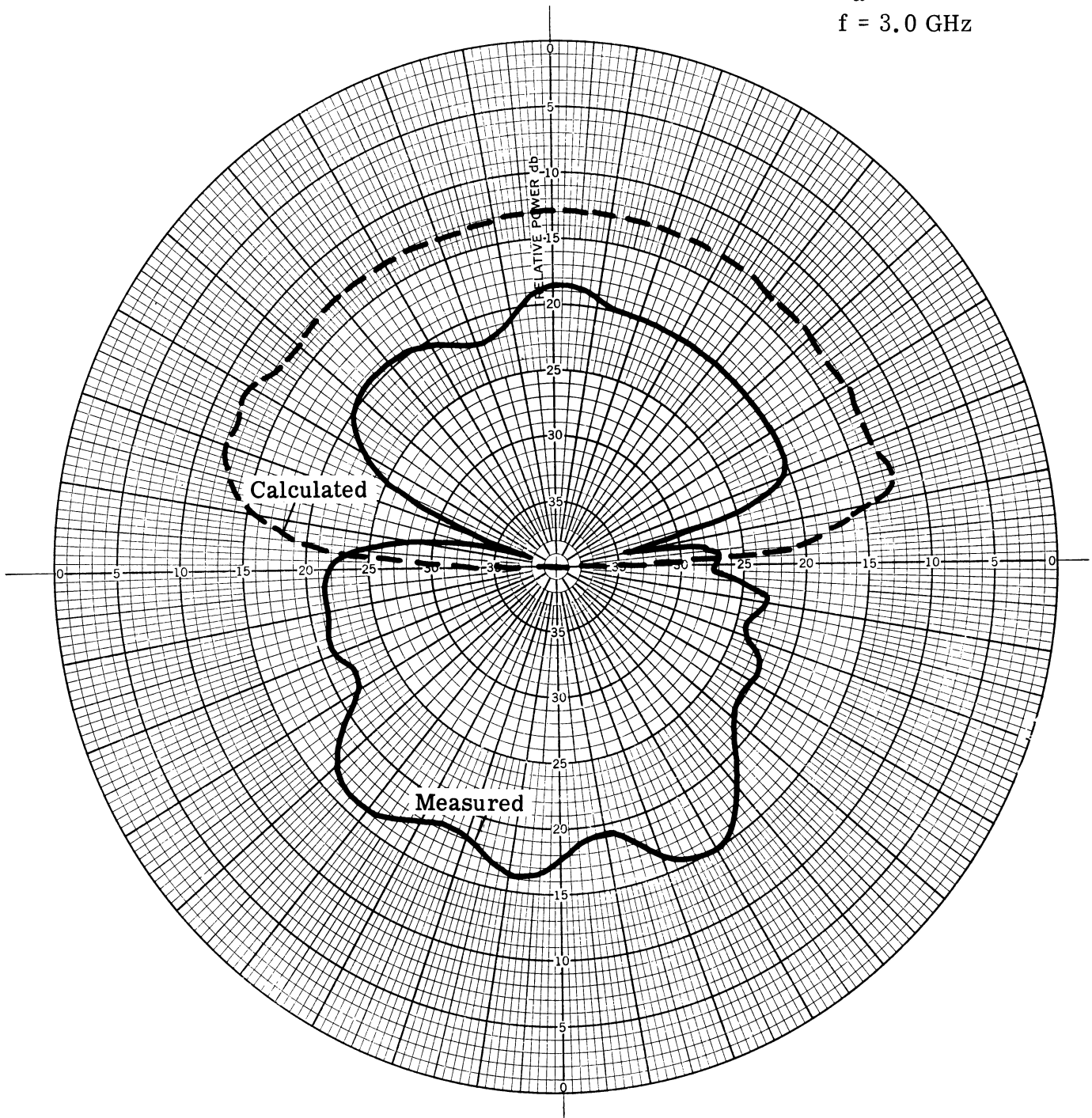
f = 3.0 GHz

FIG. 43: E-PLANE THEORETICAL AND MEASURED PATTERN FOR AN ISOTROPIC PANEL

$k = 2.76$

$x_o = 8.06$

$\theta_a = 8.05^o$

$f = 3.0$ GHz

RELATIVE POWER db

Calculated
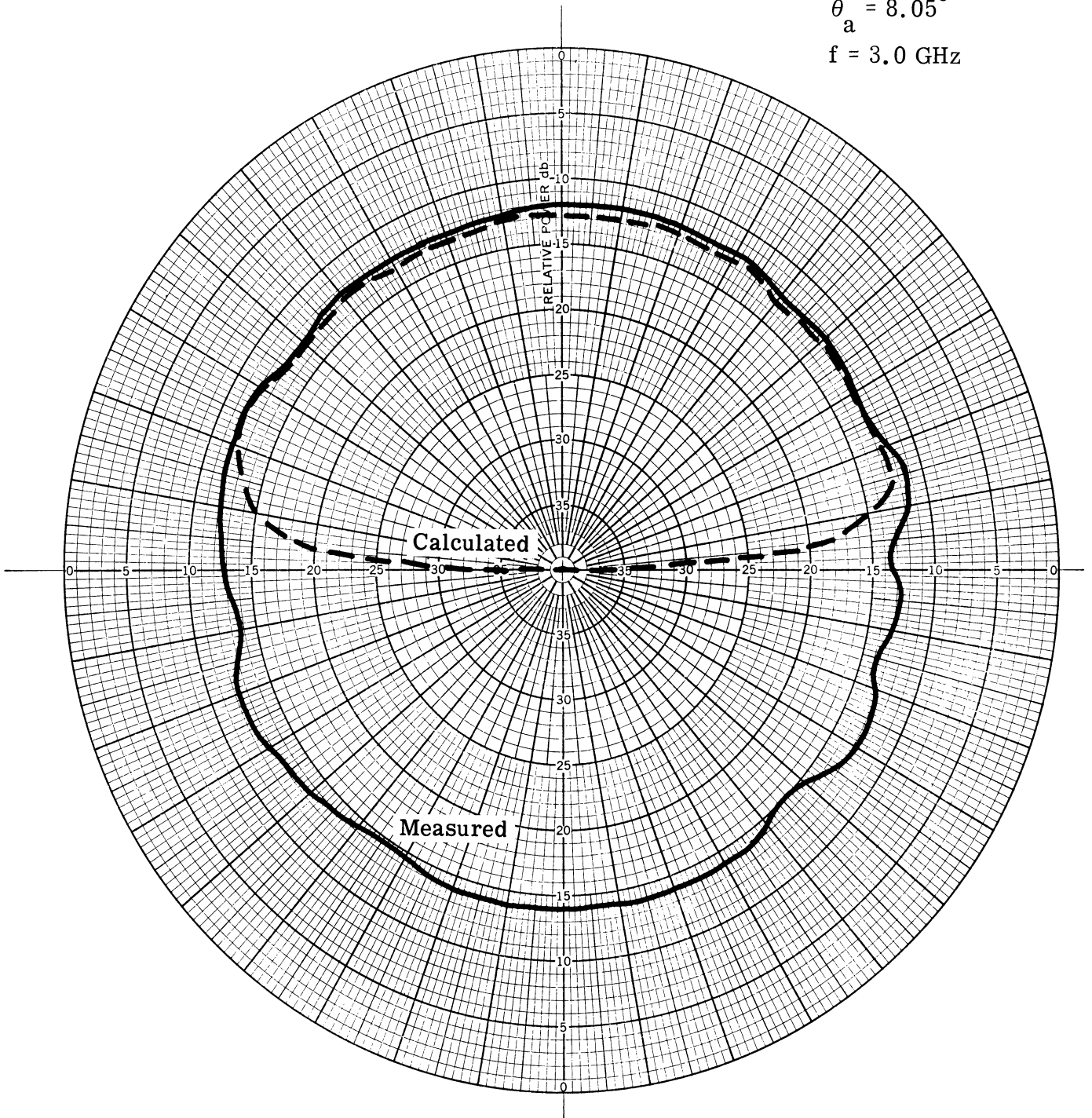
Measured

FIG. 44: H-PLANE THEORETICAL AND MEASURED PATTERN FOR AN ISOTROPIC PANEL

VI

TRANSMISSION OF ELECTROMAGNETIC WAVES
THROUGH A FINITE DIELECTRIC PANEL

6.1 Introduction

In this section we formulate the equations which determine the electric field

which a finite dielectric panel transmits when excited by an electromagnetic source.

Since the panel is finite the free space extensions of the panel surface must be

correctly accounted for. The reason for this is that the source will not only excite

the panel but also the extension of the panel area which is free space. This exten-

sion can be considered as a secondary source of Huygens wavelets which will contri-

bute to the observations point.

In order to evaluate the distant transmitted field we will need to know the

electric field on the surface of the dielectric panel. This field is obtained by using

the plane wave transmission coefficient obtained when the panel is an infinite dielec-

tric sheet. It is expected that this would be a reasonable approximation to describe

the field in the center portion of the finite panel, but near the edges such a repre-

sentation certainly does not hold true. Yet a better approximation to the electric

field on the dielectric panel is hard to obtain without solving the boundary problem

rigorously. It would be interesting to obtain the dielectric field by numerically

integrating the integral equations and comparing it to the approximation used in

these pages.

Three different sources are considered. The first is a plane wave and pre-

sents no particular problems since the integrations can be performed exactly.

The line and spherical sources are more difficult in the sense that part of the

integrations cannot be evaluated exactly. In each case the integrations are carried

out by stationary techniques. The use of the plane wave transmission coefficients

when we have point or line sources is facilitated by decomposing the point source

in an angular spectrum of plane waves.

6.2 Formulation

The vector Huygen's formula for diffraction from an aperture in a plane surface is Jackson (1962) and di Francia (1953a)

$$\underline{E}(\underline{r}) = 2 \iint_{S_\infty} \left(\hat{n}x\underline{E}(\varrho')\right) \times \nabla'G(\underline{r},\varrho')da' \tag{6.1}$$

The normal to the plane surface is $\hat{n}$ and is pointing in the half space in which the diffracted field $\underline{E}(\underline{r})$ is evaluated. In the above form with the integration over the entire surface S_∞, $\underline{E}(\underline{r})$ reproduces the field of the sources which are in the half space in which $-\hat{n}$ is pointing. If the entire surface consists of a perfectly conducting sheet with an aperture S_a in it, the field in the half space in which $\hat{n}$ is pointing is given by

$$\underline{E}(\underline{r}) = 2 \iint_{S_\infty} \left(\hat{n}x\underline{E}(\varrho')\right) \times \nabla'(\underline{r},\varrho')da' \tag{6.2}$$

This is exact if we can substitute in (6.2) the exact field $\underline{E}(\rho')$ in the aperture. Usually in practice one approximates this aperture field by the incident field and calls the above expression the vector Huygens-Kirckhoff formula.

For the case when the surfaces S_a is made up of a dielectric sheet with free space occupying the remaining surface we can write the field in the $+\hat{n}$ half space as

$$\underline{E}(\underline{r}) = 2 \iint_{S_a} \left(\hat{n}x\underline{E}_D(\varrho')\right) \times \nabla'Gda' + 2 \iint_{S_{\infty-a}} \left(\hat{n}x\underline{E}(\varrho')\right) \times \nabla'Gda' \tag{6.3}$$

where $\underline{E}_D$ is the field on the $+\hat{n}$ side of the dielectric sheet. Now if we add and subtract in (6.3) an integral over S_a we can write it as

$$\underline{E}(\underline{r}) = 2 \iint_{S_a} (\hat{n} \times [\underline{E}_D - \underline{E}]) \times \nabla'G \, da' + 2 \iint_{S_\infty} (\hat{n} \times E) \times \nabla'G \, da' \qquad (6.4)$$

The second integral on the right side of (6.4) is just the field of the sources in the -$\hat{n}$ half space; it will be denoted by $\underline{E}_S(\underline{r})$. The total electric field in the presence of the dielectric sheet of area S_a is then

$$\underline{E}(\underline{r}) = 2 \iint_{S_a} (n \times [\underline{E}_D - \underline{E}]) \times \nabla'G \, da' + \underline{E}_S(\underline{r}) \qquad (6.5)$$

Expression (6.5) is exact if we know the exact field E_D on the dielectric panel including the edges of the sheet. We will ignore any dielectric edge effects and approximate E_D by $TE_S(\underline{\rho}')$ at each point on the dielectric panel, where T is the plane wave transmission coefficient of an infinite dielectric panel. This procedure is a crucial step. The accuracy of the analysis depends very much upon the validity of this assumption. It corresponds to a physical optics analysis where the radiation from the -$\hat{n}$ half space is decomposed into rays impinging on the panel. They emerge on the other side of the panel as rays in the same direction, but modified by the transmission coefficient. Expression (6.5) can then be written as

$$\underline{E}(\underline{r}) = 2 \iint_{S_a} (T-1)(\hat{n} \times \underline{E}) \times \nabla'G \, da' + \underline{E}_S(\underline{r}) \qquad (6.6)$$

where G is the free space Green's function $G = e^{-ik_o R}/4\pi R$. The gradient operation on G can be performed explicitly

$$\underline{E}(\underline{r}) = \frac{1}{2\pi} \iint_{S_a} (T-1)(\hat{n} \times \underline{E}) \times \frac{e^{-jkR}}{R} (jk + \frac{1}{R}) \hat{R} \, da' + \underline{E}_S(\underline{r}) \qquad (6.7)$$

If we are interested in field distant from the panel we can made the far field approximation in the integration over S_a. The present formulation which results in (6.5) is particularly suitable for this, since the integration is confined to a finite area and the far field approximation can always be carried out. That is, let

$$R = |\underline{r}-\underline{\rho}'| \cong r-\hat{k}\cdot\underline{\rho}'+ \ldots \tag{6.8}$$

Substituting this in (6.7) we can write

$$\underline{E}(\underline{r}) = \frac{e^{-jik}}{j2\pi r} \underline{k} \times \iint_{S_a} (T-1)(\hat{n}x\underline{E})e^{i\underline{k}\cdot\underline{\rho}'}da' + \underline{E}_S(\underline{r}) \tag{6.9}$$

where $\underline{k}=k\hat{k}$ and $\hat{k}$ is a unit vector pointing in the direction of the observation point $\underline{r}$.

6.3 Plane Wave Sources

Let us now consider the case when a plane wave from the $-\hat{n}$ half space is incident on the dielectric panel. If the dielectric plate lies in the xy plane, as shown in Fig. 45, then $\hat{n}=\hat{i}_z$. For convenience let us consider two cases of plane wave incidence. One will be a variation in the plane of incidence, the other a variation in the perpendicular plane. Each case will then be characterized by one transmission coefficient, i.e. for variation parallel to the plane of incidence we will need only the parallel transmission coefficient $T_{||}$, for variation in the plane perpendicular to the incidence plane $T_{\perp}$.

6.3.1 Variation in the Plane of Incidence

If we have a plane wave incident on the plate an angle θ in the zy plane and polarized parallel to the plane of incidence, its electric field is

$$\underline{E}_S^{||} = E_o(\cos\theta\hat{i}_y - \sin\theta\hat{i}_z)e^{-jk(y\sin\theta + (z+d)\cos\theta)} \tag{6.10}$$

where d is the thickness of the panel. The additional factor d in the phase function $kd\cos\theta$ is introduced since we are using a transmission coefficient (6.18) for which the $-\hat{i}_z$ side of the panel coincided with the $z = 0$ plane. The $\hat{n} \times \underline{E}$ term in (6.9) becomes

$$(\hat{i}_z \times \underline{E}_S^{||})\bigg|_{z=0} = -\hat{i}_x E_o \cos\theta' e^{-jk(y\sin\theta' + d\cos\theta')} \tag{6.11}$$

For a circular plate of radius a, (6.9) reduces to

$$\underline{E}(\underline{r}) = \frac{jE_o e^{-jkr}}{2\pi r} \underline{k} \times \hat{i}_x \int_0^a \int_0^{2\pi} \Big((T_{||}(\theta')-1\Big)\cos\theta' e^{-jk(y'\sin\theta' + d\cos\theta')}$$

$$\cdot e^{jk\rho'\sin\theta\cos(\phi-\phi')}\rho'd\rho'd\phi' + \underline{E}_S^{||} \tag{6.12}$$

where ρ' is a radial distance in the xy plane. Since $y' = \rho'\sin\phi'$ we can write the above expression as

$$\underline{E}(\underline{r}) = \frac{jE_o e^{-jkr}}{2\pi r} \underline{k} \times \hat{i}_x (T_{||}-1)\cos\theta' e^{-jkd\cos\theta'} \tag{6.13}$$

$$\cdot \int_0^a \rho'd\rho' \int_0^{2\pi} e^{-jk\rho'(\sin\theta'\sin\phi' - \sin\theta\cos(\phi-\phi))}d\phi' + \underline{E}_S^{||}$$

Defining an angular function as

$$\xi = (\sin^2\theta' + \sin^2\theta - 2\sin\theta\sin\theta'\sin\phi)^{1/2} \tag{6.14}$$

71

the angular integral can be transformed into

$$\int_0^{2\pi} e^{-jk\rho\xi\cos\phi_0} d\phi_0 = 2\pi J_0(k\rho\xi) \tag{6.15}$$

The radial integral can then be integrated with the aid of

$$\int \rho J_0(\rho) d\rho = \rho J_1(\rho) \tag{6.16}$$

The resulting electric field is then

$$\underline{E}(\underline{r}) = \frac{jE_0 e^{-jk(r+d\cos\theta')}}{r} a^2 \cos\theta' \left(T_{||}(\theta')-1\right) \underline{k} x \hat{i}_x \frac{J_1(da\xi)}{ka\xi} + \underline{E}_S^{||}(\underline{r}) \tag{6.17}$$

The plane wave transmission coefficient for a dielectric panel of thickness d with electric field in the plane of incidence is (Tai et al 1965)

$$T_{||}(\theta') = \frac{(1-r_{||}^2)e^{jd(k\cos\theta'-k_z')}}{1-r_{||}^2 e^{-j2k_z'd}} \tag{6.18}$$

$$r_{||} = \frac{\epsilon_r \cos\theta' - \sqrt{\epsilon_r - \sin^2\theta'}}{\epsilon_r \cos\theta' + \sqrt{\epsilon_r - \sin^2\theta'}} \tag{6.19}$$

$$k_z' = k\sqrt{\epsilon_r - \sin^2\theta'} \tag{6.20}$$

where ϵ_r is the relative dielectric constant of the dielectric panel.

When the dielectric plate is of rectangular shape with sides 2a and 2b, the far field approximation (6.8) for R can be written more conveniently in rectangular coordinates as

$$R \cong r - \frac{xx' + yy'}{r} \tag{6.21}$$

Expression (6.9) for a rectangular plate reduces to

$$\underline{E}(\underline{r}) = \frac{jE_o e^{-jkr}}{2\pi r} \underline{k} x \hat{i}_x (T_{||} - 1)\cos\theta' e^{-jkd\cos\theta'}$$

$$\cdot \int_{-a}^{a} e^{jk\frac{x}{r}x'} dx' \int_{-b}^{b} e^{jk(\frac{y}{r} - \sin\theta')y'} dy' + \underline{E}_S^{||} \tag{6.22}$$

After integration the total electric field in the presence of a rectangular panel becomes

$$\underline{E}(\underline{r}) = \frac{jE_o e^{-jk(r + d\cos\theta')}}{\pi kr} \hat{k} x \hat{i}_x \cos\theta' \frac{2r}{x} \left(T_{||}(\theta') - 1\right)$$

$$\cdot \sin\frac{kax}{r} \frac{\sin kb(\frac{y}{r} - \sin\theta')}{\frac{y}{r} - \sin\theta'} + \underline{E}_S^{||}(\underline{r}) \tag{6.23}$$

Stating the above expression in spherical coordinates by replacing x and y by $r\sin\theta\cos\emptyset$ and $r\sin\theta\sin\emptyset$,

$$E(\underline{r}) = \frac{jE_o e^{-jk(r + d\cos\theta')}}{\pi kr} (\sin\phi \hat{i}_\theta + \cos\theta\cos\phi \hat{i}_\phi) \frac{2\cos\theta'}{\sin\theta\cos\phi}$$

$$\cdot \left(T_{||}(\theta') - 1\right) \sin(ka\sin\theta\cos\phi) \frac{\sin kb(\sin\theta\sin\phi - \sin\theta')}{\sin\theta\sin\phi - \sin\theta'} + \underline{E}_S^{||}(\underline{r})$$

6.3.2 Variation Perpendicular to the Plane of Incidence

If we have a plane wave incident on the plate at an angle θ in the zx plane and polarized perpendicular to the plane of incidence, its electric field is

$$\underline{E}_S^\perp = E_o \hat{i}_y e^{-jk[x\sin\theta + (z+d)\cos\theta]} \tag{6.24}$$

The $\hat{n} \times \underline{E}$ term in the xy plane becomes

$$(\hat{i}_z \times \underline{E}_S^\perp)\bigg|_{z=0} = -\hat{i}_x E_o e^{-jk(x'\sin\theta' + d\cos\theta')} \tag{6.25}$$

In the above expression we can replace x' with $x' = \rho'\cos\phi'$. Substituting this in (6.9) we obtain

$$E(\underline{r}) = \frac{jE_o e^{-jkr}}{2\pi r} \underline{k} \times \hat{i}_x \left(T_\perp(\theta') - 1\right) e^{-jkd\cos\theta'}$$

$$\cdot \int_o^a \rho'd\rho' \int_o^{2\pi} e^{-jk\rho'\left[\sin\theta'\cos\phi' - \sin\theta\cos(\phi - \phi')\right]} d\phi' + \underline{E}_S^\perp \tag{6.26}$$

To integrate the angular part we can define an angular function as

$$\xi = (\sin^2\theta' + \sin^2\theta - 2\sin\theta'\sin\theta\cos\phi)^{1/2} \tag{6.27}$$

With the help of this the $\emptyset'$ integral can be transformed into

$$\int_0^{2\pi} e^{-jk\rho\xi\cos\emptyset_o} d\emptyset_o = 2\pi J_o(k\rho\xi) \tag{6.28}$$

The radial part can then be integrated with the aid of (6.16) to yield

$$\underline{E}(\underline{r}) = \frac{jE_o e^{-jk(r+d\cos\theta')}}{r} a^2 \left(T_\perp(\theta')-1\right)\underline{k}x\underline{i}_x \frac{J_1(k\xi a)}{k\xi a} + \underline{E}_{\underline{S}}^{\perp} \tag{6.29}$$

The plane wave transmission coefficient $T_\perp$ for perpendicular polarization is identical to $T_{||}$ as given by (6.18) except that in (6.18) $r_{||}$ should be replaced by

$$r_\perp = \frac{\cos\theta' - \sqrt{\epsilon_r - \sin^2\theta'}}{\cos\theta + \sqrt{\epsilon_r - \sin^2\theta'}} \tag{6.30}$$

When the dielectric plate is of rectangular shape we can follow the same procedure that was used to obtain (6.23). Expression (6.9) for a rectangular plate with the incident wave E_S of (6.24) becomes then

$$\underline{E}(\underline{r}) = \frac{jE_o e^{-jkr}}{2\pi r} \underline{k}x\hat{i}_x \left(T_\perp(\theta')-1\right)e^{-jkd\cos\theta'} \int_{-a}^{a} e^{jk(\frac{x}{r}-\sin\theta')x'} dx'$$

$$\cdot \int_{-b}^{b} e^{jk\frac{y}{r}y'} dy' + \underline{E}_{\underline{S}}^{\perp} \tag{6.31}$$

Integrating this expression we obtain

$$\underline{E}(\underline{r}) = \frac{jE_o e^{-jk(r+d\cos\theta')}}{\pi kr} \hat{k}x\hat{i}_x (T_\perp - 1) \frac{2x}{y} \frac{\sin ka(\frac{x}{r}-\sin\theta')}{\frac{x}{r}-\sin\theta'} \sin\frac{kyb}{r} + \underline{E}_S^\perp (\underline{r})$$

(6.32)

as the total electric field in the presence of a rectangular dielectric plate.

6.4 Line Sources

Let us now consider an infinite dielectric strip excited by an electric or magnetic line source which is parallel to the infinite axis of the strip. After formulating the two-dimensional problem rigorously we will again make use of the physical optics approximation which will permit us to use the plane wave transmission coefficient to obtain the field in the dielectric.

The vector Huygens' formula (6.1) appropriate for a two-dimensional body like the strip can be obtained from (6.5) by letting one dimension of the area S_a go to infinity. When the excitation is a line source parallel to the strip, the $\hat{n}x\underline{E}$ term in the integrand will be independent of the axial coordinate of the line source. Let us assume that we have a strip in the xy plane, infinite in the x direction and of width 2b in the y direction which is excited by a magnetic line source positioned at $z = -(h + d) = -h'$, and $y = 0$. The geometry is shown in Fig. 46. Equation (6.5) can then be written as

$$\underline{E}(\underline{\rho}) = \frac{-1}{2\pi} \int_{-b}^{b} \hat{n}x\left[\underline{E}_D(y') - \underline{E}(y')\right] dy' x \nabla \int_{-\infty}^{\infty} \frac{e^{-jk\sqrt{(x-x')^2+(y-y')^2+z^2}}}{\sqrt{(x-x')^2+(y-y')^2+z^2}} dx' + \underline{E}_S(\underline{\rho})$$

(6.33)

Since $\nabla' = -\nabla$ when operating on the Greens' function. We can integrate the x' part with the aid of (Magnus and Oberhettinger, 1949)

$$H_o^{(2)}(k\gamma) = \frac{j}{\pi} \int_{-\infty}^{\infty} \frac{e^{-jk\sqrt{\gamma^2+t^2}}}{\sqrt{\gamma^2+t^2}}\, dt \qquad (6.34)$$

to give

$$\underline{E}(\underline{\rho}) = \frac{1}{2j} \int_{-b}^{b} \hat{n} \times [\underline{E}_D - \underline{E}] \times \nabla' H_o^{(2)}\left[k\sqrt{(y-y')^2+z^2}\right] dy' + \underline{E}_S(\underline{\rho}) \qquad (6.35)$$

If we are interested in the far field approximation we can make use of the asymptotic forms for the Hankel function with the approximation

$$\sqrt{(y-y')^2+z^2} \cong \rho - \frac{yy'}{\rho} \qquad (6.36)$$

and

$$\nabla' H_o^{(2)} \cong je^{j\frac{\pi}{4}}\sqrt{\frac{2k}{\pi\rho}}\, e^{-jk\rho+jk\frac{yy'}{\rho}}\, \hat{\rho} \qquad (6.37)$$

We obtain then

$$\underline{E}(\underline{\rho}) = \sqrt{\frac{k}{2\pi\rho}}\, e^{-j(k\rho-\frac{\pi}{4})} \int_{-b}^{b} \left(\hat{n} \times [\underline{E}_D - \underline{E}]\right) \times \hat{\rho} e^{jk\frac{yy'}{\rho}}\, dy' + \underline{E}_S(\underline{\rho}) \qquad (6.38)$$

where ρ is the radial distance in the zy plane.

If we have a magnetic line source, its electric field is given by

$$\underline{E}_s(\underline{\rho}) = \hat{i}_\theta E_o H_1^{(2)} \left[k\sqrt{(z+h')^2+y^2} \right] \tag{6.39}$$

If the argument of the above Hankel function is large, i.e. the line source is many wavelengths from the strip, the asymptotic expression of (6.39) becomes

$$\underline{E}_s(\underline{\rho}) = \hat{i}_\theta E_o j\sqrt{\frac{2}{\pi k}} \frac{e^{-jk\sqrt{(z+h')^2+y^2}+j\frac{\pi}{4}}}{\left[(z+h')^2+y^2)\right]^{1/4}} \tag{6.40}$$

We now consider this as a bundle of rays which originate at $z = -h'$, $y = 0$ and impinge on the dielectric strip at various angles θ'. It will be assumed that each of these rays passes through the dielectric modified by the transmission coefficient T and emerges on the other side of the strip as TE_s. Hence the $\hat{n}x$ term in (6.38) becomes

$$\hat{i}_z \times (\underline{E}_o - \underline{E}) \Big|_{z=0} = -\hat{i}_x \cos\theta' \left(T_{||}(\theta')-1 \right) j E_o \sqrt{\frac{2}{\pi k}} \frac{e^{-jk\sqrt{(h')^2+y'^2}+j\frac{\pi}{4}}}{\left[(h')^2+y'^2\right]^{1/4}} \tag{6.41}$$

where $T_{||}$ is given by (6.18).

The integration variables are θ' and y' and are related to each other by y' = h'tanθ'. The observation variables are ρ and y or y = ρsinθ and $\hat{\rho}x\hat{i}_x = \hat{i}_\theta$. With these transformations and (6.41) substituted in (6.38) we obtain for the total electric field

$$\underline{E}(\rho) = -\frac{e^{-jk\rho}}{\pi\sqrt{k\rho}}\, E_o\, \hat{i}_\theta \int_{-\theta_b}^{\theta_b} \left(T_{||}(\theta') - 1\right)\sqrt{kh'\sec\theta'}\; e^{-jkh'(\sec\theta' - \sin\theta\tan\theta')}\, d\theta' + \underline{E}_s(\rho)$$

$$(6.42)$$

where $\theta_b = \arctan b/h'$ and the far field of the line source $\underline{E}_s(\rho)$ is given by (6.40).
A further simplification results if we assume that the point of observation is much
farther from the origin than the line source is, i.e. $\rho \gg h'$. Equation (6.40) can
then be written as

$$\underline{E}_s(\rho) = \hat{i}_\theta E_o j \sqrt{\frac{2}{\pi k\rho}}\; e^{-jk(\rho + h'\cos\theta) + j\frac{\pi}{4}}$$

$$(6.43)$$

The total electric field in the $\hat{i}_z$ half space in the presence of the dielectric strip
can then be written as

$$\underline{E}(\rho) = -\frac{E_o\,\hat{i}_\theta}{\pi}\frac{e^{-jk\rho}}{\sqrt{k\rho}}\left[\int_{-\theta_b}^{\theta_b}(T_{||} - 1)\sqrt{k(h+d)\sec\theta'}\; e^{-jkh'(\sec\theta' - \sin\theta\tan\theta')}d\theta' \right.$$

$$\left. + \sqrt{\frac{2\pi}{j}}\; e^{-jkh'\cos\theta}\right]$$

$$(6.44)$$

where $h' = h + d$.

This can be integrated by the stationary phase method if $kh \gg 1$. Differen-
tiating the phase term one can show that the stationary phase point is given by $\theta' = \theta$.
This corresponds to a ray which impinges on the panel and emerges from the panel
in the same direction. Hence the integral will have a stationary point only as long
as the observation direction θ is less than the integration angle θ_b, i.e. $\theta < \theta_b$.

For observation angles which are less than the angle which the line source makes with the panel, the stationary phase method yields for the integral

$$\int_{-\theta_b}^{\theta_b} \ldots = \left(T_{||}(\theta) - 1\right)\sqrt{\frac{2\pi}{j}}\, e^{-jkh'\cos\theta} \qquad \theta < \theta_b \qquad (6.45)$$

Substituting this result in (6.44) the total electric field becomes

$$\underline{E}(\underline{\rho}) = \underline{E}_s(\underline{\rho})T_{||}(\theta) = \hat{i}_\theta E_o j\sqrt{\frac{2}{\pi k\rho}}\, e^{-jk(\rho + h'\cos\theta) + j\frac{\pi}{4}}\, T_{||}(\theta) \qquad (6.46)$$

From the above result we can deduce that for $\theta < \theta_b$, that is when the observation point angle is such that we cannot see the line source since it is in the shadow of the panel the fields have a plane wave behavior. Another way of stating this is that the transmitted field is due to a line source with radiation pattern or polar diagram $T_{||}(\theta)$.

For observation angle $\theta > \theta_b$ when both the line source and the panel are visible the direct radiation by the line source should be the significant contribution to the total field in the $\hat{i}_z$ half space. Since the stationary point angle is now outside the range of angles which define the integration limits a different method of approximately evaluating the integral must be found. When $kr \gg 1$ we can obtain a series in powers of $1/kr$ by partial integration (di Francia 1953b). However, it is doubtful whether such a procedure would yield results which are more accurate than simply approximating the field for $\theta > \theta_b$ by the primary field. Unless the integral can be evaluated accurately in this region it might be best to make the approximation by the primary field.

Even if the integral is evaluated accurately the results so obtained should be viewed with caution for observation angles $\theta \approx \theta_b$. This is the region where the radial plane waves vary rapidly as they change from transmission through the panel to free space. A better estimation of the $\hat{n} \times \underline{E}$ term in the integrand, i.e. one more accurate than the sudden jump from TE to E assumed in this analysis might be desirable.

For the range of observation angles $\theta < \theta_b$ we can also conclude that the stationary phase method of approximating the integral gives a transmitted total field for the strip which is identical to the field of an infinite panel. Expression (6.46) is obtained when transmission through a panel infinite in the x and y direction is considered (Senior, 1958). This could have been expected since the finite limits of an integral that is evaluated by the stationary phase method can be extended to infinity, provided that the stationary points exist in the interval defined by the integration limits. Hence the transmitted field appears as due to a line source E_s with radiation pattern or polar diagram $T_{||}$.

Let us now consider the case when a dielectric strip is excited by an electric line source, as shown in Fig. 47. The electric field of the line source is given by

$$\underline{E}_s(\rho) = \hat{i}_y E_o H_o^{(2)} \left[k\sqrt{(z+h+d)^2+x^2} \right] \tag{6.47}$$

The total electric field in the presence of the dielectric strip is then given by (6.38) with y and y' exchanged by x and x' respectively. The polar distance ρ is now in the zx plane. All of the steps that were used when the magnetic line source was considered can now be repeated for this case with the exception that the vector part of the $\hat{n} \times$ term in the integrand is now given by $\hat{i}_z \times \hat{i}_y = -\hat{i}_x$ and the observation vector is given by $\hat{\rho} \times \hat{i}_x = \hat{i}_y \cos\theta$. The total electric field in the presence of the

dielectric strip is then given by

$$
\underline{E}(\underline{\rho}) = \frac{j\hat{i}_y E_o}{\pi} \frac{e^{-jk\rho}}{\sqrt{k\rho}} \left[\cos\theta \int_{-\theta_a}^{\theta_a} \left(T_\perp(\theta') - 1 \right) \sqrt{kh'\sec^3\theta'}\ e^{-jkh'(\sec\theta' - \sin\theta\tan\theta')} d\theta' \right.
$$

$$
\left. + \sqrt{\frac{2\pi}{j}}\ e^{-jkh'\cos\theta} \right] \tag{6.48}
$$

where the width of the strip in the x-direction is 2a, hence $\theta_a = \arctan a/h'$ and $T_\perp$ is given by (6.18) and (6.30). The integration can again be performed approximately by using the stationary phase method.

6.5 Spherical Sources

Transmission through a dielectric panel excited by a magnetic or electric dipole will now be considered. The field of the point source will be treated as a three-dimensional plane wave which at each point on the dielectric is transmitted according to the plane wave transmission coefficient T. The field of a point source is composed of an angular spectrum of parallel and perpendicular polarized plane waves. Let us consider a dipole which is located a distance h' along the negative z-axis.

6.5.1 Magnetic Dipoles

If we have a finite dielectric panel of thickness d positioned such that its $\hat{i}_z$ face coincides with the xy plane, then the dipole will be at a distance h from the $-\hat{i}_z$ face of the panel (h' = h + d). If we use a small slot antenna, with dimensions much smaller than a wavelength, to excite the dielectric plate, a good approximation to its radiation pattern is the field of a magnetic dipole oriented such that its axis is parallel to the long dimension of the slot. The electric field of a

magnetic dipole oriented along the x-axis, as shown in Fig. 48 is given by (Jackson, 1962)

$$\underline{E}_s(r, \theta, \phi) = E_o(\hat{k} \times \hat{i}_x) \frac{e^{-jkR}}{R}$$

$$= E_o(\sin\phi \hat{i}_\theta + \cos\theta\cos\phi \hat{i}_\phi) \frac{e^{-jkR}}{R} \tag{6.49}$$

where $R = (r^2 + h'^2 + 2rh'\cos\theta)^{1/2}$. When the observation point r is far from the origin, R can be approximated by

$$R = r + h'\cos\theta \tag{6.50}$$

Upon further examination of the above expression we find that the $\hat{i}_\theta$ component corresponds to a parallel polarized wave and the $\hat{i}_\phi$ part to perpendicular polarization. Hence upon transmission through the dielectric the field on the $\hat{i}_z$ side of the plate can be approximated by

$$\underline{E}_D = E_o \left(T_{||}(\theta')\sin\phi'\hat{i}_\theta + T_{\perp}(\theta')\cos\theta'\cos\phi'\hat{i}_\phi \right) \frac{e^{-jkR'}}{R'} \tag{6.51}$$

where $R' = (h'^2 + \rho'^2)^{1/2} = h'\sec\theta'$ and $\rho' = (x'^2 + y'^2)^{1/2}$. The total observed far field in the presence of the dielectric plate can then be written from (6.9) as

$$\underline{E}(\underline{r}) = \frac{E_o e^{-jkr}}{j2\pi r} \underline{k} \times \iint_{S_a} \hat{i}_z \times \left[\left(T_{||}(\theta') - 1 \right)\sin\phi' \hat{i}_\theta + \left(T_{\perp}(\theta') - 1 \right)\cos\phi'\hat{i}_\phi \right]$$

$$\cdot \; \frac{e^{-jk(R' - \hat{k} \cdot \underline{\rho}')}}{R'} \; da' + \frac{E_o}{r} \; (sin\phi \, \hat{i}_\theta + cos\theta cos\phi \, \hat{i}_\phi) e^{-jk(r + h'cos\theta)}$$

(6.52)

The vector triple products simplify to

$$\hat{r} \times (\hat{i}_z \times \hat{i}_\theta) = -\hat{i}_\theta cos\theta'$$

(6.53)

$$\hat{r} \times (\hat{i}_z \times \hat{i}_\phi) = -\hat{i}_\phi cos\theta'$$

If we now have a circular plate of radius a, the total transmitted electric field is given by

$$\underline{E}(\underline{r}) = \frac{jE_o e^{-jkr}}{2\pi r} \; kh' \int_0^{\theta_a} \int_0^{2\pi} \left[(T_{||} - 1) \, sin\phi' cos\theta' \hat{i}_\theta + (T_\perp - 1) cos^2\theta' cos\phi' \hat{i}_\phi \right]$$

(6.54)

$$\cdot e^{-jkh' \left[sec\theta' - sin\theta tan\theta' cos(\phi - \phi') \right]} tan\theta' sec\theta' d\theta' d\phi' + E_s(\underline{r})$$

where ρ' is replaced by $\rho' = h'tan\theta'$ and $\theta_a = arctan\, a/h'$. The ϕ' - integration can be performed with the aid of the integrals

$$\int_0^{2\pi} cos\phi' e^{j\gamma cos(\phi - \phi')} d\phi' = 2\pi j cos\phi J_1(\gamma)$$

(6.55)

$$\int_0^{2\pi} sin\phi' e^{j\gamma cos(\phi - \phi')} d\phi' = 2\pi j sin\phi J_1(\gamma)$$

Using these expressions in (6.54), we obtain for the total field

$$
\underline{E}(\underline{r}) = \frac{-E_o\, e^{-jkr}}{r} \left\{ kh' \int_0^{\theta_a} \left[(T_{||} - 1)\sin\phi J_1(\gamma)\hat{i}_\theta + (T_\perp - 1)\cos\theta'\cos\phi J_1(\gamma)\hat{i}_\phi \right] \right.
$$

$$
\left. \cdot e^{-jkh'\sec\theta'}\tan\theta'd\theta' - (\sin\phi\,\hat{i}_\theta + \cos\theta\cos\phi\,\hat{i}_\phi)e^{-jkh'\cos\theta} \right\} \qquad (6.56)
$$

where $\gamma = kh'\sin\theta\tan\theta'$. Explicit evaluation of the integral over θ' is a difficult, if not impossible, task. A numerical integration with a computer might be a logical approach. A stationary phase evaluation can again be applied. However, doing so, the additional accuracy gained in evaluating the ϕ - integration exactly will be lost. It is well known that if one integration of a double integral is done exactly and the second by stationary phase method, the results are only as accurate as if both integrations were performed by stationary phase. As a matter of fact, to do the θ' - integration by stationary phase we must first replace J_1 by $J_1 = (H_1^{(1)} + H_1^{(2)})/2$ and then find the stationary phase point. After differentiating the phase term we find two stationary points for $\theta' = \pm\theta$. However, $\theta' = -\theta$ is outside the range of integration and in a first order analysis must be discarded. The real stationary point is at $\theta' = \theta$ which is obtained from $H_1^{(1)}$. The final results of a stationary integration of (6.56) is then

$$
\underline{E}(\underline{r}) = \frac{E_o\, e^{-jk(r+h'\cos\theta)}}{r} \left[T_{||}(\theta)\sin\phi\,\hat{i}_\theta + T_\perp(\theta)\cos\theta\cos\phi\,\hat{i}_\phi) \right] \qquad (6.57)
$$

valid for observation angles for which $\theta < \theta_a$.

If we have a rectangular dielectric plate as shown in Fig. 48, the formulation

appropriate for this geometry is, from (6.52),

$$\underline{E}(\underline{r}) = \frac{jkE_o e^{-jkr}}{2\pi r} \int_{-a}^{a} \int_{-b}^{b} \left[\left(T(x',y')-1\right) \frac{y'}{\rho'} \frac{h'}{R'} \hat{i}_\theta + \left(T(x',y')-1\right) \frac{h'^2}{R'^2} \frac{x'}{\rho'} \hat{i}_\phi \right]$$

$$\cdot \frac{e^{-jk(R'+\frac{x}{r}x'+\frac{y}{r}y')}}{R'} dx'dy' + \frac{E_o}{r} (\sin\phi \hat{i}_\theta + \cos\theta\cos\phi \hat{i}_\phi)e^{-jk(r+h'\cos\theta)} \qquad (6.58)$$

where the angular functions are replaced by

$$\cos\theta' = \frac{h'}{R'} = \frac{h'}{\sqrt{\rho'^2 + h'^2}}$$

$$\sin\theta' = \rho'/R \qquad (6.59)$$

$$\cos\phi' = \frac{x'}{\rho'} = \frac{x'}{(x'^2 + y'^2)^{1/2}} \qquad \sin\phi' = \frac{y'}{\rho'}$$

Unfortunately, the transmission coefficients are now a function of both integration variables. An explicit evaluation seems a difficult task. Resorting to stationary phase techniques, the integration of (6.58) yields an expression identical to (6.57), but valid for observation angles $\theta < \arctan\rho'/h'$. The maximum angle of observation for which (6.57) applies occurs when $\rho' = \sqrt{a^2 + b^2}$ at an azimuth angle of $\phi = \arctan b/a$.

6.5.2 Electric Dipoles

The electric field of an electric dipole, oriented along the y-axis is given by [1]

$$\underline{E}_s(\underline{r}) = E_o(\hat{k} \times \hat{i}_y) \times \hat{k} \frac{e^{-jkR}}{R}$$

(6.60)

$$= E_o \left[\cos\theta\sin\phi\, \hat{i}_\theta + \cos\phi\, \hat{i}_\phi \right] \frac{e^{-jkR}}{R}$$

Following the procedure of the last section for a magnetic dipole we obtain for the total electric field in the presence of a circular dielectric plate which is illuminated by an electric dipole

$$\underline{E}(\underline{r}) = \frac{-E_o kh' e^{-jkr}}{r} \int_0^{\theta_a} \left[\left(T_{||}(\theta') - 1 \right) \cos\theta'\sin\phi J_1(\gamma) \hat{i}_\theta + \left(T_\perp(\theta') - 1 \right) \cos\phi J_1(\gamma) \hat{i}_\phi \right]$$

$$\cdot e^{-jkh'\sec\theta'} \tan\theta' d\theta' + \frac{E_o}{r} (\cos\theta\sin\phi\, \hat{i}_\theta + \cos\phi\, \hat{i}_\phi) e^{-jk(r+h'\cos\theta)}$$

(6.61)

After a stationary phase integration the above expression reduces to

$$\underline{E}(\underline{r}) = \frac{E_o e^{-jk(r+h'\cos\theta)}}{r} \left[T_{||}(\theta) \cos\theta\sin\phi\, i_\theta + T_\perp(\theta) \cos\phi\, i_\phi \right]$$

(6.62)

valid for $\theta < \theta_a$.

For a rectangular plate the electric field is expressed by

$$\underline{E}(\underline{r}) = \frac{jkE_o e^{-jkr}}{2\pi r} \int_{-a}^{a} \int_{-b}^{b} \left[\left(T_{||}(x',y') - 1 \right) \frac{h'^2}{R'^2} \frac{y'}{\rho'} \hat{i}_\theta + \left(T_\perp(x',y') - 1 \right) \frac{h'}{R'} \frac{x'}{\rho'} \hat{i}_\phi \right]$$

87

$$\cdot \frac{e^{-jk(R' + \frac{x}{r}x' + \frac{y}{r}y')}}{R'} \, dx'dy' + \underline{E}_s(\underline{r}) \tag{6.63}$$

A stationary phase evaluation of the double integral is given by (6.62) and is valid for $\theta < \arctan\rho'/h'$.

6.6 Computations

The integrations of (6.44), (6.48) and (6.56) were performed numerically on an IBM 7090 computer and are presented graphically in Figs. 49, 50, 51 and 52. Equation (6.44) gives the total transmitted field in the presence of a dielectric strip which is excited by a magnetic line source as shown in Fig. 46. Since only the angular variation θ and the source spacing kh' are desired as parameters, (6.44) was rewritten as

$$\underline{E}(\rho) = - \frac{E_o \hat{i}_\theta}{\pi} \frac{e^{-jk\rho}}{\sqrt{k\rho}} F_{||}(\theta, h') \, . \tag{6.64}$$

Figure 49a, b shows the relative transmitted power $F(\theta, h')^2/(2\pi)$ versus observation angle θ for various spacings kh' and for two panel thicknesses $kd = \pi/8$ and π. (If d is assumed to be 1", these two values correspond to 740 Mc and 5920 Mc.) In all cases the dielectric was assumed to have a relative dielectric constant $\epsilon_r = 4$. For comparison, the square of the transmission coefficient T of (6.18) was also included in the figure. It is seen that the variation in transmitted field when the panel thickness is $kd = \pi$ is more drastic than that of $kd = \pi/8$. A similar observation can be made when $kd = \pi/2$.

The curves of Fig. 50a, b are the results of (6.48) which is the transmitted

field in the presence of a dielectric strip which is excited by an electric line source as shown in Fig. 47. Equation (6.48) was rewritten as

$$\underline{E}(\rho) = \frac{j\hat{i}_y E_o}{\pi} \frac{e^{-jk\rho}}{\sqrt{k\rho}} F(\theta, h') \tag{6.65}$$

Figure 50a, b shows the relative transmitted power $\left|F_\perp\right|^2/(2\pi)$.

Figure 51 and 52 represents the results of (6.56) which gives the transmitted field in the presence of a dielectric disc which is excited by a magnetic dipole. The geometry is shown in Fig. 48 with disc radius a. For computational purposes (6.56) was rewritten as

$$\underline{E}(\underline{r}) = -\frac{E_o e^{-jkr}}{r} F^d(\theta, \phi, h'). \tag{6.66}$$

Now we can see that we have an additional perimeter ϕ that must be specified. In the computations we limited ourselves to two values of ϕ, namely $\phi = 0$, $\pi/2$. The first value of ϕ corresponds to the H-plane pattern $F_\perp^d = F^d(\phi = 0)$ and is

$$F_\perp^d = kh' \int_0^{\theta_a} \left(T_\perp(\theta') - 1\right)\cos\theta' J_1(\gamma) e^{-jkh'\sec\theta'} \tan\theta' d\theta' - \cos\theta e^{-jkh'\cos\theta} \tag{6.67}$$

It is seen that only the transmission coefficient $T_\perp$ of perpendicularly polarized waves enters in the H-plane pattern; these graphs, $\left|F_\perp^d\right|^2$, are plotted in Fig. 51a, b.

The second value of ϕ corresponds to the E-plane diffraction pattern $F_{||}^d = F^d(\phi = \pi/2)$ which is given by

$$F_{||}^d = kh' \int_0^{\theta_a} \left(T_{||}(\theta') - 1\right) J_1(\gamma) e^{-jkh'\sec\theta'} \tan\theta' d\theta' - e^{-jkh'\cos\theta} . \qquad (6.68)$$

Here we see that only $T_{||}$ enters in the E-plane pattern. The plots of $\left| F_{||}^d \right|^2$ are shown in Fig. 52a, b.

6.7 Conclusion

The equations for the transmitted electric field through a dielectric panel are formulated by means of Huygen's principle. The electric field on the dielectric surface which is needed in the integrand expressions is approximated by using the plane wave transmission coefficient of an infinite dielectric sheet. The difficulty in obtaining the electric field is that some integrations cannot be done exactly when the exciting sources are of a cylindrical and spherical nature. Since in these cases the integrations are performed by stationary means it would now be interesting to compare the results obtained by the stationary phase method to more exact integrations of the equations by numerical means with the aid of a computer. The important conclusion that could be drawn from this would concern the validity of approximating the transmitted electric field by the field of an infinite sheet when the point source is in the shadow of the panel as viewed from the observation point and approximating by the field of the source alone whenever the source comes into view from the observation point.

An examination of Figs. 49 through 52 shows that such an approximation would not be a very good one. When the source is spaced a distance kh', which is not very large, the total transmitted field shows large variations. These variations have hardly any resemblence to the transmission coefficient T or the source variation. As the source spacing increases and the angle between the source and the

dielectric panel decreases the resemblence between the calculated fields and the variation in transmission coefficient and the variation of the source field increases: however, only for a certain range of angles. For example, when kh' $\rightarrow$ ∞ (plane wave incidence is approached), the plotted variation is very pronounced for angles θ not far from zero and no resemblence to T exists. As the observation angle θ increases, the field variation decreases. For angles very close to $\pi/2$ an approximation by the source alone is reasonable.

That a simple approximation by T and by the source alone cannot be made even when kh' $\rightarrow$ ∞ can also be seen directly from the expression for a plane wave incidence, (6.17) and (6.29). Equation (6.17) corresponds to the E-plane diffraction pattern and (6.29) to the H-plane pattern. These equations are of a sufficiently complicated nature that an approximation by the transmission coefficient and the source alone would be unreasonable to expect.
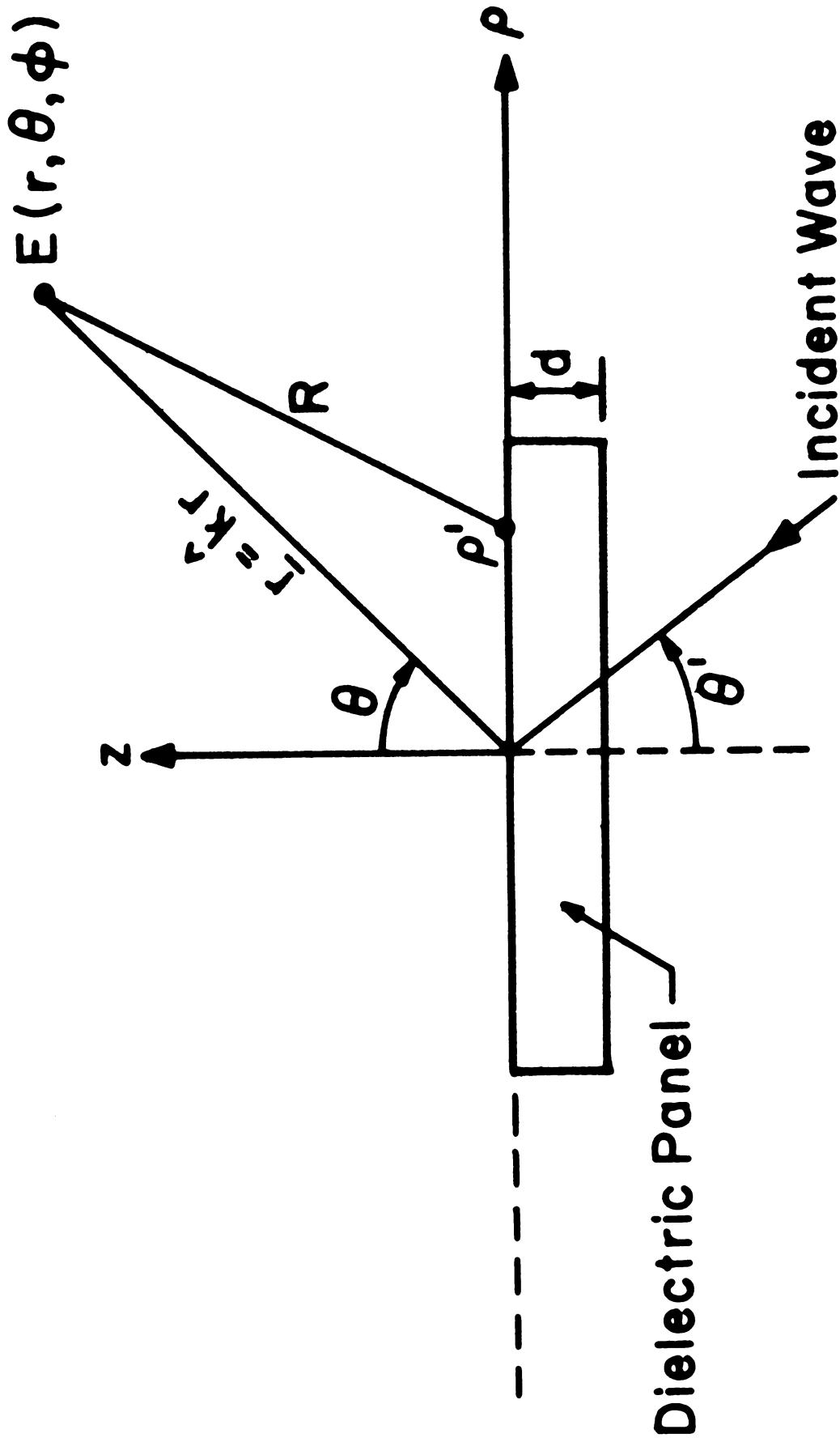
FIG. 45: A PLANE WAVE INCIDENT ON A DIELECTRIC PANEL. $\rho = (x^2 + y^2)^{1/2}$.
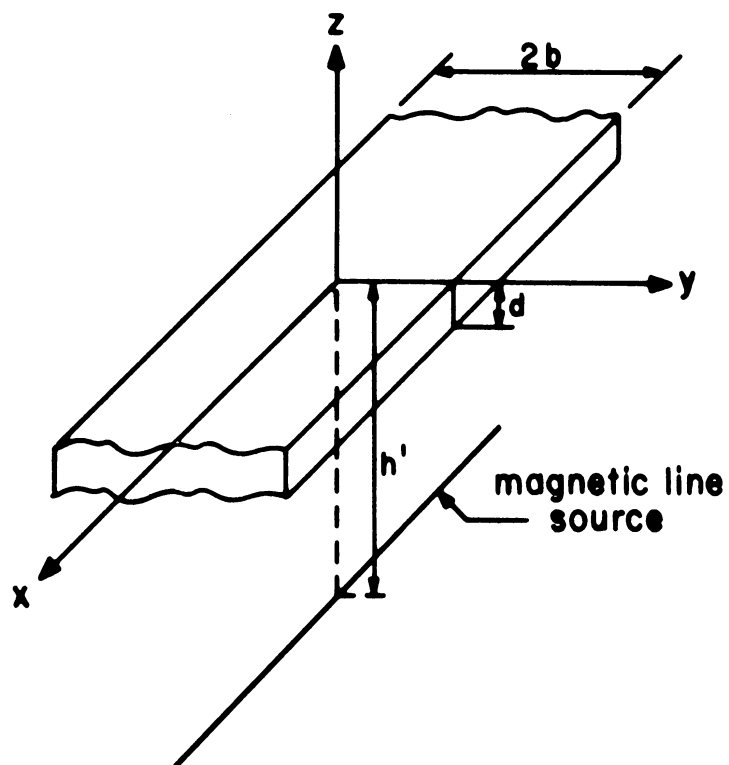
FIG. 46: A MAGNETIC LINE SOURCE LOCATED A DISTANCE h FROM A
DIELECTRIC STRIP OF THICKNESS d. (h' = h + d).
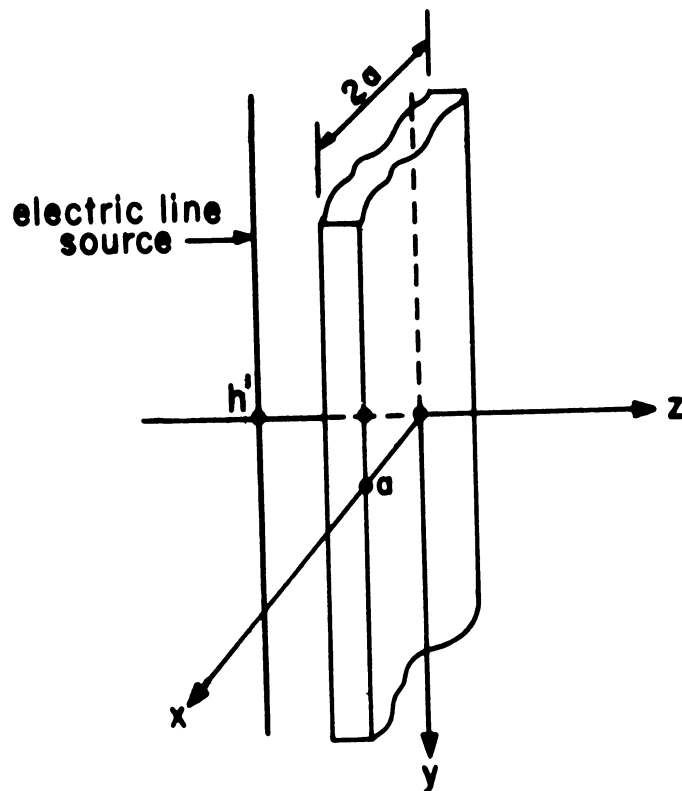
FIG. 47: AN ELECTRIC LINE SOURCE LOCATED A DISTANCE h FROM A
DIELECTRIC STRIP OF THICKNESS d. (h' = h + d).
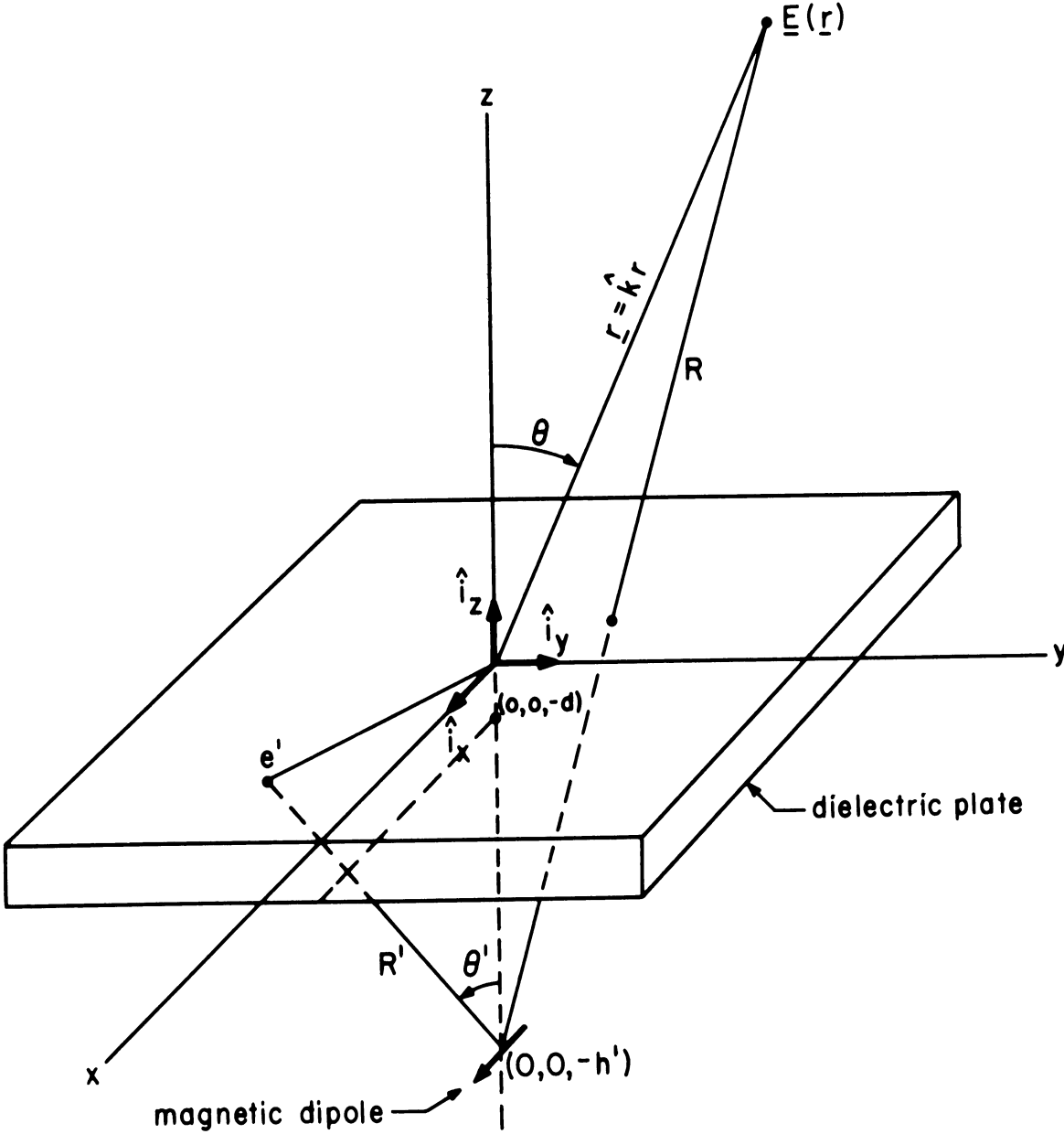
FIG. 48: GEOMETRY OF THE DIELECTRIC PLATE EXCITED BY A SPHERICAL
          SOURCE.
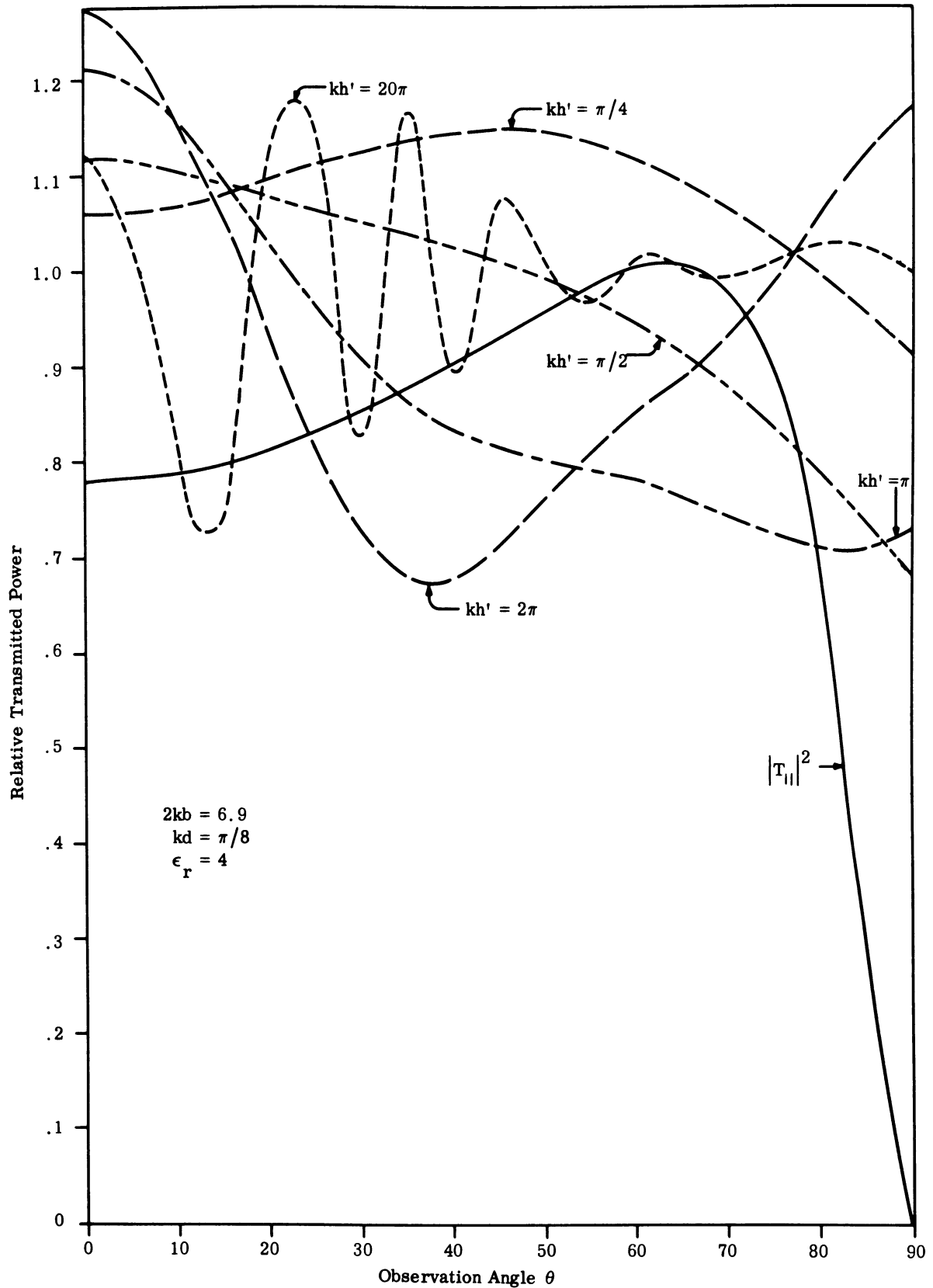
FIG. 49a: TRANSMITTED POWER VERSUS OBSERVATION ANGLE θ FOR 5 SPACINGS kh' OF THE MAGNETIC LINE SOURCE WHICH EXCITES AN INFINITE DIELECTRIC STRIP.

FIG. 49b: TRANSMITTED POWER VERSUS OBSERVATION ANGLE θ FOR 5 SPACINGS kh' OF THE MAGNETIC LINE SOURCE WHICH EXCITES AN INFINITE DIELECTRIC STRIP.
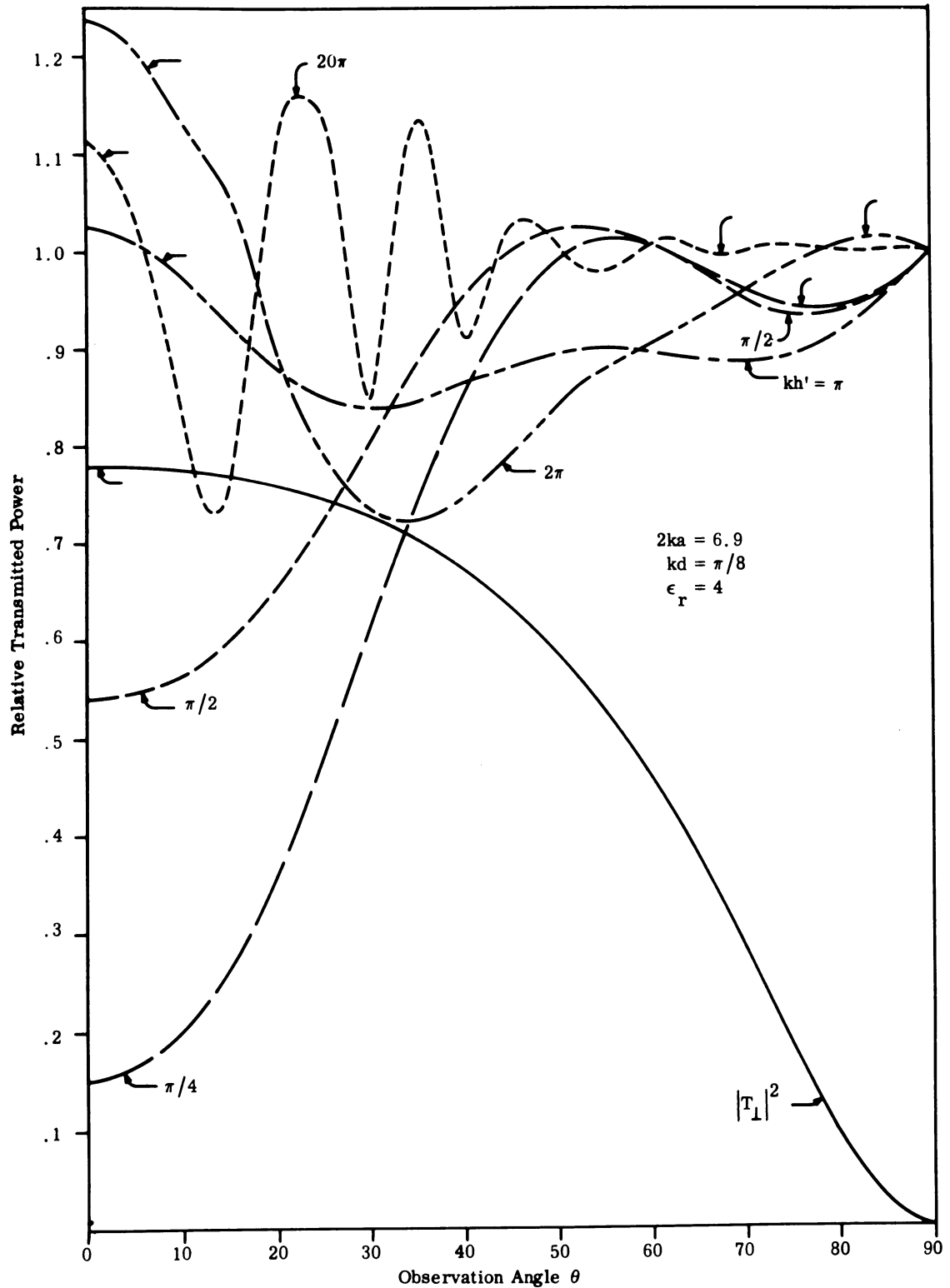
FIG. 50a: TRANSMITTED POWER VERSUS OBSERVATION ANGLE θ FOR 5
SPACINGS kh' OF THE ELECTRIC LINE SOURCE WHICH EXCITES
AN INFINITE DIELECTRIC STRIP.
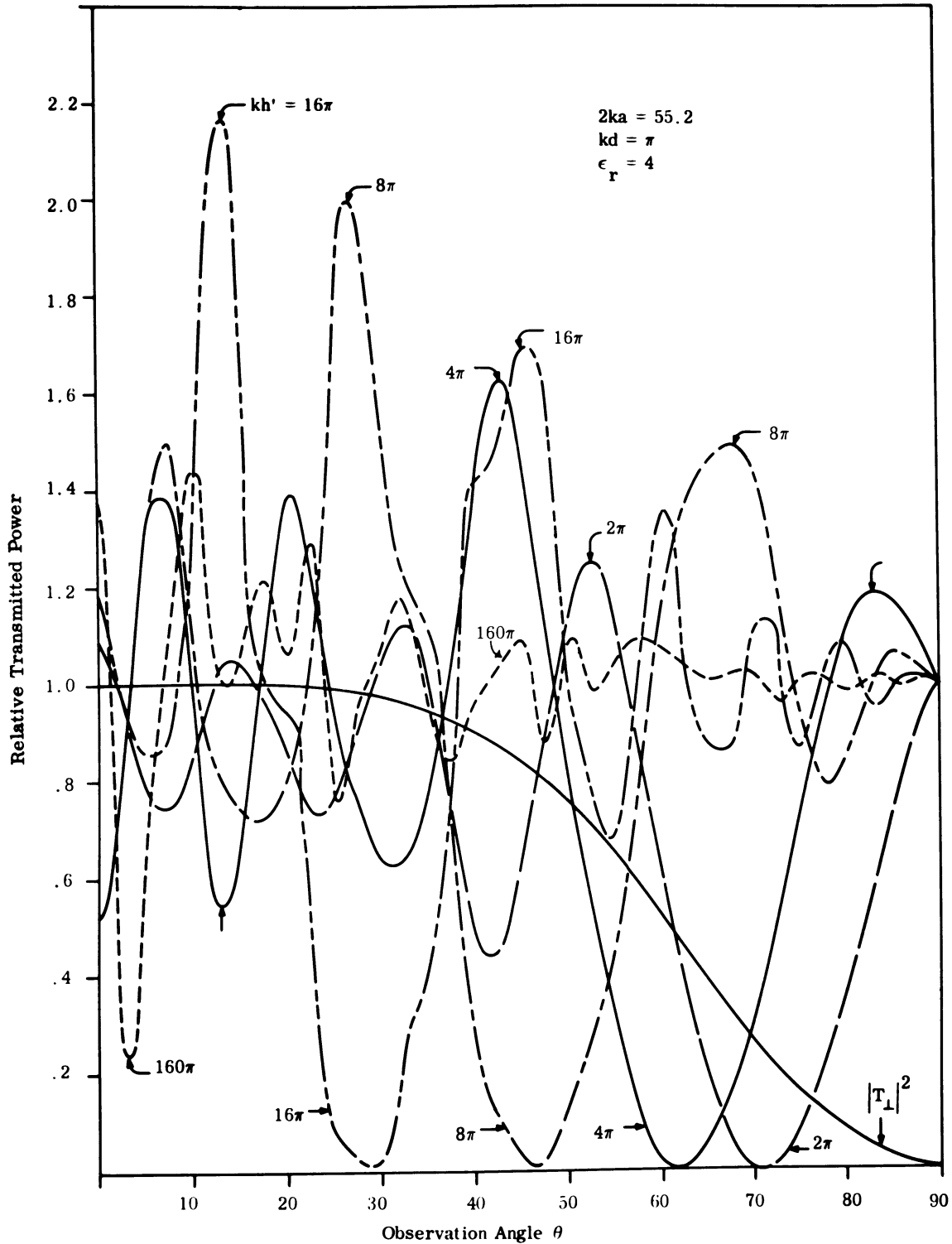
FIG. 50b: TRANSMITTED POWER VERSUS OBSERVATION ANGLE θ FOR 5
SPACINGS kh' OF THE ELECTRIC LINE SOURCE WHICH EXCITES
AN INFINITE DIELECTRIC STRIP.

FIG. 51a: TRANSMITTED POWER VERSUS OBSERVATION ANGLE θ FOR 5
SPACINGS kh' OF THE MAGNETIC DIPOLE SOURCE WHICH EXCITES
A DIELECTRIC DISC OF RADIUS a. (H-PLANE)

FIG. 51b: TRANSMITTED POWER VERSUS OBSERVATION ANGLE θ FOR 5
SPACINGS kh' OF THE MAGNETIC DIPOLE SOURCE WHICH EXCITES
A DIELECTRIC DISC OF RADIUS a. (E-PLANE)

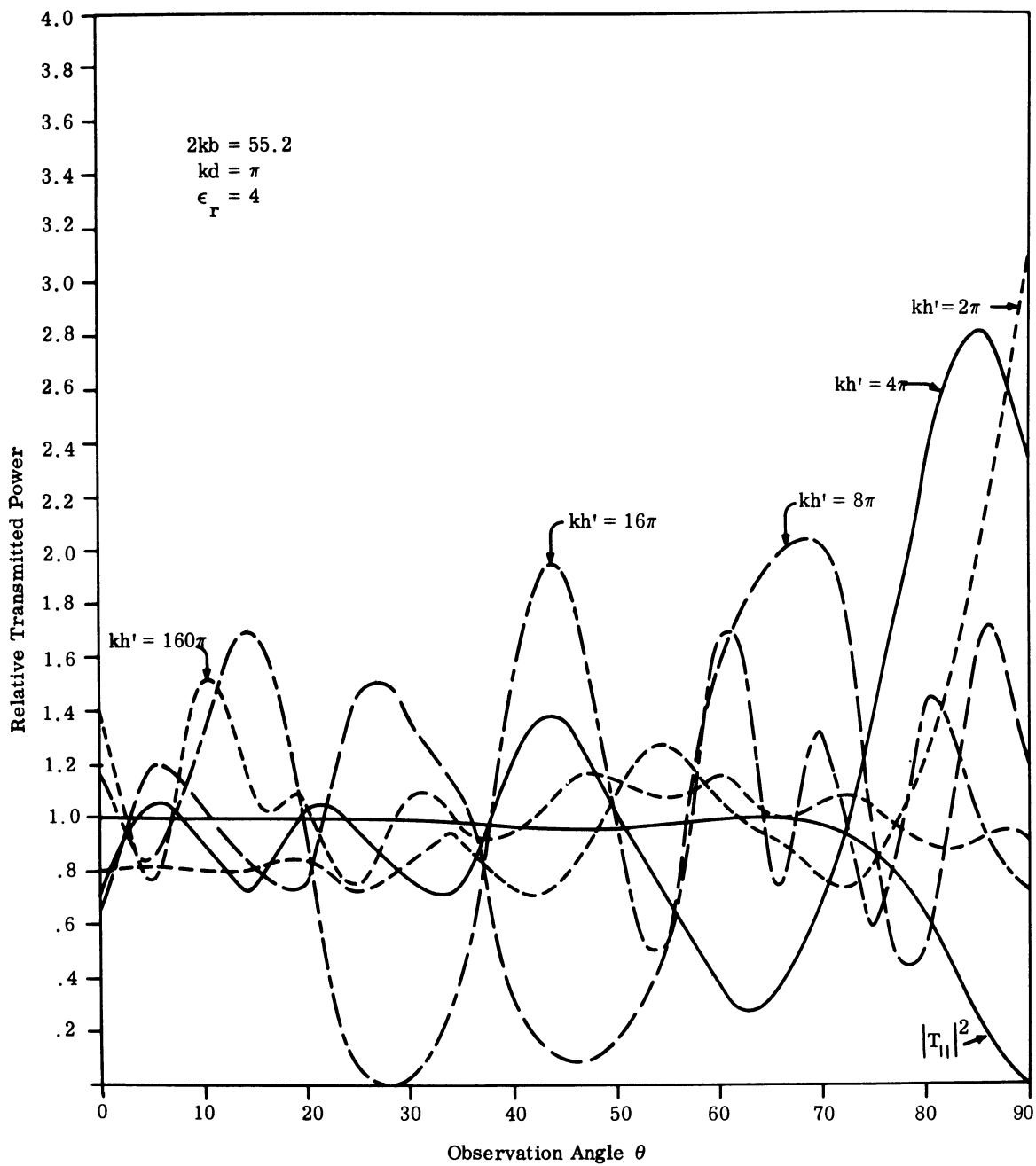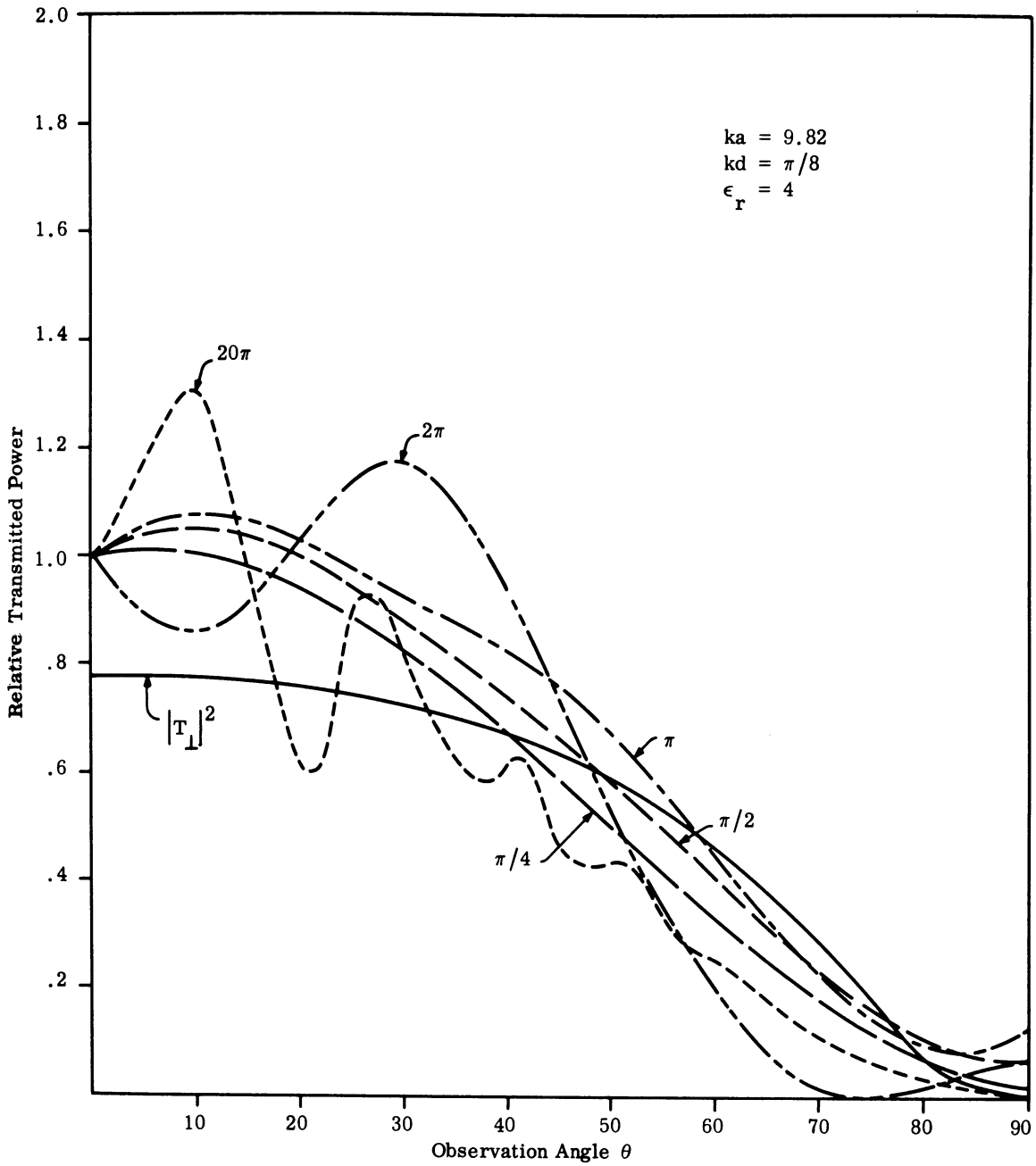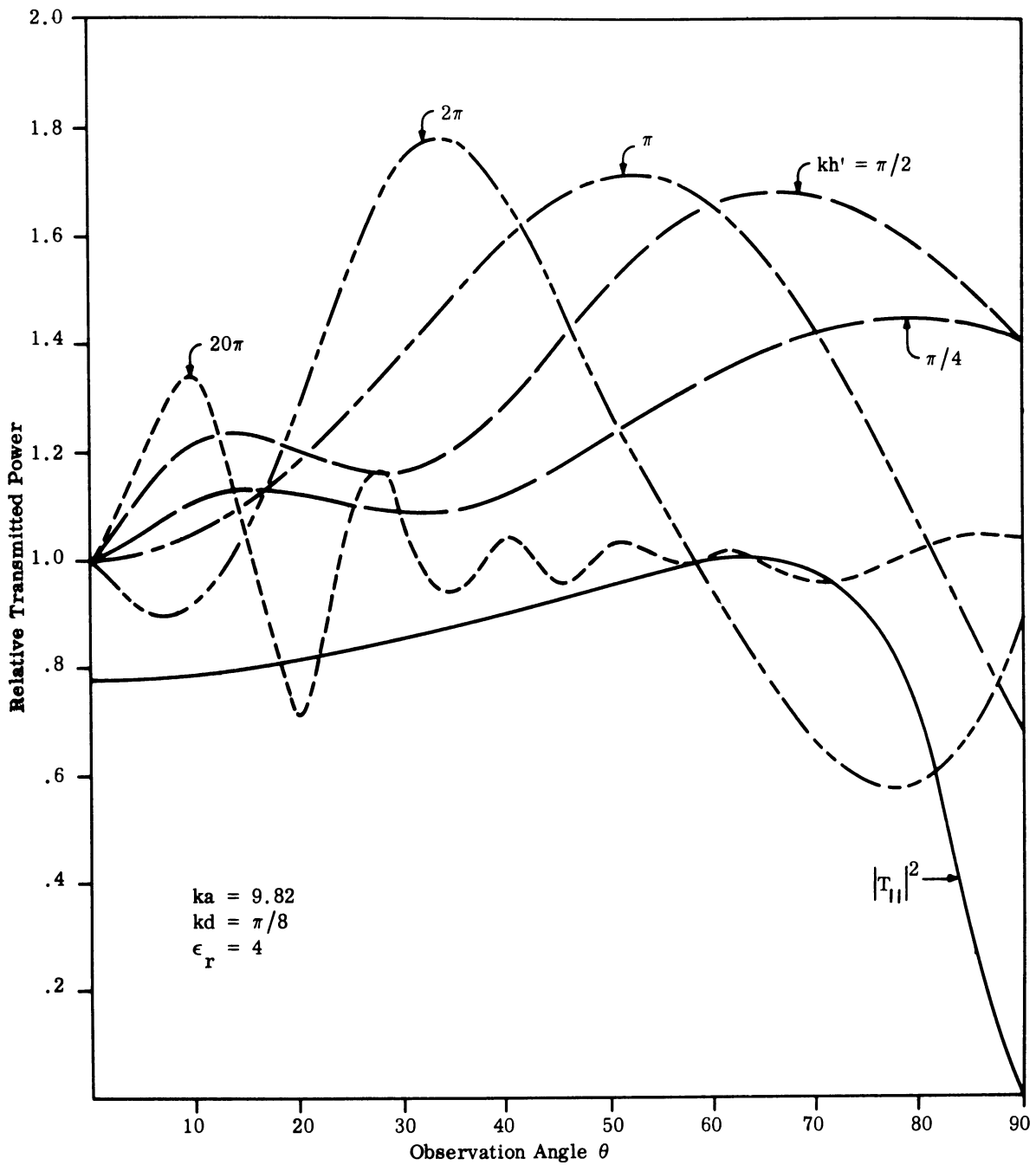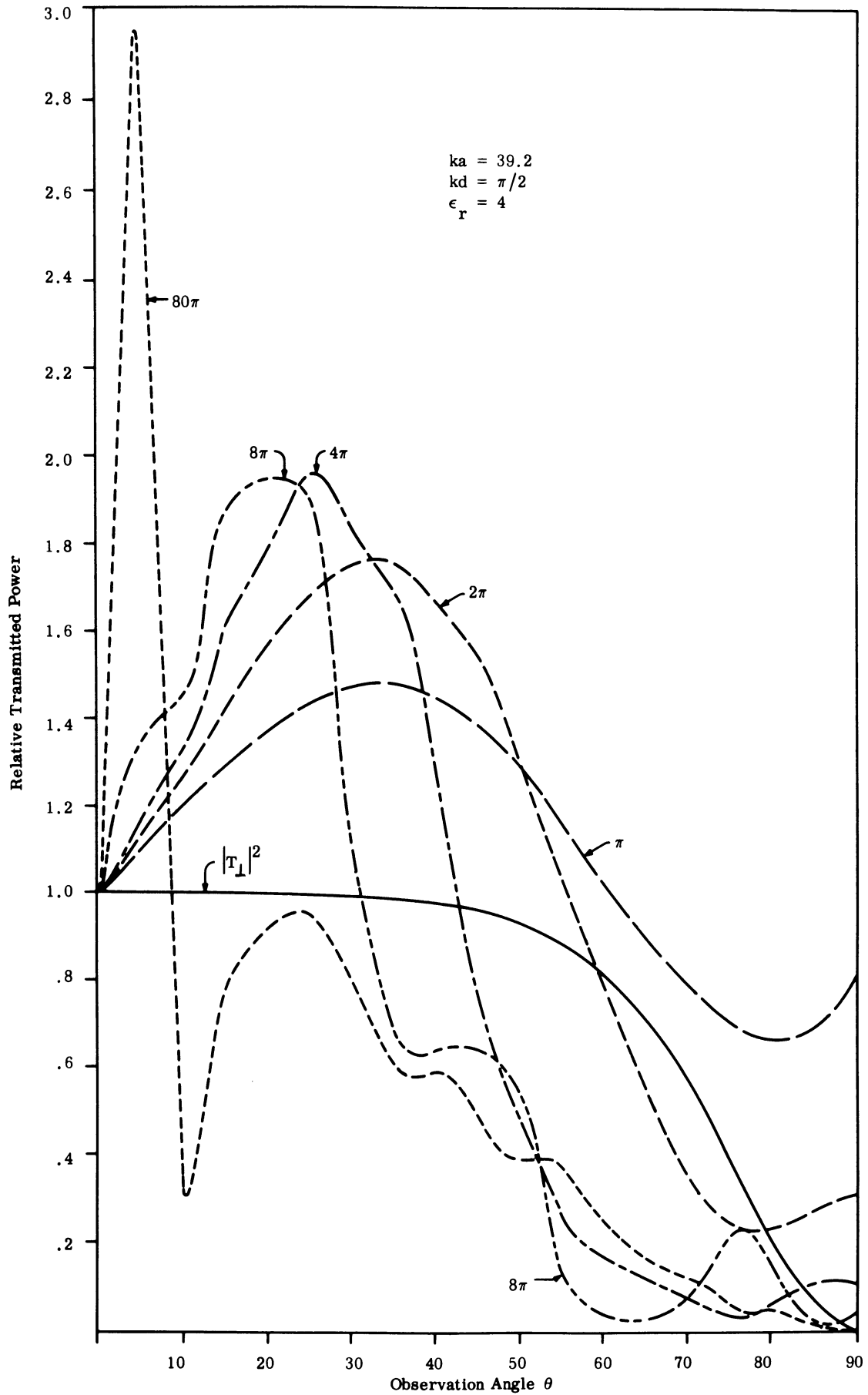FIG. 52a: TRANSMITTED POWER VERSUS OBSERVATION ANGLE θ FOR 5 SPACINGS kh'. (H-PLANE)
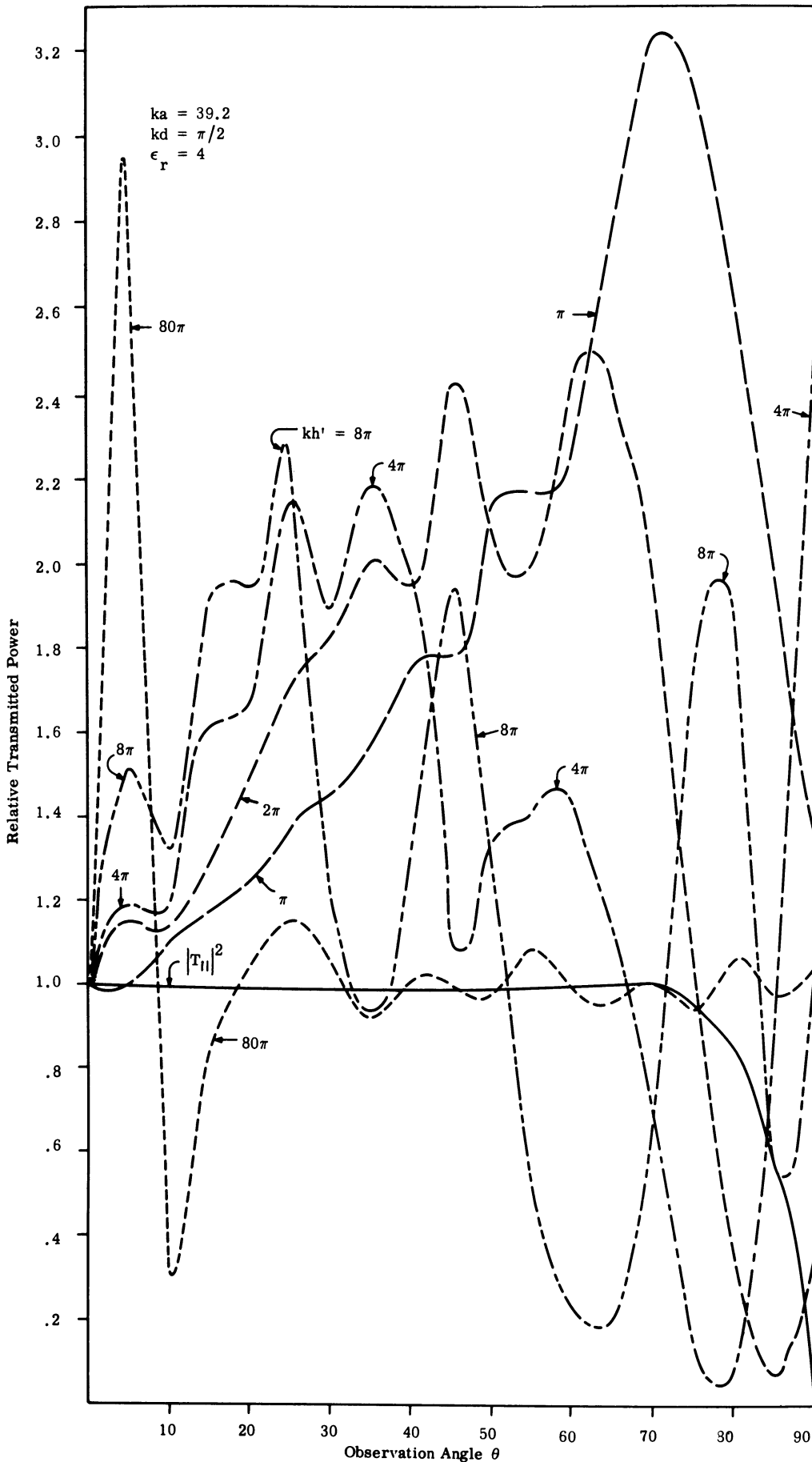
FIG. 52b: TRANSMITTED POWER VERSUS OBSERVATION ANGLE θ FOR 5 SPACINGS kh'. (E-PLANE)

VII

CONCLUSION

As a result of this study we have drawn the following conclusions in regard to the general properties of the particular radant structure, namely, the loop array mounted on two dielectric panels, supplied by the Air Force

From the analytical point of view, the panel can be considered as an aniso-tropic slab. At low frequencies, it behaves as a thin slab, hence, it does not have too much effect on the radiation pattern of a primary source which is placed behind the panel (Fig. 13, Section III). Even at moderately high frequencies, the panel is highly dispersive. It will, in general, distort very significantly the pattern of the primary source (Figs. 29 and 30, Section III). The distortion is also partly due to the finite dimension of the structure in the broadside directions as demonstrated by Figs. 23 and 24. Under certain favorable excitation conditions, corresponding to the probe position of a primary source with respect to the panel, the diffracted pattern of the radome may provide a more directive pattern than the source. For example, when a ferrite loaded antenna is used as a primary source, the directivity of the entire system shows an 8db increase [Interim Report No. 2, Section II]. In such a case, we view the radant as a part of the entire structure. The resultant direc-tivity in most cases, is commensurable to the area of the radant. Occurrence of super-directive effect is possible, but the effect would be very frequency sensitive and critical to the exact physical arrangment of the primary source and the radant. The increase of directivity can also be achieved by using a ridged horn as a primary source, [Figs. 29 and 30 of Interim Report No. 2]. The latter system, in fact, is a better arrangement compared to the ferrite-load antenna because the latter is not only frequency sensitive but also inefficient from the point view of system gain.

The distortion due to the finite area of the radant is also confirmed by a detailed experimental study on the diffracted field of a dielectric plate. Figure 43 for example, shows that the measured E-plane pattern deviates much more from the theoretical value based upon an infinite sheet of dielectric slab. On the other hand, all the H-plane patterns agree fairly well with the theoretical predication. Where the E-field is parallel to one of the broadside directions, one would expect that the linear dimension of the slab perpendicular to the E-field will not cause a pronounced resonant condition. Table IV summarizes the various experiments which performed on the radant as a secondary source.

The investigation concerning the radant as a primary source, that is excited directly by a pair of transmission line connected to one of the loops, reveals some interesting but rather complicated phenemena. Figures 36 and 37 show two typical patterns. It is practically impossible to give a precise interpretation of these patterns. All we can say is that the entire panel due to the mutual coupling between the loops is acting as an array of hybrid elements, consisting of electric dipoles and magnetic dipoles.

Our attempt to provide a reasonable theory for the diffraction by a finite dielectric slab has not yet been too successful. It is very likely that a reliable theoretical solution can only be found by solving numerically the integration which governs the field distribution inside the slab.

In regard to the future work, we feel that dielectric slabs loaded by resonant elements do not offer too much promise as a useful radant structure. When slabs are loaded by non-resonant elements, they may be treated as an artificial polarized and magnetized body with predictable characteristics. It is quite possible that one may make use of these controlable characteristics to construct a radome with tolerable distortion and the structure may offer additional mechanical strength.

TABLE IV

SUMMARY OF RADANT PERFORMANCE CHARACTERISTICS

Type of Primary Feed	Ferrite Slot Antenna	Broadband Aperture Antenna	Dipole Antenna
Bandwidth Considered	300 - 600 MHz	0.85 to 1.0 GHz	340 MHz to 3000 MHz
VSWR Characteristic for the Primary Source Alone	Less Than 3.0 to 1 For 340 to 350 MHz	Less Than 3.0 to 1 From 850 to 10000 MHz	--------------
VSWR Characteristic for the System Radant Plus Primary Source	Function of Spacing With a Frequency Shift for Minimum VSWR from 330 to 348 MHz	Peaked Characteristic With High Values as a Function of Spacing	Peaked Characteristic With High Values on VSWR Ratio as a Function of Spacing
Frequencies Where Pattern Measurements Were Performed	From 300 to 600 MHz	1000 MHz, 1500 MHz, 3000 MHz, 8500 MHz	362 MHz, 750 MHz, 1500 MHz, 3000 MHz
Experimental Half Power Beamwidth Change	140° to 108° in the E-Plane at 348 MHz, 100° to 50° in the E-Plane at 595 MHz*	110° to 50° in E-Plane at 1.0 GHz, 19.0° to 11° at 8.5 GHz	Observed Only at 362 MHz With a Change from 80° to 70° in the E-Plane Pattern
Gain Increase and Optimum Spacing Conditions	$\Delta_{db}^+ = 6.0$ for d = 1 1/2" at 595 MHz**, $\Delta_{db}^+ = 7.0$ for d = 1 1/2" at 550 MHz**	Generally Negative Due To Poor Matching Conditions Introduced by The Radant	$\Delta_{db} = 3db$ for a Spacing of 3"

* Ground Plane Dimensions 18" x 18"

** The Ground Plane Dimensions Were 48" x 48"

Δ_{db} = Power Received With Radant - Power Received Without Radant

For narrow band operation, it is believed that wire gratings should be thoroughly investigated as a possible structure to provide a desirable radant device.

REFERENCES

Adams, A. T. (1964), "The Rectangular Cavity Slot Antenna with Homogeneous Isotropic Loading", The University of Michigan Cooley Electronics Laboratory Technical Report 147, AD 603 657.

di Francia, G. T. (1953), Electromagnetic Waves, New York, Interscience Publishers, Inc., p 221.

di Francia, G. T. (1953b), Electromagnetic Waves, New York, Interscience Publishers, Inc., p 36.

Jackson, J. D. (1962), Classical Electrodynamics, New York, John Wiley and Sons, p 287.

Magnus, W. and F. Oberhettinger (1949), Formulas and Theorems for the Special Functions of Mathematical Physics, New York, Chelsea Publishing Co., p 27.

Senior, T. B. A. (April, 1958), "Propagation Through a Dielectric Slab", Electronics and Radio Engineer, pp 135-137.

Tai, C. T. and E. S. Andrade (November, 1965), "Radant Analysis Studies - Interim Report No. 2", The University of Michigan Radiation Laboratory, Report No. 7300-2-T.

Tai, C. T., M. A. Plonus and E. S. Andrade (August, 1965), "Radant Analysis Studies - Interim Report No. 1", The University of Michigan Radiation Laboratory, Report No. 7300-1-T.

DOCUMENT CONTROL DATA - R&D

(Security classification of title, body of abstract and indexing annotation must be entered when the overall report is classified)

1. ORIGINATING ACTIVITY *(Corporate author)*	2a. REPORT SECURITY CLASSIFICATION
The University of Michigan Radiation Laboratory Department of Electrical Engineering Ann Arbor, Michigan 48108	UNCLASSIFIED
	2b. GROUP

3. REPORT TITLE

Radant Analysis Studies

4. DESCRIPTIVE NOTES *(Type of report and inclusive dates)*

Final Report - 30 April 1965 through 28 February 1966

5. AUTHOR(S) *(Last name, first name, initial)*

Tai, Chen-To, Andrade, Eric S., and Plonus, Martin A.

6. REPORT DATE	7a. TOTAL NO. OF PAGES	7b. NO. OF REFS
June 1966	108	8

8a. CONTRACT OR GRANT NO. AF 33(615)-2811	9a. ORIGINATOR'S REPORT NUMBER(S)
b. PROJECT NO. 4161	7300-1-F
c. 416103	9b. OTHER REPORT NO(S) *(Any other numbers that may be assigned this report)*
d.	AFAL TR-66-186

10. AVAILABILITY/LIMITATION NOTICES This document subject to special export controls. Each transmittal to foreign governments or foreign nationals may be made only with prior approval of AFAL AVWE-3, Wright-Patterson AFB Ohio 45433. Release to Clearing House for FSTI is prohibited. U.S.Gov't agencies may obtain copies directly from DDC.

11. SUPPLEMENTARY NOTES	12. SPONSORING MILITARY ACTIVITY Air Force Avionics Laboratory, AVWE Research and Technology Division Air Force Systems Command Wright-Patterson AFB, Ohio 45433

13. ABSTRACT

This is the final report on the first phase of an investigation of radant structures. A theoretical and experimental investigation has been made of a specialized radant structure consisting of an array of loops supported by two dielectric panels. Impedance and pattern performance of the radant structure was examined over a wide frequency range. The radant structure was fed by a ferrite loaded slot, by a ridged horn and by a half wave dipole. The diffracted field due to a finite dielectric panel was analyzed using the Huygens-Kirchhoff principle. The results are evaluated and it is concluded that the performance of the specialized structure was not sufficiently unusual or promising to warrant further study. Recommendations are made for a more general approach in a study of selected radant structures or elements that appear to hold promise.

DD FORM 1473 1 JAN 64

14. KEY WORDS	LINK A		LINK B		LINK C	
	ROLE	WT	ROLE	WT	ROLE	WT
anisotropic panel						
radant structure						
experimental study						
antennas						

INSTRUCTIONS

1. ORIGINATING ACTIVITY: Enter the name and address of the contractor, subcontractor, grantee, Department of Defense activity or other organization (corporate author) issuing the report.

2a. REPORT SECURITY CLASSIFICATION: Enter the overall security classification of the report. Indicate whether "Restricted Data" is included. Marking is to be in accordance with appropriate security regulations.

2b. GROUP: Automatic downgrading is specified in DoD Directive 5200.10 and Armed Forces Industrial Manual. Enter the group number. Also, when applicable, show that optional markings have been used for Group 3 and Group 4 as authorized.

3. REPORT TITLE: Enter the complete report title in all capital letters. Titles in all cases should be unclassified. If a meaningful title cannot be selected without classification, show title classification in all capitals in parenthesis immediately following the title.

4. DESCRIPTIVE NOTES: If appropriate, enter the type of report, e.g., interim, progress, summary, annual, or final. Give the inclusive dates when a specific reporting period is covered.

5. AUTHOR(S): Enter the name(s) of author(s) as shown on or in the report. Enter last name, first name, middle initial. If military, show rank and branch of service. The name of the principal author is an absolute minimum requirement.

6. REPORT DATE: Enter the date of the report as day, month, year; or month, year. If more than one date appears on the report, use date of publication.

7a. TOTAL NUMBER OF PAGES: The total page count should follow normal pagination procedures, i.e., enter the number of pages containing information.

7b. NUMBER OF REFERENCES: Enter the total number of references cited in the report.

8a. CONTRACT OR GRANT NUMBER: If appropriate, enter the applicable number of the contract or grant under which the report was written.

8b, 8c, & 8d. PROJECT NUMBER: Enter the appropriate military department identification, such as project number, subproject number, system numbers, task number, etc.

9a. ORIGINATOR'S REPORT NUMBER(S): Enter the official report number by which the document will be identified and controlled by the originating activity. This number must be unique to this report.

9b. OTHER REPORT NUMBER(S): If the report has been assigned any other report numbers (either by the originator or by the sponsor), also enter this number(s).

10. AVAILABILITY/LIMITATION NOTICES: Enter any limitations on further dissemination of the report, other than those imposed by security classification, using standard statements such as:

(1) "Qualified requesters may obtain copies of this report from DDC."

(2) "Foreign announcement and dissemination of this report by DDC is not authorized."

(3) "U. S. Government agencies may obtain copies of this report directly from DDC. Other qualified DDC users shall request through

_____ ."

(4) "U. S. military agencies may obtain copies of this report directly from DDC. Other qualified users shall request through

_____ ."

(5) "All distribution of this report is controlled. Qualified DDC users shall request through

_____ ."

If the report has been furnished to the Office of Technical Services, Department of Commerce, for sale to the public, indicate this fact and enter the price, if known.

11. SUPPLEMENTARY NOTES: Use for additional explanatory notes.

12. SPONSORING MILITARY ACTIVITY: Enter the name of the departmental project office or laboratory sponsoring (paying for) the research and development. Include address.

13. ABSTRACT: Enter an abstract giving a brief and factual summary of the document indicative of the report, even though it may also appear elsewhere in the body of the technical report. If additional space is required, a continuation sheet shall be attached.

It is highly desirable that the abstract of classified reports be unclassified. Each paragraph of the abstract shall end with an indication of the military security classification of the information in the paragraph, represented as (TS), (S), (C), or (U).

There is no limitation on the length of the abstract. However, the suggested length is from 150 to 225 words.

14. KEY WORDS: Key words are technically meaningful terms or short phrases that characterize a report and may be used as index entries for cataloging the report. Key words must be selected so that no security classification is required. Identifiers, such as equipment model designation, trade name, military project code name, geographic location, may be used as key words but will be followed by an indication of technical context. The assignment of links, rules, and weights is optional.